FINAL REPORT



# COMBUSTION MECHANISMS OF SOLIDS

By

E.W. Price, R.K. Sigman,
R.J. Powers, Christos Markou, and J.K. Sambamurthi

Prepared for

OFFICE OF NAVAL RESEARCH
ARLINGTON, VIRGINIA 22217

Under

Contract N00014-79-C-0764, P00006

August 1986



**GEORGIA INSTITUTE OF TECHNOLOGY**
**A UNIT OF THE UNIVERSITY SYSTEM OF GEORGIA**
**SCHOOL OF AEROSPACE ENGINEERING**
**ATLANTA, GEORGIA 30332**

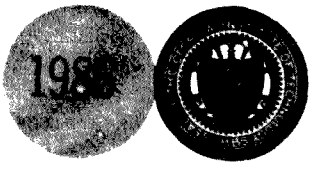

# REPORT DOCUMENTATION PAGE

| | |
|---|---|
| 1a. REPORT SECURITY CLASSIFICATION<br>Unclassified | 1b. RESTRICTIVE MARKINGS<br>AD-A173 407 |
| 2a. SECURITY CLASSIFICATION AUTHORITY | 3. DISTRIBUTION/AVAILABILITY OF REPORT |
| 2b. DECLASSIFICATION/DOWNGRADING SCHEDULE | |
| 4. PERFORMING ORGANIZATION REPORT NUMBER(S) | 5. MONITORING ORGANIZATION REPORT NUMBER(S) |
| 6a. NAME OF PERFORMING ORGANIZATION<br>SCHOOL OF AEROSPACE ENGINEERING<br>6b. OFFICE SYMBOL (If applicable) | 7a. NAME OF MONITORING ORGANIZATION<br>OFFICE OF NAVAL RESEARCH<br>MECHANICS DIVISION |
| 6c. ADDRESS (City, State and ZIP Code)<br>GEORGIA INSTITUTE OF TECHNOLOGY<br>ATLANTA, GEORGIA 30332-0150 | 7b. ADDRESS (City, State and ZIP Code)<br>DEPARTMENT OF THE NAVY<br>800 N. QUINCY STREET<br>ARLINGTON, VA 22212 |
| 8a. NAME OF FUNDING/SPONSORING ORGANIZATION<br>8b. OFFICE SYMBOL (If applicable) | 9. PROCUREMENT INSTRUMENT IDENTIFICATION NUMBER<br>ONR Cont. No. N00014-79-C-0764, P00006 |
| 8c. ADDRESS (City, State and ZIP Code) | 10. SOURCE OF FUNDING NOS.<br>PROGRAM ELEMENT NO. / PROJECT NO. / TASK NO. / WORK UNIT NO. |
| 11. TITLE (Include Security Classification)<br>Combustion Mechanisms of Solids (Unclassified) | |
| 12. PERSONAL AUTHOR(S)<br>E. W. Price, R. K. Sigman, R. J. Powers, Christos Markou, J. K. Sambamurthi | |
| 13a. TYPE OF REPORT<br>FINAL | 13b. TIME COVERED<br>FROM 8-1-1979 TO 7-31-85 |
| 14. DATE OF REPORT (Yr., Mo., Day)<br>1986 August 31 | 15. PAGE COUNT<br>206 |
| 16. SUPPLEMENTARY NOTATION | |

| 17. COSATI CODES | | | 18. SUBJECT TERMS (Continue on reverse if necessary and identify by block number) |
|---|---|---|---|
| FIELD | GROUP | SUB. GR. | |
| | | | |
| | | | |

19. ABSTRACT (Continue on reverse if necessary and identify by block number)

A study was made of combustion mechanisms of composite solid rocket propellants, using the "sandwich burning" method to minimize the statistical aspects of experimentation and interpretation of results inherent in propellant studies. The results provide a more clear picture of the complex combustion process than has been possible previously.

Because of the importance of knowledge of the decomposition mechanisms of individual propellant ingredients at combustion zone temperatures, a combination of facilities was planned for studies of this subject. The primary effort under the contract was development of a new thermal analysis instrument that can measure weight change as a function of time while heating a sample at 100°C/sec. Heating may be done by laser, furnace, or radio frequency induction. The test sample is deposited on the free end of a rod that vibrates during a test, and

| | |
|---|---|
| 20. DISTRIBUTION/AVAILABILITY OF ABSTRACT<br>UNCLASSIFIED/UNLIMITED ☒ SAME AS RPT. ☐ DTIC USERS ☐ | 21. ABSTRACT SECURITY CLASSIFICATION<br>Unclassified |
| 22a. NAME OF RESPONSIBLE INDIVIDUAL | 22b. TELEPHONE NUMBER (Include Area Code)<br>22c. OFFICE SYMBOL |

19. ABSTRACT, continued

mass change is determined by recording the change in vibration frequency of the rod. Results are reported comparing the decomposition behavior of two propellant binders as measured by this high rate thermogravimetric analyzer and a conventional TGA.

ACKNOWLEDGEMENTS

This research has been sponsored by the Mechanics Division of the Office of Naval Research, Arlington, Virginia, under the Contract No. N00014-79-C-0764, P00006. Dr. Richard S. Miller served as the technical monitor and program manager for this contract. His support of this research investigation is greatly appreciated.

TABLE OF CONTENTS

# INTRODUCTION

Progress in the theory of combustion of heterogeneous solid propellants has stagnated for many years as a result of continued ignorance of the decomposition mechanisms (and kinetics) of propellant ingredients, the difficulty of measuring the microscopic details of the combustion process, and the difficulty of analytical description of this three-dimensionally- and chemically-complex process. The research reported here was aimed specifically at these "stagnant points" in the progress toward understanding. The research included two primary strategies. One strategy was to develop means of observing decomposition of ingredients by several complementary controlled heating experiments that spanned the range of heating rates and temperatures from the low rates characteristic of conventional differential thermal analysis and TGA to very high rates in laser pyrolysis comparable to those in the propellant combustion zone. The second strategy was to develop and use a combination of model combustion experiments that collectively guided combustion theory to a more realistic representation of the propellant combustion zone. The results of these two strategies are presented in Appendices A and B, which constitute the bulk of this report. The following is a short summary of these Appendices and of other activities not contained therein.

## HIGH TEMPERATURE DECOMPOSITION

In order to establish the behavior of individual ingredients in the combustion zone, experiments were set up to produce controlled heating of samples while observing their response to heating. The following methods were "assembled":

1. Leitz optical microscope with heating stage (typical heating rate $1^{o}C/sec$)

2. Perkin-Elmer Model TGS-2 thermogravimetric analyzer (typical heating rate 0.1 to $10^{o}C/sec$)

3. Perkin-Elmer differential thermal analyzer DTA 1700 (0.1 to $10^{o}C/sec$)

4. Custom built (see Appendix A) thermal gravimetric analyzer (heating rate up to $200^{o}C/sec$)

5. 1200 watt $CO_2$ laser (Penn Research Corp, Model FHI-140) (heating rate $10^{5}\ ^{o}C/sec$)

The above experiments were aided by a DoD Equipment Grant (AFOSR-84-0183) and are in varying degrees of use as described below.

### Hot Stage Microscope

The microscope was purchased on an earlier AFOSR grant (#84-0183) and the heating stage, purchased with Georgia Tech funds, has been in routine use for 10 years. In the present contract, the "HSM" was used to verify the conditions for melting, conditions for out-gassing, and character of dry residue from tests on polymers used in companion experiments.

### TGA and DTA

This apparatus was used to develop low heating rate data on polymer decomposition (Appendix A). This data was compared with results from the Georgia

Tech-developed high heating rate thermogravimetric analyzer (HHRTGA), first to evaluate performance of the HHRTGA and then to give a comparison base for determining heating rate effects. Comparisons were made for HTPB and PBAN polymers (See Appendix A).

The TGA-DTA unit was also used as a programmable heating control in some tests on the HHRTGA.

## High Heating Rate Thermogravimetric Analyzer

Development was undertaken of a novel device for high heating rate experiments using a "Curie Point Pyrolizer" as a starting point. This device uses radio frequency induction heating of a ferroelectric sample holder to produce rapid heating. The test sample is deposited on the sample holder in a thin film to assure tracking of the sample holder temperature. Heating rates of up to $10^3$ $^oC$ are attainable by this method and a variety of sample and product analyses are possible. In the present study, it was decided to concentrate on time resolved measurement of sample mass (hence the name, "HHRTGA"). In order to make mass measurements, the ferroelectric sample holder was installed as the outer extremity (free end) of a cantilever-mounted quartz tube. Provisions were made for mechanical excitation of vibrations of the rod at its resonant frequency, which was then measured as a function of time during sample heating. Because the sample is at the outer (free) extremity of the vibrating rod, the frequency is quite sensitive to sample mass and sample masses can be relatively small (.25-.50 mg). The change in vibration frquency vs time is a measure of sample mass change. In a typical test, the sample is heated from ambient temperature to 550$^oC$ in 10 seconds. The system records frequency and temperature in digital form in a Nicolet Oscilloscope disk storage (as functions of time). The data are transferred to an IBM PC, which uses stored calibration data to convert frequency to mass and display mass fraction vs temperature. The computer program also calculates effective activation energy and a pre-exponential factor for an Arhenius rate approximation of the data. The system is now operational and has been used to observe decomposition of PBAN and HTPB binders and ammonium perchlorate (See Appendix A). Decomposition at heating rates comparable to conventional DTA and TGA experiments yielded activation energies similar to values from those experiments ( $\sim$ 18,000 cal/mole: see the "VTGA" curves in Fig. 5-4b and Table 5-3b of Appendix A). The effective activation energy of HTPB

decomposition was much higher at high heating rate than at conventional rates (~ 80,000 cal/mole: Table 5-5 of Appendix A), comparable to the weakest bond energies of the molecules. This result suggests that the weight loss during conventional low heating rate experiments is governed by an evaporation process and that the kinetics do not control the rate until rates of 10 to $100^{o}$/sec are used. In the case of PBAN polymer, the activation energy remained low even at a heating rate of $50^{o}$C/sec (Fig. 5-4a and Table 5-4 of Appendix A). It is worthy of note that the heating rates reached in the propellant combustion zone are still 2-3 orders of magnitude higher than those achieved here, so that the complex dependence on heating rate needs to be more fully explored, and extended to higher rates (and temperatures). It was in anticipation of such results that the present study included development of a laser pyrolysis facility.

## $CO_2$ Laser Pyrolysis Facility

This facility is intended to permit observation of polymer decomposition at heating rates of $10^5$ $^{o}$C/sec. It is not proposed that time resolved measurements be made during the heat-up event of any single mass element as this would require time resolution more appropriate to burst heating. It is proposed to propagate a steady state pyrolysis wave in a sample at velocities comparable to propellant burning rates. Measurements will be made of velocity of the pyrolysis wave, sample surface temperature, temperature profile in the thermal wave, and gas composition above the surface. Planning for this project was started during the present contract, funding for a 1200 watt Penn Research Corporation fast axial flow laser was provided under DoD Equipment Grant AFOSR-84-0183, and the laser was ordered for delivery in November 1985.

## COMBUSTION ZONE STUDIES

As noted earlier, a combination of combustion experiments and theory was used to determine the nature and dimensions of the flame complex that occurs above the propellant burning surface and to study the coupled three-dimensional heat field in the heterogeneous solid. This work was done primarily with two-dimensional models of the propellant (i.e., oxidizer-binder "sandwiches"). These studies were a continuation of earlier ones reported in Ref. 1, 2 and the new results are summarized in Appendix B. The studies have established a description of the flame complex shown in Fig. 12 of Appendix B, and of its pressure dependence shown in Fig. 18 of Appendix B. Some of the novel features of the combustion zone that are either established or strongly indicated by the results are:

1. The AP flame that is usually pictured as occurring over all the AP surface (at pressures above the AP low pressure deflagration limit) does not occur in the region close to the binder, because of subsurface heat flow from the AP to the binder. In this "quenched" region of the AP surface, the AP vaporizes by dissociative sublimation.

2. The rest of the AP surface deflagrates at a velocity that depends on proximity of the hot oxidizer-binder flame.

3. The AP-polymer vapors diffuse together above the AP-binder contact surface. The extent of mixing increases with distance above the contact surface. At some distance above the surface, conditions become favorable to support a local "pre-mixed" flamelet, which is the nearest part of the O-F flame complex to the surface.

4. The location of the "pre-mixed" flamelet is determined by the necessity for heat release to balance upstream heat loss. The flame is held off from the surface to a location where large fuel molecules are broken down into "oxidizable" fragments and an adequate supply of O-F mixture is available for a self-sustaining flamelet. This was labeled the "Kinetically limited leading edge flamelet" (KLLEF) of the O-F flame complex.

5. The heat from the KLLEF supplies heat to the surface to sustain surface decomposition near the AP-fuel contact surface and to enhance self-deflagration of the AP in a limited region where the AP surface is close but not quenched (location 4 in Fig. 12 of Appendix B).

6. The balance of the O-F flame consists of a diffusion flamelet trailing beyond the KLLEF, generally too remote from the surface to affect burning rate much. At low pressure, the KLLEF stands far out from the surface, consumes a larger part of the O-F mixture, and leaves less reactants for the diffusion flame (Fig. 13, 18 of Appendix B).

7. At sufficiently low pressure, the KLLEF experiences a threshold condition beyond which it cannot be sustained. This is related to the thickness of the binder lamina (in a sandwich) or the size of the oxidizer particle (propellant). In a sandwich, this yields a low pressure deflagration limit. In a propellant, the mechanism causes small oxidizer surfaces to pyrolize without near-surface attached O-F flamelets, reducing the effectiveness of fine particles as a means to high burning rate (Fig. 11 of Appendix B).

8. At high pressure, the AP self-deflagration proceeds ahead of the O-F flame controlled region, dominating the burning rate (7-10 MPa) (Fig. 18 of Appendix B).

## REFERENCES


1. Price, E. W., Handley, J. C., Panyam, R. R., Sigman, R. K., and Ghosh, A., "Combustion of ammonium perchlorate-polymer sandwiches, AIAA Journal, vol 19, March 1981, pp. 380-386.

2. Price, E. W., Handley, J. C., Strahle, W. C., Sheshadri, T. S., Sigman, R. K., and Ghosh, A., "Combustion Mechanisms of Solid Propellants," Final report to Office of Naval Research on Contract N00014-75-C-0332 Mod. P00005, Georgia Institute of Technology, Atlanta, Georgia, September 1980.

Appendix A

# RAPID PYROLYSIS

# OF

# POLYMERIC SOLID PROPELLANT BINDERS

A THESIS
Presented to
The Faculty of the Division of Graduate Studies

By

**Robert John Powers**

In Partial Fulfillment
of the Requirements for the Degree of
Doctor of Philosophy
in the School of Aerospace Engineering

Georgia Institute of Technology
**June, 1986**

RAPID PYROLYSIS

OF

POLYMERIC SOLID PROPELLANT BINDERS

Approved

E. W. Price

Edward W. Price, Chairman

Gary A. Mandro

Gary A. Mandro

J. Jagoda

Jechiel I. Jagoda

Robert K. Sigman

Robert K. Sigman

Date Approved by Chairman 5/22/86

## ACKNOWLEDGEMENTS

I wish to express my sincerest gratitude to my Professor, Edward W. Price, without whom my graduate career would not have been possible; his guidance, his experience, his insight have been invaluable throughout the course of this work. To the members of my committee, Drs. I. A. Jagoda, F. L. Cook, G. A. Flandro, R. K. Sigman, I am indebted for their many hours of discussion and their suggestions. Special thanks to my friend William Meyer whose skill with the microcomputer is second to none, and upon whose expertise the graphics in this work depends. To my friend Robert S. Albright, whose advice and assistance on micro-computers and electronics was indispensable, again my thanks. In addition, I would like extend my appreciation to Christos Markou, for his interest and help with the experimental portion of the work; the advice of my fellow graduate students is gratefully acknowledged. My special thanks the Office of Naval Research and to Dr. R. Miller for their support of this work; this research was carried out under contract N00014-79-C0764.

**To my wife Virginia, for her patience, her encouragement, and for her devotion . . . my gratitude and my love.**

# TABLE OF CONTENTS

Appendices

# LIST OF TABLES

# LIST OF ILLUSTRATIONS

## NOMENCLATURE

| | |
|---|---|
| a | Area, ($cm^2$) |
| A | Pre-exponential Term in Arrhenius Rate Law |
| c | Specific Heat (cal/g-°K) |
| E | Youngs Modulus, (dynes/$cm^2$) |
| e | Napierian Constant |
| Ea | Energy of Activation, (cal/mole) |
| f | Conversion Function |
| h | Specific Enthalpy (cal/g) |
| H | Magnetic Field Intensity |
| I.D. | Inside Diameter of Probe, (mm) |
| I | Area Moment of Inertia, ($cm^4$) |
| k | Reaction Rate Constant |
| K | Kinetic Constant, Lumped Coefficient |
| L | Probe length, (mm) |
| m | Mass, (g) |
| M | Molecular Weight, (g/mole) |
| n | Reaction Order, (dimensionless) |
| $\underline{n}$ | Generic Product |
| O.D. | Outside Probe Diameter, (cm) |
| P | Generic Reactant |
| Q | Heat of Reaction, (cal) |
| $R_o$ | Specific Gas Constant, (cal/g-°K) |
| r | Surface Regression Rate, Burning Rate, (cm/s) |
| S | Entropy, (cal/°K) |

| | |
|---|---|
| $t$ | Time, (s) |
| $T$ | Temperature, (°K) |
| $u$ | Dummy Variable, (Dimensionless) |
| $V$ | Velocity of Species with Respect to Surface, (cm/s) |
| $w$ | Weight (mass), (g) |
| $x$ | x-direction |
| $y$ | y-direction |
| $z$ | z-direction |

**Greek Symbols**

| | |
|---|---|
| $\alpha$ | Reaction Coordinate (Fraction Reacted), (dimensionless) |
| $\beta$ | Heating Rate, (°K/s) |
| $\tau$ | Reaction Coordinate (Fraction Remaining), (dimensionless) |
| $\delta$ | Skin Depth, (μm) |
| $\underline{\delta}$ | Constant, (dimensionless) |
| $\mu$ | Linear Tube Density, (g/cm) |
| $\mu_r$ | Relative Magnetic Permeability, (dimensionless) |
| $\mu_o$ | Magnetic Permeability of Free Space |
| $\lambda$ | Thermal Conductivity, cal/cm-s-°K |
| $\rho$ | Density, (g/cc) |
| $\phi$ | Resistivity of Heating Element (micro-Ohms-cm) |
| $\Phi$ | Euler's Integral, (Dimensionless) |
| $\Theta$ | Frequency, (Hertz) |
| $\omega$ | Rate of Production of Species, (g/s-cc) |
| $\Omega$ | Dimensionless Heating Rate |

**Subscripts**

| | |
|---|---|
| i | i-th Species |
| c | condensed phase |
| f | final |
| g | vapor phase |
| v | vapor phase or vaporization |
| o | initial |
| s | condensed phase |

## ABBREVIATIONS

| | |
|---|---|
| AE | Avrami-Erofeyev Equation |
| AP | Ammonium Perchlorate |
| AR | As Required |
| BW | Bandwidth |
| CC | Contracting-Cube Formula |
| CPP | Curie Point Pyrolyzer |
| CR | "Coats and Redfern" Kinetic Analysis [35] |
| CTPB | Carboxy-Terminated Poly(butadiene) |
| DC | Direct Current |
| DCO | DC-Offset |
| DSC | Differential Scanning Calorimetry |
| DSM | "Direct Solution Method" [53] |
| DTA | Differential Thermal Analysis |
| FVC | Frequency-to-Voltage Converter |
| HTPB | Hydroxy-Terminated Poly(butadiene) |
| LP | Linear Pyrolysis |
| PBAN | Poly(butadiene-co-acrylonitrile) |
| PGC | Pyrolysis Gas Chromatography |
| PMMA | Poly(methyl-methacrylate) |
| RMS | Root Mean Square |
| RF | Radio Frequency |
| RHBP | Rapid-Heating Bulk Pyrolysis |
| SHBP | Slow-Heating Bulk Pyrolysis |

| | |
|---|---|
| S/N | Signal-to-Noise |
| TGA | Thermogravimetric Analysis |
| TVA | Thermal Volatilization Analysis |
| VDC | Volts DC |

## SUMMARY

An investigation into the rapid pyrolysis of polymers has been conducted; this investigation focuses on experimental methods to measure global Arrhenius parameters of polymers under conditions approaching those found in combustion. Prior work in the field of rapid pyrolysis is reviewed.

From theoretical considerations, it is concluded that using Arrhenius parameters, determined at low pressures and low-heating-rates, to extrapolate reaction rates to regions far outside of this domain is unwarranted, and often incorrect. Global kinetic parameters of complex substances are not necessarily constants, and must be measured in the domain of interest, wherein "effective" energies of activation and pre-exponential terms can be interpolated based upon the local conditions.

A novel "Vibrational Thermogravimetric Analyzer" (VTGA) has been constructed which uses a vibrating quartz tube to make continuous mass measurements during sample pyrolysis at heating rates up to 60 °C/s. The samples, thin films coated on a metal substrate, are rapidly heated using a non-contact radio frequency induction heater; these samples are in contact with a thermocouple throughout the course of the

pyrolysis. Global Arrhenius parameters are calculated for the thermal decomposition of Hydroxy-terminated poly(butadiene) (HTPB), Poly(butadiene-co-acrylonitrile) (PBAN), and Ammonium Perchlorate (AP); low-heating-rate results from the VTGA compare favorably with data obtained under similar conditions using a conventional TGA. A limited number of kinetic measurements have been made on these materials at heating rates between 20 and 60 °C/s - rates which would be relevant to the low pressure combustion of polymers.

The work demonstrates that vibration is a suitable technique to make rapid and continuous mass measurements of samples undergoing pyrolysis at moderate heating rates. Modifications to the VTGA are suggested which should permit operation at heating rates in excess of 100 °C/s.

# CHAPTER I

# INTRODUCTION

## 1.1 Background

Recent years have seen the ever increasing use of synthetic polymers in virtually all aspects of aerospace engineering. Polymers are the essential ingredient in light-weight composite structural materials, as well as in modern heat resistant fabrics. They are used in very low temperature environments, such as space-storable systems, and in very high temperature environments where they are required to retain their desirable mechanical properties for substantial periods of time. In addition, synthetic polymers have important applications in high temperature ablative systems, and currently, are finding wide spread use in advanced solid propellants. New classes of energetic polymers are emerging which will revolutionize solid propellant technology. Consequently, polymers are exposed to a wide range of thermal environments. Continued effective use of these materials necessitates a complete mechanistic understanding of the details of their degradation, pyrolysis, and combustion. A thorough understanding of these details would figure prominently in analytically predicting the behavior of solid propellants; quantifying the burning

characteristics of polymers, synthetic structural materials, and fabrics; and predicting performance of ablation systems, etc.

The capability of analytically predicting the behavior of burning solid materials, and in particular polymers, over a broad spectrum of conditions has long been the goal of combustion researchers. However, due to the physical and chemical complexity often encountered in the combustion environment, no such general capability currently exists. The inner details of the combustion zone are ordinarily extremely difficult to measure, primarily due to the microscopic, transient, and hostile nature of the combustion wave. Prediction and control of the burning characteristics of solid materials continues to be an important and completely unresolved problem.

A number of workers [1-9] have developed combustion models which hold over a limited range of conditions. Recognizing that the chemistry of the combustion zone presents an insurmountable mathematical and experimental dilemma, recourse is taken to global kinetics to describe the chemical rate processes. For these models to hold over a broad range of conditions, it is necessary to include constitutive relations of appropriate functional form, and to have an accurate knowledge of the associated physical and chemical parameters for the entire domain over which the model is to remain valid. These parameters include: the

thermal conductivity and diffusivity of the condensed and gas phase species; coefficients of viscosity and mass diffusivity; reaction rate constants, orders, Arrhenius parameters; etc.

The chemical kinetic parameters, especially activation energy, have the greatest impact upon the problem; it is readily apparent from Table 1-1 that small errors in estimating the activation energy produce serious errors in predicted rates.

Table 1-1. Error Estimate in Arrhenius Parameters.

Arrhenius Parameters for
a Theoretical Polymer

$E_a$ = 45000.00 cal/mole
A = $1.82 \times 10^{13}$ $s^{-1}$ : RT/Nh
T = 500 °C

| Presumed $E_a$ cal/mole | k $s^{-1}$ | Error in $E_a$ % | Error in k % |
|---|---|---|---|
| 36000. | 17722. | - 20 | + 17622 |
| 40500. | 1325. | - 10 | + 1225 |
| 42750. | 362. | - 5 | + 262 |
| 45000. | 100. | 0 | 0 |
| 47250. | 27. | + 5 | - 73 |
| 49500. | 7. | + 10 | - 93 |
| 54000. | .6 | + 20 | - 99 |

It is unfortunately not possible to calculate these kinetic values for such complex systems. Furthermore, currently available analytical equipment does not permit the measurement of many these quantities at the temperatures, pressures, and heating rates commonly encountered in combustion. As the global kinetic parameters can be strong functions of the system state variables, it is also in general not possible to extrapolate this data from the more manageable low temperature, low heat flux, and low pressure test environments used in contemporary thermal analysis equipment [10]. As a result there is clearly a need for analytical and empirical methods which address these difficult test conditions. It is the purpose of this work to investigate such methods and apply them to study of selected polymeric materials.

## 1.2 Statement of the Problem

The combustion zone in the vicinity of a polymer can be loosely envisioned as composed of two parts: a gas phase reaction zone - the flame, and a condensed phase zone encompassing a region at and slightly below the deflagrating surface. Heat fed back to the surface via conduction, radiation, and convection, produces: condensed phase reactions, phase changes, and decomposition in the condensed materials. The degree of decomposition is of course dependent upon the temperature and the heat flux to the surface

- this is especially true of polymeric materials. The products of the decomposition vaporize, and provide new reactant species to the gas phase reaction zone.

In a typical propellant, burning at 34 atm., the gas phase combustion wave has a thickness of $10^3$ μm, thermal gradients as large as 30 °C/μm, and temperatures on the order of $10^3$ °C [11]. Polymeric binders in the condensed phase exhibit surface temperatures of about 600 °C (the exact figure is unknown), and sub-surface thermal gradients of about 15 °C/μm [11]. Overall burning rates are around 10 mm per sec. This translates into average heating rates of the condensed phase material of the order of $10^5$ °C/s!

In contrast, a polymer burning at pressures of around 1 atm, has a much more expanded gas phase combustion wave with thermal gradients at the surface of about 0.25 °C/μm [12]; this greatly reduces the heat-flux to the surface, and therefore, reduces linear regression rates to about $10^{-2}$ mm./s. The surface temperatures are still approximately 600 °C, however, with the result that average heating rates are on the order of $10^1$ °C/s.

Polymers used as ablatives in high temperature erosive environments have linear regression rates which fall in between these two extremes typically $10^{-1}$ mm/s [7]. Assuming a similar surface temperatures and sub-surface gradients this gives average heating rates on the order of $10^3$ °C/s. Table 1-2 summarizes these order of magnitude estimates.

Table 1-2. Order of Magnitude Estimates of Various Combustion Zones.

| Combustion Zone | Low Pressure Combustion | Ablation | Propellant Combustion |
|---|---|---|---|
| GAS PHASE | | | |
| Thickness, μm | $10^{4}$ | - | $10^{3}$ |
| Temperature, °C | $10^{3}$ | - | $10^{3}$ |
| Thermal Gradients, °C/μm | 0.25 | Convection | 30 |
| CONDENSED PHASE | | | |
| Thickness, μm | 40 | - | 40 |
| Surface Temperature, °C | ≈600 | ≈600 | ≈600 |
| Sub-Surface Gradients, °C/μm | 15 | 15 | 15 |
| Burning Rates, cm/s | $10^{-6}$ | $10^{-1}$ | 10 |
| Average Heating Rates, °C/s | $10^{1}$ | $10^{3}$ | $10^{3}$ |

When analytically modeling such complex combustion processes, the modeler is faced with the task of solving the appropriate conservation equations of mass, species, momentum, and energy for both the gas and condensed phases. Generally simplifying assumptions are made to render the problem tractable, but nevertheless the task is still formidable. Of particular importance and difficulty are the associated rate processes of species and energy conversion in the condensed phase, which enter the analysis through the conservation of species and energy equations. For the one dimensional, steady case, and in a coordinate system which

is fixed with respect to the regressing surface, these are [7]:

$$r\frac{d\rho_i}{dy} = -\frac{d[\rho_i V_i]}{dy} + \dot{\omega}_i \qquad (1-1)$$

$$\frac{dT}{dy}\sum_i \rho_i c_i [\, r + V_i \,] = \frac{d[\,\lambda\, dT/dy\,]}{dy} - \sum_i h_i \dot{\omega}_i \qquad (1-2)$$

where the last terms in these equations are the rate of species generation per unit volume and the rate of enthalpy production due to chemical reactions per unit volume, respectively. In practical situations the overall rate is normally defined in terms of global zero-order kinetics [13] and an assumed Arrhenius-type temperature dependence, Eqn. 1-3.

$$\omega = A\, e^{-Ea/RT} \qquad (1-3)$$

To use this relation in connection with Eqns. 1-1 and 1-2, it is absolutely essential to accurately know Ea, "the energy of activation" and A, the "pre-exponential term," as

a function of the temperatures and pressures over which the model is to be used. This is particularly true of Ea upon which the burning rate is exponentially dependent. Again, it is not possible to calculate these quantities; and the modeler is forced to rely on their empirical determination - generally from thermal analysis/decomposition experiments.

Experimental difficulties and equipment limitations have largely limited thermal analysis to temperatures, heating rates, and pressures that are well below those found in combustion. There is no reason to assume that data from decomposition studies at conventional conditions are relevant to combustion situations, although, they are often used for lack of better information. DSC, DTA, TGA, TVA, etc., with heating rates on the order of 0.5 °C/s, have been used to estimate Arrhenius parameters of a number of propellant related materials. However, Bouck, Baer, et al. [14] note that "Several important questions concerning the applicability of these laboratory tests to . . . combustion conditions have never been adequately answered." The most serious question concerns validity of extrapolating data obtained at heating rates of 1 °C/s to combustion situations, wherein the rates may range from $10^1$ °C/s. in one-atmosphere flames, to as high as $10^5$ °C/s in propellant combustion. While these low rate techniques are very suitable for material characterization, for example, propellant ingredient aging studies and polymer degradation, they

are not necessarily relevant to combustion and other high rate phenomenon! F. Farre-Ruis and G. Guiochon [15] have shown that heating rate and heat flux to the sample are the controlling factors in polymer decomposition. It has also been shown [14] that various crosslinked polymers gave high-rate pyrolysis results that were quite different than those in low temperature DSC studies. In addition, high temperature exotherms were observed in high-heating-rate experiments (conducted in air) that were not observed in DSC.

> Presumably, when temperature-sensitive materials are heated at low rates to high temperatures, slow low-temperature reactions are permitted to proceed, extensively modifying the virgin material before high temperatures are reached; thus the same high temperature pyrolysis mechanisms are not observed. [14]

Indeed, at conventional heating rates, the sample is usually completely decomposed long before reaching the temperatures at which most of the decomposition occurs in combustion. The relevance of typical decomposition studies to combustion is therefore necessarily suspect.

This situation dictates that new experimental methods must be developed with a strategy for applicability to higher temperatures, elevated heating rates, and high pressure environments. The experimental designs should be predicated on: the objectives of the study, the nature of the material under investigation, and most importantly, the

conditions of the process to be emulated.

## 1.3 Present Work in Perspective

### 1.3.1 Thermal Decomposition of Polymers

Polymers are a unique class of materials. Unlike low molecular weight substances, their physical and chemical properties, such as, molecular weight, density, melting point, boiling point, thermal conductivity, decomposition temperature, vapor pressure, solubility, and reactivity are not well defined. These properties often vary from sample to sample or even within a sample; polymers have been shown to be non-isotropic with respect to thermal, mechanical, and even chemical behavior. These unique properties are engendered by variations in: molecular weight distribution, the degree of crosslinking, crystallinity, methods of preparation, additives, as well as the ratios of constituents in co-polymers. Indeed polymers may be viewed as composite materials in their own right.

This complexity underscores the need to interpret experimental results with some reserve. These results can depend heavily on the physical and chemical makeup of the sample, with the result that inter-laboratory agreement is often poor. Thorough characterization of samples is the only way to mitigate this problem.

Mass loss which occurs during polymer pyrolysis is

essentially a degradative-vaporization process; polymer molecules are too large for vaporization to occur without substantial "cracking" [16]. Kinetically, pyrolysis can be divided into three categories: rate proportional to surface area - the rate limited by molecular vaporization; rate proportional to surface area and inversely proportional to sample thickness - diffusion controlled vaporization; and rate proportional to current weight of sample - kinetically limited.

In kinetically limited pyrolysis, the rate of mass loss, and hence vaporization, is controlled by the rate of bond rupture, which would of course be directly proportional to the weight of the decomposing polymer. Bond rupture is normally the rate determining step in polymers having no low molecular weight constituent, however, under certain conditions the rate of vaporization can be the rate controlling factor.

The maximum theoretical rate of vaporization of a material at a given temperature will occur in a vacuum, this represents the greatest upper bound on the mass loss rate due to vaporization. As long as the rate of conversion to products remains less than this rate, the process will be kinetically limited.

Diffusion controlled vaporization is primarily of importance in cases where the sample size is large, and decomposition takes place throughout the bulk of the sample.

Due to the poor thermal conductivity of polymers, temperature gradients in combustion are large and thermal waves in the solid are thin. Therefore, diffusion should prove unimportant, although, it may be a factor in the low heating rate pyrolysis of bulk samples. (See TGA results Figs. 5-1a and 5-1b.)

Several broadly defined mechanisms are recognized in the non-oxidative thermal decomposition of polymers: a number of polymers "unzip" from the chain ends to yield almost one-hundred percent monomer, while on the other extreme, many polymers exhibit a "random" chain scission mechanism, yielding varying amounts of monomer along with smaller and larger fragments. The behavior of other polymers falls somewhere in between these two extremes. In addition, some polymers, Poly(vinylchloride) for example, decompose through the elimination of small stable molecules. This can occur with simultaneous or subsequent main chain breakup. A given polymer can transition among these mechanisms depending upon the physical conditions controlling the pyrolysis at the time.

"Unzipping" to monomer is highly favored in polymers with tertiary carbon atoms such as PMMA and poly(α-methylstyrene). This mechanism is characterized by the easy volatilization of pyrolysis products with little or no change in the molecular weight of the sample, at least in the early stages of the decomposition. Monomer yield is

also favored in structures and reaction environments where the formation of free radicals is favored. Large amounts of available hydrogen and chlorine (not fluorine), which scavenge free radicals, discourage their formation, and promotes the generation of random fragments. Teflon, for example, completely devoid of hydrogen, yields 100% monomer at moderate temperatures.

Even so-called random chain scission is not entirely random; it has been demonstrated that many of these type of polymers decompose through a "backbiting" mechanism, at least at low temperatures. Chain ends loop back to form ring structures with the main chain, and chain scission occurs at the point of loop-back, followed by ring opening. The number of carbons per ring is influenced by such factors as ring-strain, steric hindrance, and stereo-chemical factors. The most probable number of carbon atoms in the fragment are six or seven depending upon temperature. Random chain scission is characterized by a rapid reduction in molecular weight of the sample during the early stages of decomposition.

These mechanisms hold below about 500 °C depending upon the thermal stability of the polymer. At temperatures in excess of this value, the amounts of monomer are significantly reduced, and products contain more fundamental fragments. Table 1-3 gives the yield of monomer for various polymers undergoing pyrolysis in vacuum (the large mean-

free-path eliminates obscuring secondary reactions); the decreased monomer yield with temperature is apparent.

The pyrolysis products of a particular polymer are, therefore, not necessarily unique. The product yield can depend upon temperature, heat flux, and pressure. Variation in product distribution, which implies variation in the overall mechanism, could also affect vaporization rates; both could certainly influence the magnitude of measured of global kinetic values.

Table I-3. Monomer Yield of Polymers with Temperature. [17]

| Polymer | Percent yield of monomer based upon total volatiles | | |
|---|---|---|---|
| | At 500 °C | At 800 °C | At 1200 °C |
| Polyethylene | 0.03 | 5.5 | 26.4 |
| Polypropylene | 0.4 | 17.9 | 15.8 |
| Polyisobutylene | 36.5 | 69.0 | 13.0 |
| Polystyrene | 51.0 | 10.5 | 0.5 |
| Poly(methylmethacrylate) | 94.2 | 81.8 | 12.9 |
| Poly(tetrafluoroethylene) | 96.6 | 91.2 | 78.1 |
| Poly(α-methylstyrene) | 100 | 38.5 | 37.7 |

### 1.3.2 Global Arrhenius Parameters

Virtually all combustion models to date [1-7] assume an Arrhenius type dependence to describe the binder decomposition on the propellant surface, and, for the most part, these parameters have been taken as constants - independent of

temperature, heat-flux, and pressure. Only recently have attempts been made to measure these quantities under conditions similar to combustion. [18-30] In the past, values obtained at low heating rates and temperatures, were often used to extrapolate reaction rate constants to regions far outside of the domain of applicability; implicit in this approach is the assumption is that the pyrolysis proceeds through a one-step reaction whose rate is a function of temperature and is independent of other physical processes. More realistically these "global" values should be measured throughout the domain interest, where "effective" Ea's and A's could be interpolated based upon the "local" conditions. Without a priori knowledge of the details of the pyrolysis process (which is often unavailable), Arrhenius parameters must be assumed to be "global". In order to examine how these global parameters depend upon the details of the system, it is helpful to recall some of the fundamental aspects of chemical kinetics.

Energies of activation and frequency factors are familiar and fairly well understood concepts of chemical kinetics. They are usually explained in terms of elementary gas phase reactions. In this context, the energy of activation can be loosely envisioned as an energy barrier between reactants and products, while frequency factors can be related to the molecular collision or vibration frequency, and the reactant concentration. For the reaction to proceed

to completion at an appreciable rate, there must be a sufficient number of reactants or activated complexes possessing energies in excess of this barrier potential.

This simple description can be extended to species in solution or even to reactions in the solid state, particularly if the reaction is a simple, one-step processes, which occurs at modest rates. The literature is replete with analytical and numerical methods to determine Arrhenius parameters which are based upon this simple model. When an attempt is made to apply these analytical methods to "complex processes", where species can undergo a variety of chemical and physical changes as function of the state variables, serious questions arise as to the validity of the calculated Ea's and A's.

Gontkovskaya, et al. [31,33], have recently investigated the thermal decomposition of a material, subjected to a linear temperature rise, decomposing via two parallel exothermic reactions, Eqn. 1-4.

$$P \begin{cases} \xrightarrow{k_1} n_1, \quad Q_1 \\ \xrightarrow{k_2} n_2, \quad Q_2 \end{cases} \qquad (1\text{-}4)$$

Here P is the reactant and $n_1$ and $n_2$ are the respective products. Their theoretical investigation involved the

solution of the following equations:

$$\beta \frac{d\eta_1}{dT_s} = A_1 e^{-E_1/RT} (1 - \eta_1 - \eta_2) \qquad (1\text{-}5a)$$

$$\beta \frac{d\eta_2}{dT_s} = A_2 e^{-E_2/RT} (1 - \eta_1 - \eta_2) \qquad (1\text{-}5b)$$

$$c\rho\beta \frac{dT}{dT_s} = \sum_i Q_i A_i e^{-E_i/RT} (1 - \eta_1 - \eta_2) - \alpha \frac{S}{V} (T - T_s) \qquad (1\text{-}5c)$$

$$T = T_s = T_i \qquad \eta_1 = \eta_2 = 0 \qquad (1\text{-}5d)$$

where Eqns. 1-5a and b are the rates of generation of the products, $\eta_1$ and $\eta_2$ respectively, and Eqn. 1-5c represents the energy balance for the material in an environment (subscript s) heated at a constant rate, $\beta$. Eqns. 1-5d, state the initial conditions. In the numerical solution of the non-dimensional form of these equations, $Q_1$ and $Q_2$, the heats of reaction, were taken as equal and $E_1$ was always

less than $E_2$. Calculations for various ratios of the pre-exponentials, and for ratios of the activation energies show that, from the thermograms (decomposition curves) alone, it is impossible to determine whether one or several reactions are taking place! In any case, the first reaction to start is always the one with lowest activation energy, however, the question of how rapidly the second reaction starts and by what path the bulk of the conversion takes place, depends upon the ratio of the rate constants and the heating rate. The higher heating rates promote the course of the reaction with the higher activation energy, indeed, for $A_2/A_1 \approx 10^4$ and $E_1/E_2 \approx 0.8$, over 90% of the reaction proceeded via the path with the largest activation energy! It is further shown that, in principal, it is possible to describe the net rate of conversion of P decomposing by several parallel reactions through an effective rate expression Eqn. 1-6., where $n$ represents the fraction of P remaining at any temperature.

$$\Omega \frac{dn}{d\Theta} = \gamma A_{eff} e^{[-\sigma_{eff}\Theta/(1 - \epsilon\Theta)]} (1 - n) \qquad (1-6)$$

In this expression, $\sigma_{eff}$, is the effective nondimensional activation energy where, $E_{eff} = \sigma_{eff} \cdot E_2$.

$$E_{eff} = \sum_i \underline{\delta}_i E_i \qquad (1\text{-}7)$$

where $\underline{\delta}_i$ is the relative rate of the i-th reaction. This implies that the effective activation represents linear combination of the activation energies of all parallel reactions which are in progress. These $\underline{\delta}$'s and consequently the $E_{eff}$ depend upon heating rate. Since most traditional methods of analysis presume that the kinetics are described by Eqn. 1-6, it is not surprising that results found in traditional TGA experiments and high-heating rate work often differ substantially.

The situation is further complicated if one considers vaporization in the overall rate of mass loss. Chaiken [28] observed a decrease in Ea at high temperatures to levels which could not be accounted for on the basis of molecular structure. (In principal, the lower limit of the activation energy should be the bond energy of the weakest bond in the molecule.) He postulated that an apparent activation energy of 11 kcal/mole from the linear pyrolysis of PMMA at temperatures above 600 °C, corresponded to the heat of vaporization of PMMA monomer - the mass loss is limited by the rate of vaporization. The overall process can be represented by

Eqn. 1-8.

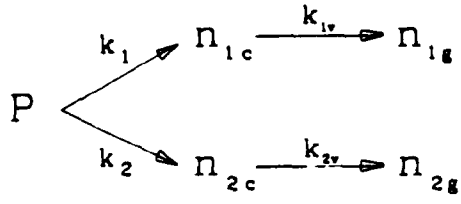


(1-8)

The upper molecular limit for the vaporization of large organic structures has been investigated by Wall [16]. Contrary to statements made in [9], it has been shown that the rate of mass loss, in grams/s, due to evaporation can be represented by an Arrhenius type expression, Eqn. 1-9,

$$\frac{dw}{dt} = \left[ 6.25 \left(\frac{M}{T}\right)^{\frac{1}{2}} a e^{-\Delta S_v / R} \right] e^{-\Delta E_v / RT} \qquad (1-9)$$

from which may be derived a temperature dependent activation energy, Eqn. 1-10.

$$E_v = \Delta E_v + RT/2 = \Delta H_v + 3RT/2 \qquad (1-10)$$

Vaporization is therefore a result of the fraction of

molecules which have sufficient energy (Ea in the previous equation) to overcome their cohesive forces of the medium. Since both kinetics and vaporization have the same functional form, both effects may contribute to the $\sigma_{eff}$ in Eqn. 1-6. In addition, Since heating rate can influence the overall kinetics of sequential reactions [32,33], under appropriate conditions it is possible that either $k_{1v}$ or $k_{2v}$ may dominate in Eqn. 1-8. Therefore, the assumption of constant Arrhenius parameters, implicit in virtually all traditional data analysis schemes, is not necessarily correct in the case of complex processes.

A global Ea is not an Energy of Activation in the strict sense - a col point on a reaction-coordinate vs. potential-energy surface. It is a lumped parameter which must be empirically determined. It is "constant" only in so far as the relative contribution of the participating reactions and physical processes do not greatly change during the course of the decomposition. Therefore constancy in these parameters can be safely assumed only if the decomposition is steady, and takes place over a relatively narrow range in temperature, heat-flux, and pressure.

In connection with polymer pyrolysis, the Arrhenius equation should be used as a heuristic relation based upon notions from statistical mechanics and collisional gas dynamic theory. The Arrhenius parameters should be taken as representing some sort of weighted average of the individual

parameters for the of instantaneous reaction set. These parameters should be viewed as merely numbers used to fit the Arrhenius equation to the experimental data. However the importance of the numbers should not be underestimated. These numbers, if experimentally known, over the conditions for which the model is used, represent the definitive description of the processes occurring in the domain of interest.

### 1.3.3 Rapid Pyrolysis - State of the Art

In recent years, a number of scientists [18-30] have been designing experiments which try to more nearly approximate conditions found in combustion. Experiments of this type can be divided into two groups: "rapid uniform heating or bulk-pyrolysis" (RHBP) experiments, and the so-called "surface or linear" pyrolysis (LP) experiments.

The bulk pyrolysis experiments attempt to rapidly heat samples, sufficiently uniformly, such that thermal gradients are reduced to a minimum and may be neglected in the analysis. Some workers [18] assume that samples can be heated to a known temperature without substantial loss of material, in which case, an "isothermal" analysis is applied at the various final temperatures. Other methods provided for a non-isothermal analysis on samples subjected to a rapid "uniform" temperature rise. In general, both methods require extremely thin samples coupled with very powerful heating techniques.

Linear pyrolysis experiments are designed so as to replicate details of the combustion as much as possible. They attempt to reproduce the high heating rates, surface temperatures, and high thermal gradients, found in combustion. However, this is often coupled with some uncertainty in these values; as these experiments become more "combustion-like", the same difficulties are encountered in measuring these quantities as are encountered in actual combustion situations. The benefits of this type of approach over conventional TGA normally out weigh these uncertainties. The highlights of this work appear in a review by McAlevy and Blazowski [24].

Surface pyrolysis measurements include surface regression rates and temperature; estimates of thermal gradients are made where possible. "Surface kinetic" parameters are extracted from this data using Arrhenius plots[28] . More elaborately, Houser [9] determines these quantities from "measured" surface temperatures, and estimated thermal profiles at several mass regression rates. The HRBP experiments rely on the more traditional methods of analysis of Arrhenius plots and modification of techniques used in the slow heating rate methods [10].

Linear Pyrolysis. Experiments to investigate the pyrolysis of materials in environments somewhat similar to combustion began in the mid-nineteen-fifties. This work was in part motivated by the proposal of Wilfong, Penner, and

Daniels [8], that the burning rate of a solid material should be equal to the decomposition rate of the solid at a temperature equal to the steady-state temperature of the burning surface, $T_s$. They further proposed that the rate-determining step would be the unimolecular decomposition of molecules at the burning surface. This all implied that the rate of linear regression could be described using the an Arrhenius expression and zero order kinetics, Eqn. 1-11

$$r = A\, e^{-E/RT_s} \qquad (1\text{-}11)$$

(Zero order, since, the concentration of surface reactant/area is constant (in a homogeneous material) - surface molecules are continually being renewed by the formation of fresh surface.)

Among the first linear pyrolysis experiments were the so-called "hot-plate" experiments originally devised by Shultz and Dekker [26] and later improved by Barsh[27]. In these experiments, a sample is pressed with constant force against a hot-plate of known temperature, and the linear regression rate is measured. Temperatures are either determined by a thermocouple in the hot plate or a thermocouple sandwiched between the hot-plate and the sample. Arrhenius

type plots of the mass regression rate vs. 1/T allow for the calculation of apparent energies of activation. Shultz and Dekker [26], using a "hot-wire" pyrolysis technique, measured the Arrhenius parameters of PMMA and found Ea = 27.5 kcal/mole, A = 1.88 x $10^{6}$, at temperatures between 450 and 503 °C. They conclude that the rate controlling mechanism is probably the same as that in low-heating-rate bulk pyrolysis - the depolymerization of the condensed polymer on the surface. In subsequent work by Coates on AP [23], the solid hot-plate is replace by a porous plate, thus reducing the build-up of pyrolysis gas in the vicinity of the surface - the principal cause for ambiguity in surface temperature in earlier work. Pyrolysis gases are removed from the back side of the porous plate through the application of a vacuum. Coats work focused mainly on solid oxidizers. Chaiken, et al. [28] applied the hot-plate method to the pyrolysis of PMMA, using an apparatus that permitted much higher temperatures than could be obtained by Shultz and Dekker, but, without the benefit of the porous plate. (Presumably, polymers would clog the porous plate). Investigations on both linear and crosslinked PMMA revealed two distinct energies of activation: ≈26 kcal/mole at temperatures less than 400 °C, in close agreement with that of Shultz and Dekker and a value of 11.2±0.06 kcal/mole at temperatures between 636 and 400 °C. The effect of crosslinking was to increase rates across the entire temperature range but not

affect the Ea's. It is pointed out that this unusually low value for Ea cannot be reconciled on the basis of bond rupture as the rate controlling step, but, is more consistent with surface desorption of the monomer whose heat of vaporization is reported to be 9.2 kcal/mole at 100 °C. The experimental data suggests that the polymer decomposes by a "first-order" surface-depolymerization to monomer which at low temperature is kinetically limited. Whereas at high temperature, the surface becomes saturated with monomer and the vaporization is the rate controlling step!

The principal criticisms leveled at the "hot-plate" experiments are largely aimed at the interferences of the pyrolysis products with experimental measurements/conditions. The actual surface temperature of the sample and hot-plate may differ due to the interposed pyrolysis gas layer. Moreover, the regression rate may be influenced by the accumulation of gases at the interface; these emerging pyrolysis gases flowing radially across the surface may produce erosive conditions not found in combustion. As far as is known to the author, no report of this technique being used at pressure has been published. Whether this is an oversight, or that experimental difficulties preclude this, is not clear. Notwithstanding these limitations, the hot plate technique, especially the porous plate experiments, provides the most clear cut approximation to combustion to date which permit a definitive estimation of the important

variables.

In a attempt to overcome some of the uncertainties associated with the hot-plate experiments, McAlevy et al. [22], performed experiments using a "self-heating diffusion-flame" technique. In this work, an oxidant gas is directed at the surface of a PMMA sample and a diffusion flame is established above the surface. The sample, the lower portion of which is water cooled, automatically advances, thereby keeping the sample surface stationary. The "apparent surface brightness temperature" is measured optically using an infrared radiometer which "looks" through the pyrolysis gases, and also by a 15μm bead thermocouple embedded in the polymer. Using this apparatus, the authors were able to determine "surface energies of activation" for a number of polymers, (but not pre-exponentials), at heat fluxes around 10 cal/cm²-s, surface temperatures around 500 °C, surface regression rates of .32 - .08 mm/s, and pressures of one atm. Accurate measurement of pre-exponentials requires precise measurement of the emissivity of the polymer surface. Temperature data obtained from thermocouple measurements showed considerable scatter as was the case in earlier studies [11]. McAlevy found an Ea for PMMA of 37 kcal/mole over a temperature range of 530 - 490 °C. A liquid layer was observed on the surface of the PMMA. It was concluded that in the hot plate technique, the temperature measured is that of the solid-liquid interface, whereas the optical tech-

nique measures the temperature of the liquid-vapor interface. Values of E, reported for linear PMMA are between 47 and 62 kcal/mole while the values for the crosslinked material are 39-47; it is not clear over what "apparent surface brightness temperature" the PMMA data was collected although it appears to be in the range 500 - 600 °C. The spread in these values is interpreted as a temperature dependence of the activation energy, nevertheless, these values are substantially higher than those obtained by Chaiken. No explanation is given for this discrepancy. It is concluded that there is not a single temperature independent mechanism which controls the decomposition mechanism in the case of PMMA. Experiments were performed on PBAN and CTPB, but surface charring prevented meaningful temperature measurements: apparently, radiometric temperature measurements are unsuitable for the temperature measurement of some important propellant binders.

Cohen, et al. [25], in an important paper, examined a number of propellant related polymers in a linear pyrolysis experiment which used radiative heating to pyrolyze samples at heat fluxes up to 200 cal/cm$^2$-s and pressures up to 1000 psi. Mass loss was again measured by discontinuous weighing of the sample on an analytical balance after an exposure to various heat-fluxes for arbitrary periods of time. Surface temperatures were measured using an infrared radiometer "looking" through the pyrolysis products of the samples;

these samples contained carbon to permit the assumption of black-body conditions. Kinetic and heat of decomposition data were determined for the various polymers, the results of which are given in Table 1-4.

Table 1-4. Kinetic Constants from Ref. [25].

| | HTPB | CTPB | PBAN |
|---|---|---|---|
| Ea, kcal/mole | 16.9 | 10.5 | 16.7 |
| A, g/cm² | 299 | 12.8 | 270 |
| Q, cal/g | 433 | 381 | 564 |

As with the work of Chaiken, the striking feature of this data is the unusually low values of the Ea's; these results cannot be correlated with polymer structure since, for example, the bond energies of the C-C bond are of the order of 80 kcal/mole and C-H bond is about 108 kcal/mole in HTPB. Without the presence of AP all polymers exhibited molten surface layers. Evolved gas analysis was performed using a mass spectrometer (low pressure tests). The major species to appear were heavy hydrocarbons with the greatest variety in the HTPB tests (mass numbers 82 and 84 predominate - a value consistent with a backbiting mechanism); results indicate that heavy hydrocarbons are more representative of

fuel species in the AP-binder diffusion flame than the previously assumed methane fuel. The authors also measure heats of decomposition for the polymers which are an order of magnitude greater than previously assumed. Calculations performed by Cohen [25], using these newly measured values in the so-called Derr, Beckstead, Price combustion model [4], suggest that: the flame temperature and primary flame kinetics are the most important factors influencing the burning rate, the heat of decomposition has only a secondary effect on the rate and, the magnitude pre-exponential term for the pyrolysis has only a minor effect. In addition, they arrive at the surprising conclusion that the kinetics of polymer pyrolysis are independent of heat flux and pressure. The various binders exhibit a range of kinetic constants, but the activation energies do not exceed 17 kcal/mole, they believe that bond rupture is not the rate determining factor. The magnitude of the forgoing kinetic parameters, coupled with the mass spectrometer tests, appear to support the work of Chaiken. The forgoing tends to lend support to the argument of Chaiken that the rate determining step is the vaporization of large hydrocarbon fragments from the surface - at least under conditions of high-heat-flux and high temperature. If, however, vaporization is the rate controlling mechanism, the rate, contrary to the findings in [25], would certainly be a function of pressure. Considerable controversy exists in the literature as to whether the

rate limiting step for the surface pyrolysis is a chemical or physical process.

While all these linear-pyrolysis techniques have made significant strides toward making meaningful kinetic measurements, all possess certain limitations which impede the accuracy of the data. Hot-plate experiments, which permit the determination of excellent mass regression rates, suffer from uncertainty in the temperature and possible erosive effects. On the other hand the diffusion flame approach of McAlevy also suffers from ambiguity in temperature measurement due to the lack of information of on the emissivity of the polymer surface as a function of temperature. This is partially overcome in Cohen's work by the addition of carbon black to the specimen, but here mass regression estimates are made by discontinuous weighing which introduces some uncertainty in the result. Nevertheless, this method permits samples to be pyrolyzed at heating rates more meaningful to combustion than do most other approaches.

Rapid Heating Bulk Pyrolysis. In 1961, S. Kohn [19], in connection with work on high temperature ablation of polymers, recognized the importance of elevated heating rates, and designed a "rapid" TGA and DSC. The "rapid" TGA suffered from several shortcomings. Samples were heated by rapid introduction into a furnace to effect heating; heating rates were on the order of 20 °C per second. Mass measurements

were made discontinuously - the experiment was interrupted after a given time and the sample removed and weighed. Time required to cool the sample prior to weighing was as much as eighty seconds! This, the author points out, was a major drawback of the apparatus which makes it difficult to interpret results. Sample sizes are relatively large, 100 mg, and due to the poor thermal conductivity of polymer, thermal gradients across the sample are large. Temperature time relationships could not be determined during the tests. Given these facts, determination of kinetic parameters proved impossible; "at most, it may be expected that some information about the endo- or exothermal nature of the degradation may be. . ." ascertained.

Somewhat later, Shannon and Erickson [21], studied the thermal decomposition of some polymers used as binders in solid propellants. The methods used included DSC (80 °C/min.), radiation furnace (4 - 10 cal/cm²-sec), and flash-heating techniques ( no estimate given); the three techniques being used to provide three levels of heat flux. In the radiation furnace method, samples were rapidly inserted into a furnace for certain periods of time, and weight-loss was intermittently recorded as a function of total energy absorbed. In the flash-heating experiments, samples were suspended from a micro-balance and mass continuously recorded as a function of total energy absorbed. Results in all cases were largely qualitative in nature. No

effort was made to estimate sample temperature, nor was any attempt made to determine kinetics.

Some of the best work in rapid-heating bulk-Pyrolysis and in high speed decomposition has been done by A. D. Baer et al. [10,14,18,20]. In 1973 [14] Bear reported work on a high speed thermal decomposition technique which produced data very similar to that of a DTA. In this work, "unsupported", 100μm thick, polymer films were heated by radiation from a 1200W projection lamp; heating rates were measured using an infrared radiometer at about 300 °C/s. Since the sample is not in contact with an "infinite" energy reservoir as in DTA, heat evolved due to reaction produces a permanent temperature change in the sample. The data is reported in the form of $\Delta T$ vs. T. The $\Delta T$ is derived from the difference in the measured sample temperature and a calculated temperature of an inert sample exposed to an equivalent heat flux. Estimates of temperature differences across the sample were not more than 10 °C. The principal advantages of the arrangement are: low thermal inertia, small sample size, may be operated at pressure, and is suitable for crosslinked polymers. The principal disadvantages are that low heating rates are not possible in this technique, therefore data cannot be compared with classical methods; data is insufficient to estimate kinetic parameters; and that $\Delta T$ estimates rely in part on calculated values. The most significant result of this work is that polymers exhibited high tempera-

ture "exotherms" which were not observed in low temperature thermal analysis! The authors suggest, that at the even higher temperatures and heating rates characteristic of propellant processes, yet other reactions may be observed. In addition, polymers investigated remained intact to temperatures as high as 700 °K. In 1977, Baer, Hedges, Seader, et al., in a singular paper [20], reported another fast heating approach, which was used to characterize materials used as ablative insulators. The instrument, a form of TGA, heated 25 - 125μm polymer films at rates of 70 °C/sec in a $N_2$ atmosphere. Samples were coated on an electrically heated 25μm metal strip; the temperature of the strip was determined using an infrared radiometer on the side opposite to the sample coating. Pre-weighed samples were heated at a constant rate to a predetermined temperature. Samples were then quickly cooled, by a blast of cold nitrogen, at rates estimated to be 830 °C/s and subsequently weighed. Repetition of this procedure produced a non-continuous set of data in the form of residual-weight as a function of temperature for constant heating rates. Samples were evaluated on this apparatus at variety of heating rates, and on a conventional TGA at low heating rates. In addition, the authors determine kinetic parameters for the samples - three Neoprene/acrylonitrile butadiene composites. The finding of major significance in this work, is that decomposition curves predicted by extrapolation of the

conventional TGA data are greatly different than observed under the rapid pyrolysis experiment. As far as is known this is the first example of kinetic data from a rapid bulk pyrolysis experiment, unfortunately, no data is provided on common polymers. Some uncertainty is implicit in these results, since mass measurements are made discontinuously, and there is no way to determine the effectiveness of the "rapid" quench procedure. Some decomposition may occur in the time between max-temperature and sample weighing. In subsequent work in 1978 [20] and a related paper of 1981 [18], ignition and degradation test were conducted on several neat-polymers, however, these tests were performed in air which makes comparison with the $N_2$ tests impossible. It would be fortunate if these tests could be repeated in an nitrogen atmosphere and analyzed according to the methods of [14]. The purpose of the work presented in [18] was to investigate polymer ignition under approximated fire conditions, and to determine polymer decomposition kinetics at high heating rates. The instrument used in the ignition tests was similar to that used in the 1977 study; it heated 25 - 125μm polymer films at 200 °C/s; this experiment measured ignition temperature as function of heating rate. In the decomposition work, unlike the 1973 study, samples were heated in air at 1000 °C/s to a constant pre-defined temperature, where the material was allowed to decompose "isothermally". The implicit assumption of course is that

no decomposition takes place during heating. The rapid decomposition experiments produced mass loss vs. temperature data. Somewhat arbitrary, mechanisms were proposed for the isothermal decomposition of mylar and polyethylene; global kinetic parameters were calculated.

The rapid heating bulk-pyrolysis methods permit pyrolysis to be performed under more definable conditions than is apparently possible with linear pyrolysis. Rapid heating of thin films, in contact with metal surfaces (heat sinks), provides for uniform sample heating, and permits accurate measurement of temperatures. Emissivities of the metal supports can be determined as a function of temperature, and therefore permit more accurate optical temperature measurements. These methods are also amenable to high pressure operation. Besides the assumption of no mass loss during sample heating, the principal drawback of this type of experiment appears to be discontinuous mass measurement.

## 1.4 Objectives

Mindful of the foregoing, an investigation into rapid pyrolysis was undertaken. This investigation focused on the construction of a TGA which would operate at heating rates beyond those obtainable with conventional instruments. Samples were limited to pure materials, thereby avoiding the complexity of ingredient interaction.

The long term objectives of the research are to

underscore the need for experimental methods which address the combustion environment, and to explore theoretical and experimental techniques which can provide the needed data.

The short term objectives of this work were: firstly, to review previous theoretical and experimental developments in rapid pyrolysis. Secondly, build an apparatus capable of measuring, at elevated heating rates, the extent of sample decomposition as a function of temperature. Thirdly, to extract Arrhenius parameters from this data, and lastly, to apply the foregoing techniques to kinetically analyze HTPB and PBAN during high rate pyrolysis.

# CHAPTER II

# APPROACH

## 2.1 Overview

The determination kinetic parameters during rapid pyrolysis, requires techniques which can rapidly heat samples, while simultaneously making the necessary high speed mass and temperature measurements. As indicated in the last chapter, the performance of any of these tasks independently is a relatively straight forward matter; however, designing an instrument to make the concerted measurements is much more difficult. An investigation into rapid heating and mass measurement techniques was therefore conducted; this investigation resulted in the design and construction of new type of thermogravimetric analyzer. A sketch of this instrument is shown in Fig. 2-1. The device relies on vibration to perform rapid mass measurements. The sample ( $\leq$ 1 mg. ), a polymer dissolved in a solvent, is "painted" on a small metal strip which has been cemented in the free end of a quartz tube. It is surrounded and pyrolyzed by a non-contact heating device, such as a furnace or an RF induction-heater.

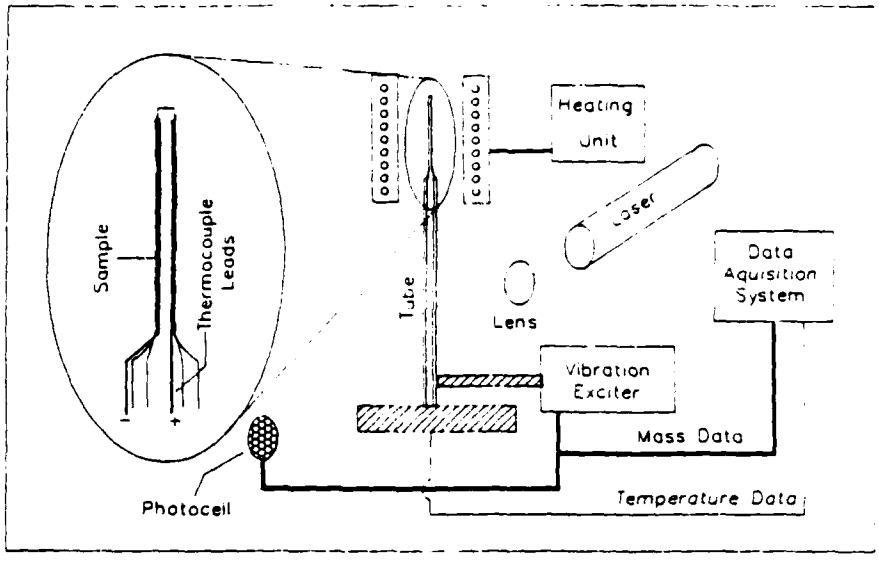


Fig. 2-1 Sketch of the Vibration-based-TGA. (VTGA)

If the tube is excited in transverse oscillation, the period of oscillation is directly proportional to the instantaneous sample mass. As the material pyrolyzes, the resonant vibration frequency of the tube (really the system) increases. Monitoring the change in frequency or period provides a means of estimating the instantaneous sample mass. The frequency is determined using a laser-photodiode pair. The laser ( 1.0 mWatts ) "looks" across the tube at the photodiode, the output from which is a sinusoidal signal whose frequency is identical to the frequency of the vibrating tube. This signal is fed-back into the vibration exciter which excites the tube at the current resonant frequency of the system. This electrodynamic feedback-loop

causes the tube to be continuously excited at the instantaneous resonant frequency, thereby making a continuous mass measurement possible. The system can be calibrated by application of known masses. The actual amplitude of oscillation is less than a millimeter. Sample temperatures are measured by a fine wire thermocouple "embedded" in the metal strip upon which the sample is coated. This, unlike conventional TGA's, places the sample in good thermal contact with the thermocouple and permits the measurement of the actual sample temperature rather than the furnace temperature. The functional parts of the system are enclosed in an chamber so that tests may be performed in an inert atmosphere. Frequency and temperature data are acquired on a two-channel, 2 MHertz digital oscilloscope interfaced to a microcomputer, to which data is transferred for subsequent analysis. (See Appendix A.) A typical output is illustrated in the oscillograph shown in Fig. 2-2; this figure shows the output of the mass and temperature data lines during the low-heating-rate decomposition of HTPB. The top curve in this figure is the amplified thermocouple output, while the lower curve is generated by passing the feedback loop signal through a frequency to voltage converter (FVC). This last curve, is proportional to the instantaneous resonance frequency of the system, and therefore inversely proportional to the instantaneous mass loading, represents the fraction of material vaporized. In

Table 2-1, the parameters associated with the data of Fig. 2-2 may be found. In essence, the system depicted in Fig 2-1 is a Vibrational-TGA (VTGA).

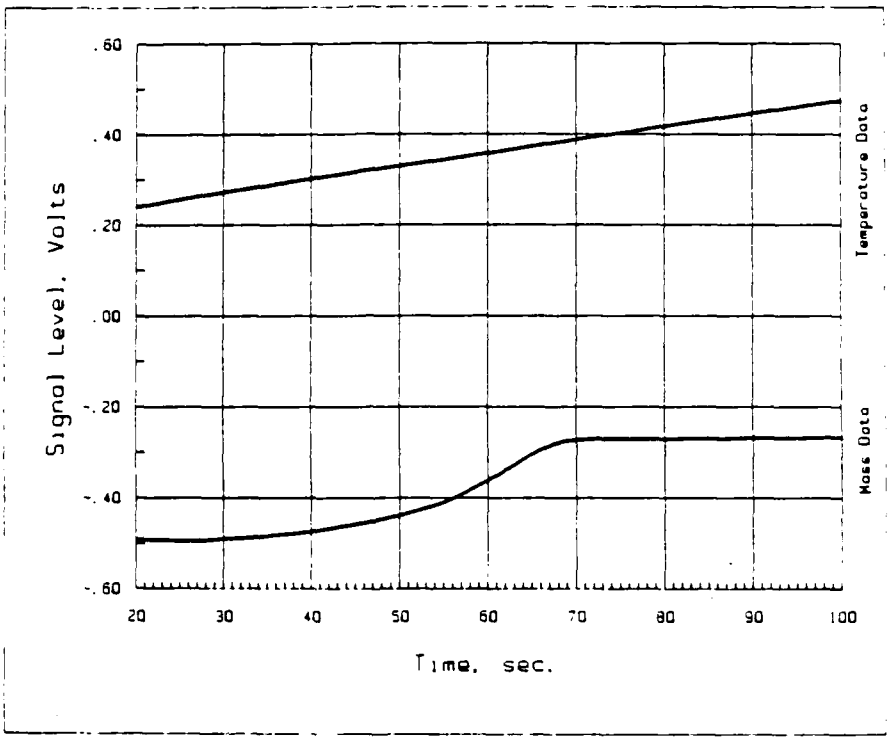


**Fig. 2-2. Oscillograph - Typical Output of VTGA.**

In order to demonstrate the functionality of the instrument several tasks were accomplished. Firstly, selected polymers were kinetically analyzed on a conventional thermogravimetric analyzer.

Table 2-1. Parameters for Curves in Fig. 2-2.

| | |
|---|---|
| Apparatus: | VTGA |
| Material: | HTPB |
| Heating Rate: | 3.3 °C/s |
| Sample Size: | ≈ 1.0 mg |
| Quartz Tube Geometry: | See Fig. 3-1 |

Secondly, Arrhenius parameters were then extracted from this data using a modified form of a classical data reduction scheme from the literature. These values serve as baseline data. Thirdly, these polymers were re-evaluated on the new VTGA under comparable conditions. This was to demonstrate that the new instrument is indeed a functional thermogravimetric analyzer. Lastly, these polymers were again evaluated on the VTGA at increased heating rates to assess the capabilities of the new instrument; results are examined in terms of the scant elevated heating-rate data in the literature.

## 2.2 Pressure Dependence

No high pressure tests were performed in this work, although, the functional parts of this prototype instrument were selected such they would be suitable for implementation at high pressure. Unlike combustion, results from the proposed experiment should be a weak functions of pressure, particularly if the rate controlling step for the mass loss

is the surface decomposition kinetics. Strictly speaking, rates of condensed phase reactions are independent of pressure. In combustion situations, however, pressure controls the position of the gas phase combustion wave relative to the deflagrating surface, this in turn influences the heat flux to the surface. In the present experiment heat flux is controlled by the power input by the heating unit; a gas phase combustion wave does not exist. Therefore, pressure is expected to have a minimal effect on the overall results. If, however, the rate controlling process is vaporization, pressure would certainly influence the results. It is interesting to point out that in experiments such as the diffusion flame work of McAlevy [22], and in most combustion type experiments, the effects of pressure and heat flux are coupled. In most RHBP, which includes the present experiment, heat-flux and pressure are decoupled and can be varied independently. Subsequent work should examine the dependence of the results on the systematic variation of these parameters. This also re-emphasizes the importance of performing experiments under conditions where the heat-flux matches that of the "real world" process being emulated.

## 2.3 Data Analysis

As is usually the case in TGA analyses, reactions of the form:

$$a\ A(s) \xrightarrow{\Delta} b\ B(s) + \ldots + c\ C(g) + \ldots$$

$$b = 0, \text{ or } b \neq 0$$

are considered. In general it is possible that several such reactions may take place concurrently or consecutively in the course of the decomposition, especially when dealing with complex substances such as polymers. The calculation of global Arrhenius parameters requires, in the isothermal case [34], an accurate measurement of the fraction of sample decomposed as a function of time, $\alpha(t)$, and in the non-isothermal case [35], a measure of the fraction decomposed as a function of temperature $\alpha(T(t))$. The ratio of the change in mass to the total change in mass provides a convenient measure of $\alpha$, a non-dimensional representation of which is given by Eqn. (2-1).

$$\alpha = 1 - \gamma = \frac{m_o - m}{m_o - m_f} \qquad (2\text{-}1)$$

In this expression, $\alpha$ represents the "fraction reacted"; $\gamma$ is the "fraction remaining", $m_o$ is the initial mass of the sample, $m_f$ is the final mass of the sample, and $m$ is the instantaneous sample mass. The rate of disappearance of the sample can be described in terms of the so-called conversion function, $f(\gamma)$ in Eqn. 2-2. This equation asserts that the

rate of mass loss is proportional to a constant, k, the rate constant, times some function of the remaining mass.

$$\frac{d\gamma}{dt} = -k\, f(\gamma) \qquad (2\text{-}2)$$

Since $\gamma$ is by definition equal to $1-\alpha$, Eqn. (2-2) becomes:

$$\frac{d\alpha}{dt} = k\, f(1-\alpha) \qquad (2\text{-}3)$$

Implicit in the foregoing is the assumption used in most TGA analyses that the sample is thermally thin - uniform temperature throughout. That is, the measured reaction rates must be independent of the sample thickness; this is especially important in rapid heating experiments [25] and must be verified on a case-by-case examination.

The principal difficulty in the determination of Arrhenius parameters from thermal analysis experiments is that there is basically one equation - the rate equation, and three unknowns - E, A, and n. The general approach is to integrate the rate expression and linearize the result, such that a plot of the data in some reduced coordinate system yields a straight line, where the slope is some

function of Ea and the intercept is some function of A; n is determined parametrically.

In general, two main approaches are normally considered: isothermal and non-isothermal methods. If the experimental method can ballistically heat samples to some high constant uniform temperature before substantial decomposition occurs, the balance of the decomposition will occur at constant temperature and an isothermal treatment of the data may be used. This is preferable since the functional form of $f(\gamma)$ can be empirically determined in this type of analysis, and a greater understanding of the decomposition mechanism is possible [36]. If, however, a large weight loss occurs during heat-up, recourse must be taken to a non-isothermal analysis; this is always accompanied by some ambiguity in result, due to the uncertainty in the functional form of $f(\gamma)$. Farre-Ruis, and Guiochon [15] point out that substantial decomposition occurs in thermally stable polymers even at the highest heating rates. It is due to this and other compelling practical considerations that a non-isothermal analysis has been selected in this work.

There are many techniques in the literature [37] which permit the calculation of Arrhenius parameters using non-isothermal data if one assumes a general functional form for $f(\gamma)$. Indeed, polymer decomposition in a combustion wave is a non-isothermal process, and in the final analysis one would like to program the heating rate such that the sample

would experience the same "thermal history" as a small volume element in the burning solid.

2.3.1 Non-Isothermal Data Analysis.

In the past 30 years, a number of techniques have been proposed to estimate Arrhenius parameters from non-isothermal decomposition data; these are outlined in an excellent review by Wall [37]. These can loosely be divided into: integral methods, differential methods, and difference-differential methods, each method having its own advantages and disadvantages.

Integral methods obtain Arrhenius values through direct integration of the rate expression. These methods, are the most straight forward, but generally require a priori knowledge of the order of reaction. Differential methods suffer from loss of accuracy due to the amplification in data scatter due to numerical differentiation, and at times it may be impossible to use this approach with empirical data [37]. Difference-differential methods employ finite difference relations which are applied to data that is collected at various heating rates. This analysis suffers many of the same limitations as differential methods. All share the following key assumptions: that the Ea, so determined, is kinetically meaningful in a chemical sense, and more seriously, that the Ea and the pre-exponential term are constant over the entire temperature domain of the decomposition. ( This temperature range is commonly over 200 °C. )

These methods, in addition, assume that Ea is constant with respect to the various heating rates employed. Some methods assume first order decomposition while others determine the order parametrically. All require a thermally thin sample, i.e. thermal gradients within the sample are small. Cognizant of "data scatter" associated with differential methods, an integral approach was selected in the following work.

If the sample heating rate, $\beta(T) \equiv dT/dt$, is used in Eqn. (2-3), and an Arrhenius type dependence is assumed for the rate constant, k, this relation becomes:

$$\frac{d\alpha}{dT} = \frac{A}{\beta(T)} e^{-E/RT} f(1-\alpha) \qquad (2-4)$$

which is the basic differential rate expression for a material decomposing under a programmed temperature rise. The corresponding integral expression is given in Eqn. (2-5).

$$\int_0^{\alpha} \frac{d\alpha}{f(1-\alpha)} = \int_0^{T} \frac{A}{\beta(T)} e^{-E/RT} dT \qquad (2-5)$$

If we assume in the first analysis, for low heating rate cases, that $f(1-\alpha) \equiv (1-\alpha)^n$, and that E, A, and n are constant over the entire range of decomposition (which is not necessarily true), and impose a linear heating program ( $\beta$ = constant), then Eqn. (2-5) becomes:

$$F_n(\alpha) = \int_0^{\alpha} \frac{d\alpha}{(1-\alpha)^n} = \frac{A}{\beta} \int_0^{T} e^{-E/RT}\, dT = \frac{A}{\beta}\, \Phi(T) \qquad (2\text{-}6)$$

The left-hand-side of this equation evaluates easily to $F_1(\alpha)$ or $F_n(\alpha)$ where,

$$F_1(\alpha) = -\ln(1-\alpha) \qquad (2\text{-}7a)$$

$$F_n(\alpha) = \left[\frac{1-(1-\alpha)^{1-n}}{(1-n)}\right] \qquad (2\text{-}7b)$$

depending whether or not n = 1. The right-hand-side of Eqn. 2-6, however, has no closed form solution. The literature is replete with approximations to this integral. Coats and Redfern [35] have evaluated this integral by making the substitution, u = E/RT and expanding the result in an asymptotic series [38] to yield,

$$\Phi(T_i) = -\frac{E}{R}\int_u^\infty e^{-u}u^{-2}\,du = -\frac{E}{R}\left[\frac{e^{-u}}{u}\sum_{n=0}^{\infty}\frac{(-1)^n(2)_n}{u^{n+1}}\right] \qquad (2\text{-}8)$$

If the independent variable, u, is large (which is usually the case in solids pyrolysis), it is sufficient to neglect terms of order $O(1/u^3)$ and higher; through this procedure one may obtain three Equations, 2-9a, b, and c, for the zero, first, and n'th order cases respectively. Here $\Gamma$ is the "Coats and Redfern Ordinate" or the ordinate in the reduced coordinate system.

$$\Gamma_0 = \ln\left[\frac{\alpha}{T^2}\right] = \ln\left[\frac{AR}{\beta E}\left\{1 - \frac{2RT}{E}\right\}\right] - \frac{E}{RT} \qquad (2\text{-}9a)$$

$$\Gamma_1 = \ln\left[\ln\frac{(1-\alpha)}{T^2}\right] = \ln\left[\frac{AR}{\beta E}\left\{1 - \frac{2RT}{E}\right\}\right] - \frac{E}{RT} \qquad (2\text{-}9b)$$

$$\Gamma_n = \ln\left[\frac{1-(1-\alpha)^{1-n}}{T^2(1-n)}\right] = \ln\left[\frac{AR}{\beta E}\left\{1 - \frac{2RT}{E}\right\}\right] - \frac{E}{RT} \qquad (2\text{-}9c)$$

Unfortunately, as with all integral methods, evaluation of the Arrhenius parameters requires a priori knowledge of n, the order of reaction. Many schemes have been devised to circumvent this problem where the order of reaction is determined parametrically [39,40,41].

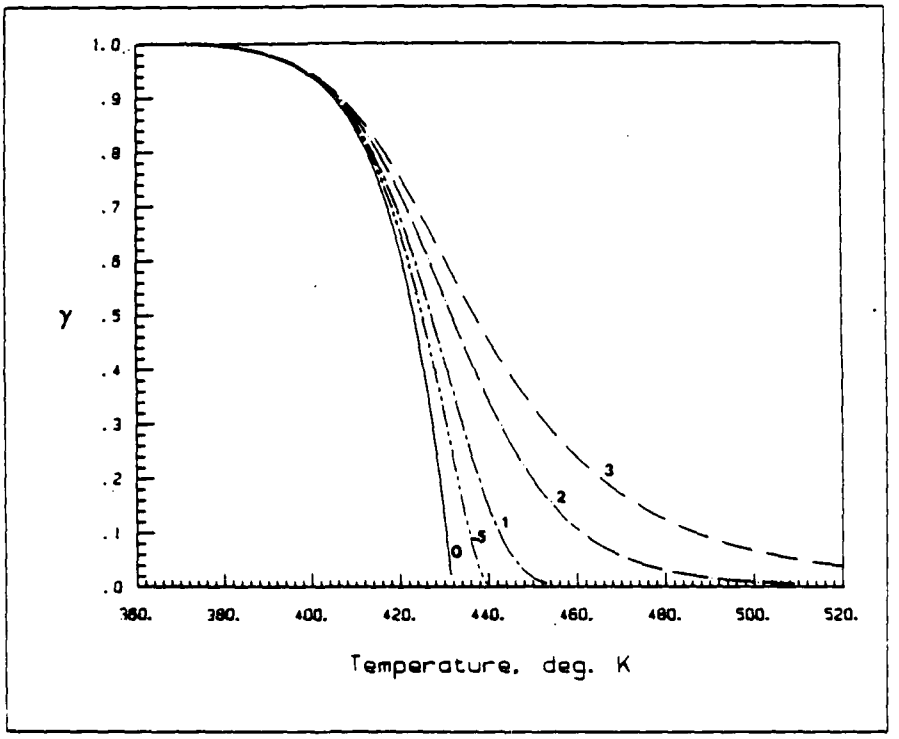


**Fig. 2-3a. Solutions to the Differential Form of Eqn. 2-6.**

Table 2-2. Fourth Order Runge-Kutta Solution Parameters to Eqn 2-6.

| Parameters | Initial Conditions |
|---|---|
| $E_a$ = 28,000.00 calories/mole | $T_o$ = 370.00 °K |
| A = $6.00 \times 10^{+11}$ $s^{-1}$ | $\alpha_o$ = 0.0 : $r_o$ = 1.0 |
| R = 1.987 calories/ mole / °K | |
| n : 0; ½; 1; 2; 3 | |
| $\beta$ : 0.05 °K/s | |

To illustrate one resolution to this dilemma, the differential form of Eqn. 2-6 has been solved numerically using a fourth order Runge-Kutta method; the solution curves for various reaction orders are shown in Fig 2-3a and the solution parameters are given in Table 2-2. The corresponding differential curves are given in Figure 2-3b.

It has been observed [37] that, in the limit, as $\alpha$ approaches zero, reactions of all orders follow zero order behavior, Fig. 2-3c. This can be exploited to determine Arrhenius parameters during the early stages of reaction without prior knowledge or assumption of the reaction order. Therefore, by equation (2-9a), a plot in the "reduced coordinates" of $\Gamma \equiv \ln(\alpha/T^2)$ versus $1/T$, should produce a straight line with a slope of $-E/R$, since $(1-2RT/E)$ is essentially constant and equal to unity. The pre-exponential may be obtained from the intercept, I, and the relation $A = (\beta E/R)e^{I}$. Applying this procedure to the theoretical data of

Figure 2-3a produced the curves shown in Figure 2-3d. Table 2-3 contains the tabulated Arrhenius data so obtained.

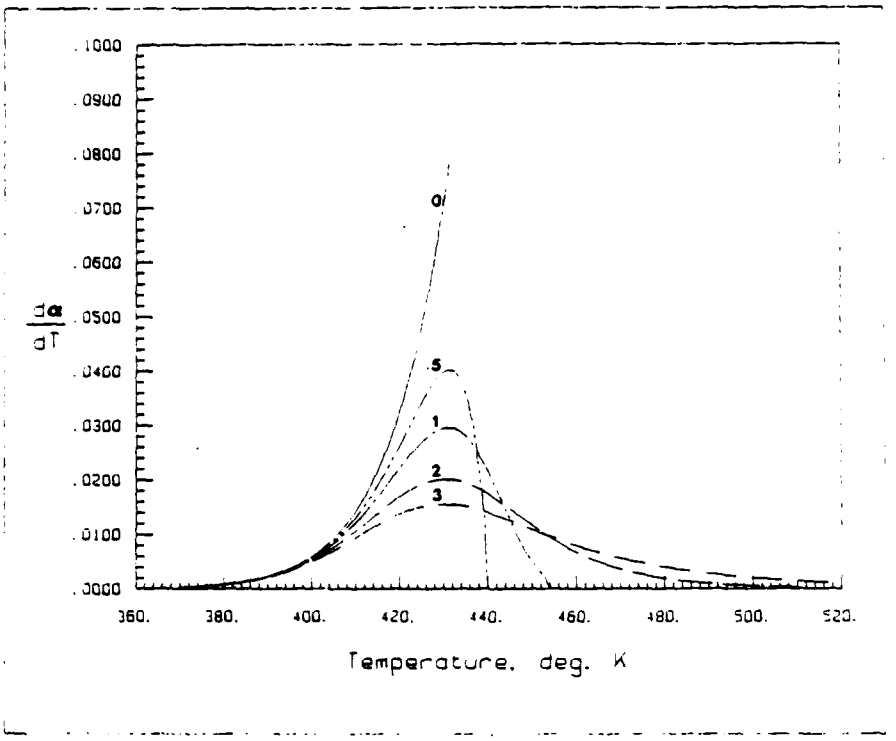


**Fig. 2-3b. Differential Curves for Parameters in Tbl. 2-2.**

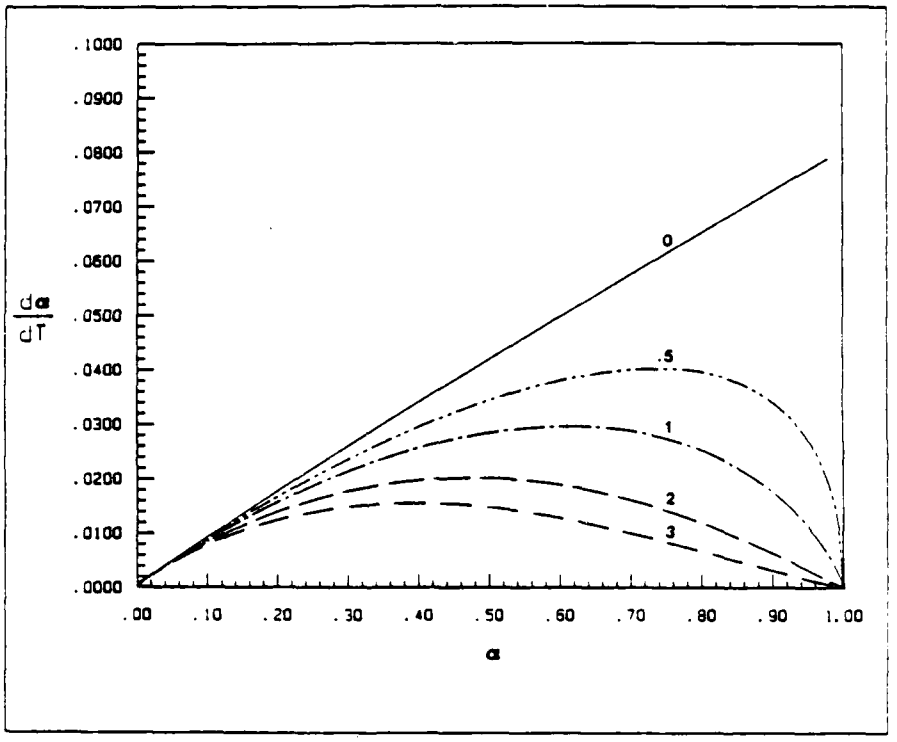


Fig. 2-3c. Rate vs. Extent of Reaction.

Table 2-3. Calculated Arrhenius Data by a Zero Order Analysis - $0.10 < \alpha < 0.30$.

| Actual Order | Calculated Values Assuming Zero Order | | |
|---|---|---|---|
| | Ea cal/mole | A $\times 10^{-11}$ $s^{-1}$ | Correlation Coefficient |
| 0 | 30,160 | 85.9 | .9991 |
| ½ | 29,489 | 35.6 | .9986 |
| 1 | 28,830 | 14.7 | .9976 |
| 2 | 27,459 | 2.49 | .9961 |
| 3 | 26,186 | 0.438 | .9937 |

It apparent that for $\alpha < 0.30$, the data is virtually independent of order. Analyzing the early stages of decomposition frees the experimenter from the necessity of a priori assumptions as to order. In fact, "although there are some special cases for which a theoretical order has real significance, n must be looked upon as a purely empirical parameter, sometimes useful in curve fitting. [37]" Global reaction order can be a complex function of sample geometry, heating rate, etc., and depends largely on experimental method. Moreover, analyzing the first 30% of the reaction, has the added advantage of narrowing the temperature range over which the Arrhenius parameters are determine, and the temperature range over which they are assumed constant. The foregoing is the theoretical basis for the data reduction method which was applied to the TGA

and VTGA data produced in this work; the exact details of the analysis procedure will be explained in Chapter IV.

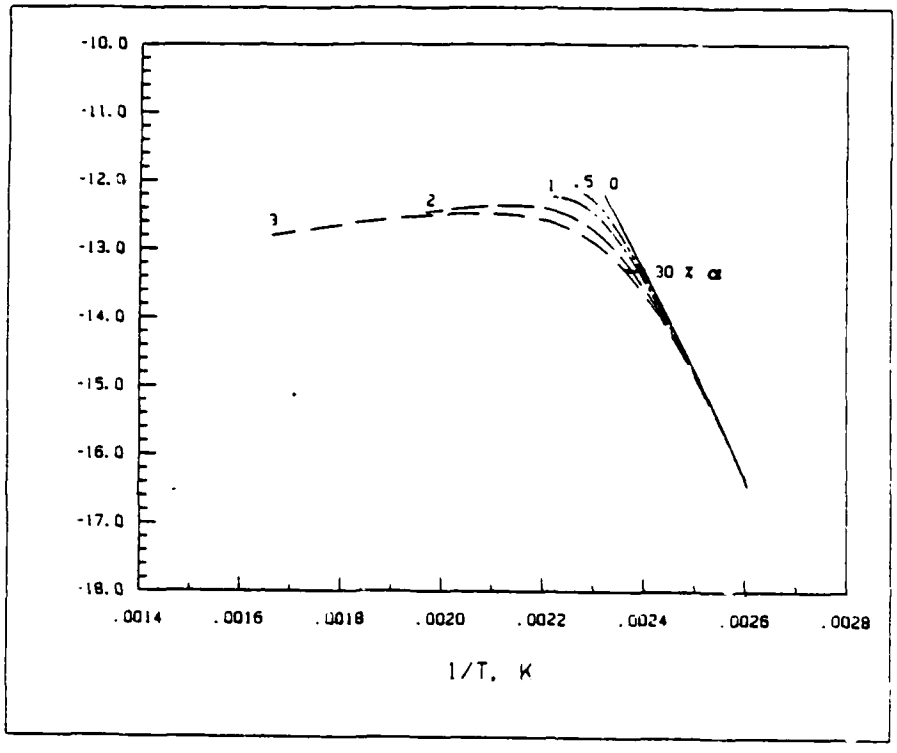


Fig 2-3d. $\Gamma_\infty$ vs 1/T

# CHAPTER III

# INSTRUMENTATION - DESIGN AND CALIBRATION

## 3.1 The Instrument

Recent years have seen an ever increasing level of sophistication in the design of thermal analysis equipment [42]. These improvements have resulted in instruments which are capable of more accurate mass and thermal measurements, improved temperature control and automatic calibration, as well as units with the ability of attaining higher and lower ultimate temperatures. While these enhancements have facilitated the investigation of polymer stability and other low rate phenomena, they have done little to improve the understanding of polymer combustion. This is mainly due to the inability of such devices to heat samples at rates much above 1 °C/s without significant thermal lags between the sample and its environment. In thermogravimetric analyses, for example, the usual mass measuring device is the double-arm micro-balance; it has too much thermal and mechanical inertia to provide the necessary response at more ambitious heating rates. Factors such as buoyancy, condensation of pyrolysis products on the cooler parts of the balance, and the influence of the pyrolysis-product vapor on mass deter-

minations, all combine to interfere with the most sensitive measurements. Moreover, in conventional TGA systems, the thermocouple is rarely in contact with the sample, and is therefore unable to detect endothermal and exothermal transitions which normally accompany pyrolysis. In definitive work, these thermal deviations within the sample must be minimized by placing the sample in contact with a good heat sink, or they must be accounted for in the data analyses. The ability to overcome such limitations is incompatible with the design of present thermal analysis equipment; this necessitates the development of new techniques which are more suited to operation at higher heating rates.

Therefore, in order to quantitatively evaluate polymers at increased heating rates, a new type TGA was constructed; this prototype instrument, unlike conventional TGA's, uses vibration for mass determination. Moreover, in this new design the sample is in intimate contact with the thermocouple. A considerable portion of present work was devoted to the development of this apparatus and to the evaluation of this method with respect to rapid pyrolysis.

The principal features of the apparatus are illustrated in Figs. 3-1 through 3-3. The main components are mounted on triangular "optical benches" which have been bolted to a half-inch steel plate equipped with leveling legs; the whole assembly is placed on a table fitted with anti-vibration pads.

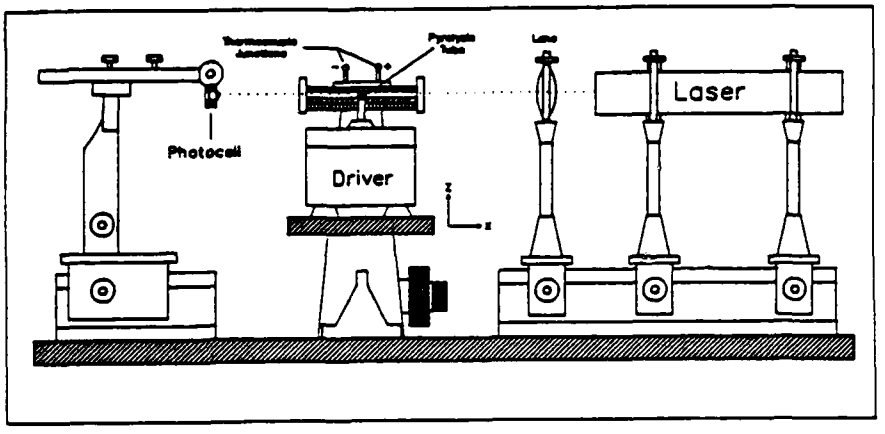


Fig. 3-1. Front View of VTGA Apparatus.

The focal point of the apparatus is a cantilevered quartz tube which has been clamped to a central mount fashioned from a microscope stage and support. A ferromagnetic metal strip with an imbedded fine-wire thermocouple (1 mil) is cemented (2000 °F ceramic cement) in the tip of the quartz tube. The positive lead of the thermocouple is routed through the center of the tube; the negative lead is routed along the outside of the tube to prevent shorting of the leads. These leads are soldered to the base of the thermocouple "pick-ups". The shaft of the vibration exciter is brought into contact with the tube by means of the stage z-axis vernier adjustment.

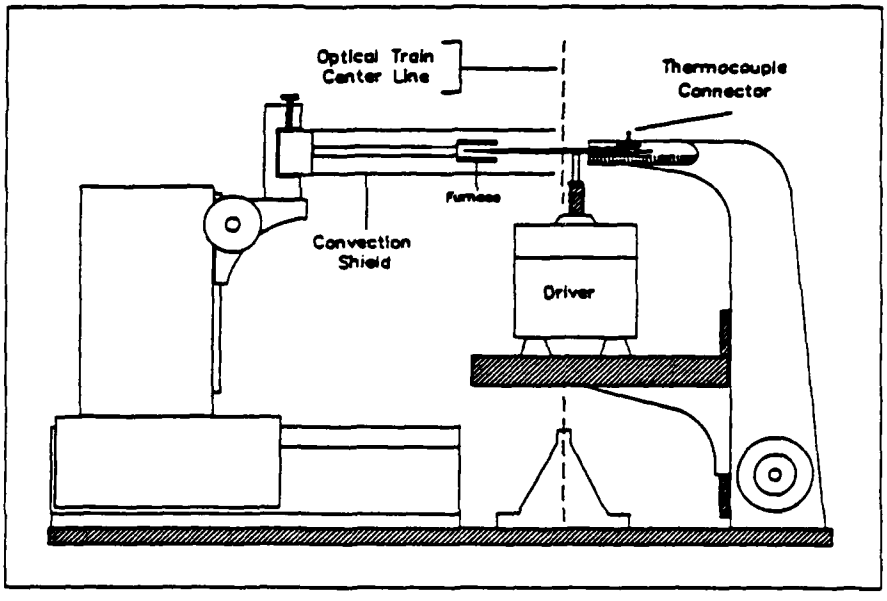


Fig. 3-2 Side View VTGA with Linear Furnace.

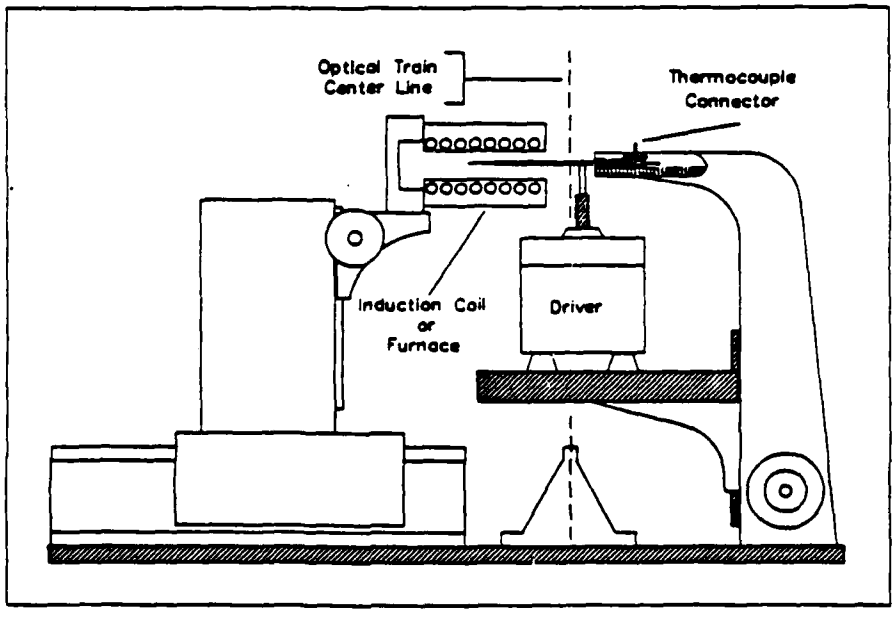


Fig. 3-3 Side View VTGA with Induction Furnace.

Side views of the apparatus are shown in Figs. 3-2 and 3-3. In the former illustration, the instrument is configured with a low heating rate linearly programmed furnace, while the later drawing shows the instrument configured with an induction furnace. The point of contact of the vibration exciter with the quartz "pyrolysis tube" is adjusted using the x-y stage verniers. Likewise, the furnace mount is configured with a vernier adjustments for positioning in the z-direction and may incrementally positioned and locked in other directions. The instrument can be functionally divided in to three main sub-systems: mass determination, sample heating and temperature measurement, and data acquisition.

## 3.2 Apparatus

### 3.2.1 Mass Measurement

The problems associated with making a continuous mass measurement of a sample during rapid heating have been pointed out by Kohn [19]. He states, that:

> . . . there are great practical difficulties in making an experimental device to continuously determine the specimen weight durirg ( rapid pyrolysis ). Restrictions are set, on one hand, by the time needed to determine the thermal equilibrium of the weighing device, and on the other, by the difficulty of calculating or of experimentally ascertaining the weight corrections, made necessary by the variation in the Archimedean pressure due to a density decrease in the gaseous atmosphere of the furnace and by the pressure caused by the gas emission accompanying pyrolysis.

Mindful of these difficulties, Th. Gast and H. Jakobs [43,44] have used vibration to make mass measurements of materials subjected to rapid temperature increases. In their work a platinum ribbon was mounted under tension between two fixed supports. Samples were coated on this ribbon, which was then heated by the passage of an electric current. Temperature measurements were made by simultaneously using this ribbon as a platinum resistance thermometer. A continuous mass measurement was made possible by fashioning an electrodynamic feedback-loop; however, no description of the feedback loop is given, nor, is there any mention of how the frequency of the vibrating ribbon is determined. Their measurements included mass and heat capacity of the samples; no attempt was made to extract kinetic data. On the whole, the description of the details of their apparatus and their method are somewhat sparse. While their approach is very interesting with respect to the present work, it was felt that it would be difficult to maintain constant tension in the ribbon during heating, this problem, which was not discussed by the authors, is pivotal to the success of the measurement. After some deliberation, a method using a vibrating cantilevered quartz tube was selected as best suited to the present work.

The mass measurement scheme of the present method derives from the fact that the natural frequency of vibration of a cantilevered tube is inversely proportional to the

linear density of the tube, Eqn. 3-1.

$$\Theta = \left[ \frac{EI}{\mu L^4} \right]^{\frac{1}{2}} \qquad (3\text{-}1)$$

If a mass is coated on the end of a cantilevered tube, the period of oscillation is directly proportional to the instantaneous loading.

The basis of the system depends upon an electrodynamic feedback loop, a block diagram of which is shown in Fig. 3-4. The essential features of this feedback system are: a 1 mW laser; a lens, to diffuse the laser beam; the quartz tube; a photodiode; some ancillary circuitry; an amplifier; a power supply; and a vibration exciter. The photodiode is positioned in such a way that the shadow of the tube partially obscures the active part of this device. Transverse motion of the tube causes more and then less of the diode to be obscured. This results in a sinusoidal output from the photodiode, rather than a square-wave which would result if the tube "chopped" the light beam. This signal is fed back to the vibration exciter, via some electronics, to close the loop. The purpose of the electronic circuit, shown at the bottom of Fig. 3-4, is to "kill" any DC-offset induced by the DC power supply and to prevent saturation of the loop amplifier. By using the DC-Offset vernier adjustments on

this amplifier, any remaining DC component may be precisely set or eliminated, as necessary; this adjustment is crucial to the fine tuning of the system. The true RMS signal strength going to the vibration exciter is controlled by the vernier gain adjustment also on this amplifier.

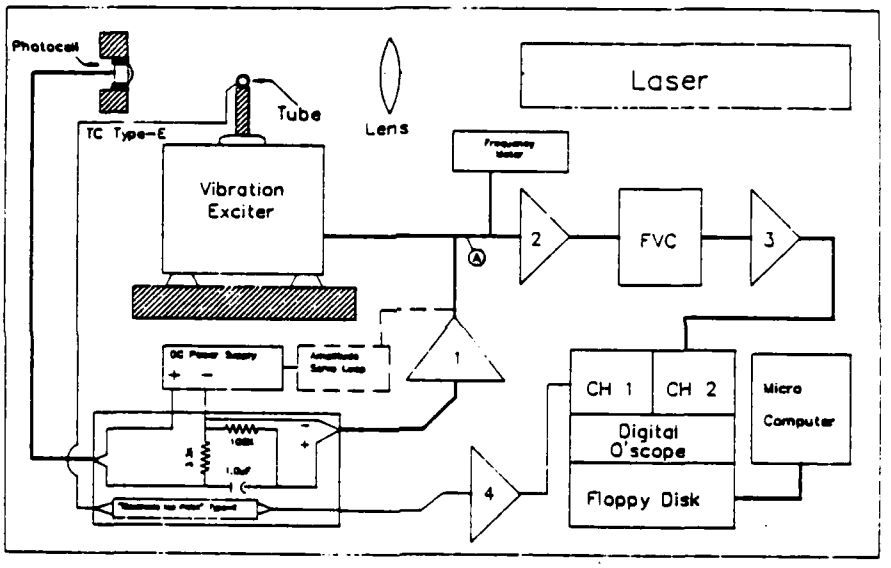


**Fig. 3-4. Block Diagram of VTGA.**

Any decrease in mass at the end of the tube causes oscillation at a slightly higher frequency thereby producing an analogous change in the output of the photodiode. This causes the tube to be excited at this new natural frequency of the system. Monitoring of the frequency or period, makes a continuous mass measurement possible.

Interestingly enough, the system does not have to be started! If DC power is supplied to the feedback loop, any disturbance or vibration is sufficient to cause the system to start oscillation and to seek its natural frequency. An acoustic analogy may be drawn between the present system and the "feedback" phenomenon common to audio speakers and microphones. In the audio case, the speaker corresponds to the vibration exciter, the microphone to the photodiode, and the transverse oscillation of the tube to the longitudinal oscillations in the air between the speaker and the microphone. In this case, if the density of the medium is changed, as by the introduction of a foreign gas, the system shifts automatically to the new resonance frequency. When properly adjusted, the system will automatically track the variation in mass loading on the tube, the output signal will be a near perfect sinusoidal wave, with zero DC offset, whose period is proportional the instantaneous mass loading. The quality of the signal produced by the oscillation of the composite quartz/metal tube can be seen in the oscillograph shown in the inset of Fig. 3-5. This signal was acquired at location A in Fig. 3-4 under the conditions given in Table 3-1. The almost unimodal character of the oscillation is further illustrated by the Fourier transform of this signal shown in Fig 3-5. This signal, and hence the tube motion, was only virtually unaffected by the magnetic and RF fields generated by the induction heater during rapid

heating. This is primarily due to the large frequency difference between the mechanical oscillations (150 Hertz) and the field oscillations (1.2 MHertz).

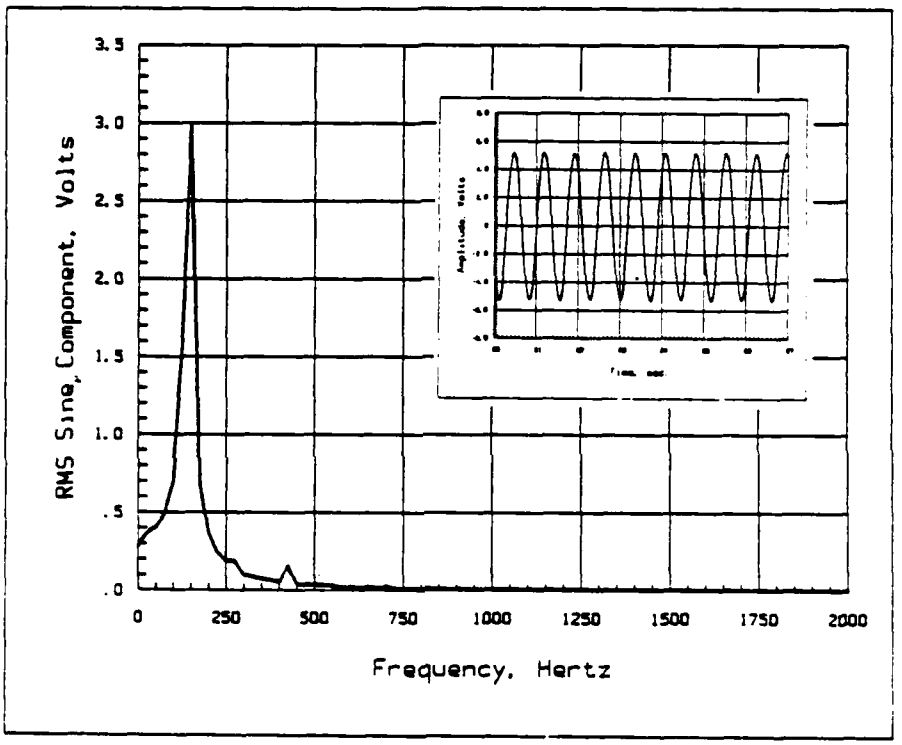


**Fig. 3-5. Feedback-loop Signal and Fourier Transform.**

Table 3-1. Measured Parameters for Data in Figs. 3-5a and b. #

| | Quartz Tube | Metal Tube | Composite Tube |
|---|---|---|---|
| Length + | 5.40 cm | 0.70 cm | 6.1 cm |
| Outside Diameter * | 0.55 mm | 0.33 mm | - |
| Inside Diameter * | 0.40 mm | 0.178 mm | - |
| Linear Density + | | 6.71 mg/cm | - |
| Youngs Modulus * | $3.3 \times 10^{11}$ dynes/cm$^2$ | | |
| | | Flattened Tip | |
| Weight + | | 4.19 mg | |
| Thickness + | | 101 μm | |
| Surface Area (one side)+ | | 0.0586 cm$^2$ | |

* Effective
+ Measured
# The values in this table are typical of those used in this work. The linear density of the thermocouple wire is essentially negligible.

### 3.2.2 Thermal Systems

In the low heating rate experiments, samples are heated in a linear furnace, Fig. 3-2. For convenience, and ease of comparison with conventional TGA results, the furnace used in these tests is the very one used in the commercially available TGA-2 made by Perkin-Elmer. The temperature rise is programmed and controlled using the TGA-2 System 7/4 control device.

In the high heating rate experiments, an induction furnace of the type found in Curie point pyrolyzers is used to indirectly heat the samples. Induction heating uses the

magnetic field from a high power radio frequency (RF) coil to induce eddy currents in a ferromagnetic conductor (or heating element). At radio frequencies these induced currents are confined to a small region near the surface of the conductor. The depth of these currents is defined as the skin depth - that depth where the surface magnetic field strength, $H_o$, drops to 1/e of this value. Ferromagnetic materials are characterized by very small skin depths due to their large relative magnetic permeability, $\mu_r$. The skin depth, $\delta$, is a function of the frequency, $\theta$, of the RF oscillator, and the magnetic permeability, $\mu$. (See Eqn. 3-2). The eddy currents release heat near the surface of the conductor; ninety percent of the heat release takes place in the first skin depth [46]. At radio frequencies, $\delta$, is of the order of 25 $\mu$m. The computed skin depths and specifications for the induction heater used in this work

$$\delta = \left[ \frac{2\,\phi}{\mu\,\theta} \right]^{\frac{1}{2}} \qquad (3\text{-}2)$$

are given in Table 3-2. These small skin depths permit extremely high surface heating rates up to the Curie point temperature of the ferromagnetic conductor ( the ferromagnetic tip on a the quartz tubes ). Proper selection of the tube geometry and the RF field parameters causes the system

to heat ballistically to, and stabilize at the Curie

Table 3-2. Calculated Skin Depths for Ferromagnetic Materials

$H_o$ = 382 Oe
$\mu_o$ = $4\pi \times 10^{-9}$ V-sec-turn/A-cm
$\omega$ = 1.2 MHertz
$\mu$ = $\mu_r \cdot \mu_o$

| Material | Curie Pt. °K [56] | $\mu_r$ [56] | Resistivity Ohm-cm x $10^6$ 20 °C | $\delta$ μm |
|---|---|---|---|---|
| Nickel | 631 | 16.5 | 7.8 | 31.5 |
| Iron | 1043 | 50 | 9.71 | 20.2 |
| 304SS | 845 | ≈35 | 69.5 | ≈4.7 |
| Cobalt | 1401 | 21 | 9.8 | 31.4 |

temperature. It has been reported [45] that the surface of a 0.6 mm Fe wire, as measured by a 1 mil thermocouple, goes from 20 °C to 760 °C in about 40 ms (RF oscillator 480 kHz; magnetic field 1170 Oe; power generator 2000W). This translates into an average heating rate of 25,000 °C/sec. The heating rate can be modified by varying the power input to the coil or the coil geometry. Different final temperatures can be obtained by alloying the ferromagnetic heating materials with various paramagnetic metals.

Near the Curie point, $\mu_r$ for the heating element drops precipitously from a value of around five-hundred to about unity. This significantly reduces further absorption of energy from the magnetic field and consequently limits further heating. Any temperature decrease due to radiation or conduction causes magnetic permeability to increase and re-initiates heating to the Curie temperature.

Curie point pyrolyzers have been used for years in connection with pyrolysis gas chromatography, and have gained a reputation of very high precision. This is due to very reproducible heating rates which can be obtained. The principal criticism applied to RF induction heating by most authors [46] is that the sample cannot be subjected to a continuous range of temperatures, but only to the discrete Curie temperatures characteristic of the ferromagnetic material. They make the unwarranted assumption that the heating time to the Curie point is essentially instantaneous. In their understandable desire to design an isothermal experiment, they fail to realize the potential of the system in a non-isothermal mode. Also most authors give very little concern to the heating rate at all, and they mistakenly concentrate only on the final temperature. ( Even with induction heating, the half-decomposition time of poly(tetrafluoroethylene), one of the most stable polymers is less than the time required to heat the sample to 600 °C [15].) Given this it is not surprising that, there is only

one report of using a Curie point apparatus to make kinetic measurements [46,47] (Mass measurements were not made continuously.)

The elements of the temperature measurement system are also shown in Fig. 3-4. Samples are coated on a flat metallic surface at the end of the pyrolysis tubes. The temperatures of the surface is measured using a type-E thermocouple, which has been embedded in the surface. To insure that the output of the thermocouple corresponds to the published thermocouple tables [48,49], an electronic "ice point" or compensator is included in the output line. The output is amplified (#4, Fig. 3-4) and filtered to increase the S/N ratio. Fabrication of tubes with embedded thermocouples is described in Appendix A. In the finished tube, the thermocouple resides approximately 50 μm below the surface; this is within one "skin depth". There is an additional advantage of using induction heating with type-E thermocouples. Since the thermocouples are ferromagnetic alloys themselves, they are also heated by magnetic field, but at a lower rate. Therefore their response time is increased over that which can be obtained strictly by conduction. In addition, the RF field generated by the induction coil caused only minimal interference on the temperature data line; this high frequency noise was easily eliminated using by low-pass filtering in amplifier #4, Fig. 3-4.

### 3.2.3 Data Acquisition System

The data acquisition system consists of separate analog data lines for the mass and temperature information as shown in Fig. 3-4; these signals are sent to two separate channels of a digital oscilloscope. The electronic components of the feedback loop and data lines were assembled from available equipment and are far from optimized. As a result, undesirable signal characteristics arising from incompatibilities were eliminated by filtering of the data lines and the use of differential inputs at the oscilloscope, Fig. 3-6. These measures limit the response of the system and introduce a "time constant" in the data lines.

Thus this prototype instrument is limited in its overall time response; this of course could be corrected in a more ambitious electronic design. The digital oscilloscope samples data at a preset rate which can be varied from 200 s/point up to a maximum of 0.5 μs/point (2 MHertz). A maximum of sixteen-thousand . data points can be acquired during a test with an accuracy of 12 bits in preselected ranges of ±100 mV to ±40 mV. The data from individual tests are stored on a floppy disk on the oscilloscope disk drive and are later transferred to a microcomputer through an RS-232 serial port; the necessary data transfer software was written [ Program 1, Appendix B ] to link the oscilloscope and the computer. Raw data, in the form of Volts vs. time, is stored on the computer's disks for subsequent data

reduction.

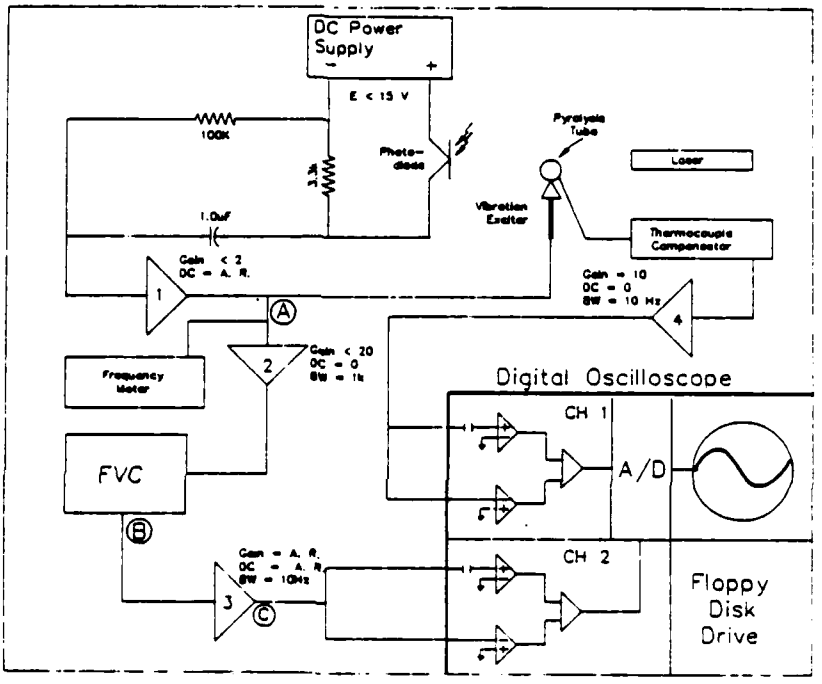


Fig. 3-6 Electronic Block Diagram-Schematic - VTGA.

## 3.3 Calibration

### 3.3.1 Mass Calibration

Prior to each calibration of the mass measurement system, the positions of the vibration exciter and the photodiode are mechanically adjusted to produce maximum signal amplitude at location A in Fig. 3-6. The DC power

supply is adjusted such that the amplitude of oscillation of the tube is approximately 1 mm. The input and output DC-offsets of amplifier #1, which has previously been zeroed, are adjusted to give maximum signal at location A with a zero DC offset. The emf to the loop is again adjusted to return the amplitude of the pyrolysis tube to 1 mm. The peak-to-peak voltage of the sinusoidal wave at circuit location A is normally about 0.5 Volts and has a frequency less than 300 Hertz depending upon the geometry of the pyrolysis tube. The purpose of amplifier #2 in the data line is to boost the signal strength sufficiently to drive the Frequency-to-Voltage (FVC) converter. This amplifier is nominally set to: DC offset = 0; gain = 20; and bandpass < 1000 Hertz. The signal from this amplifier is fed to the FVC whose zero has been appropriately adjusted. This DC signal is sent to amplifier #3 whose purpose is to increase the sensitivity of the output to frequency changes. This amplifier is set to: DC offset = A.R.; variable gain ≈ 10; and a bandwidth of 10 Hertz to "kill" any 60 cycle noise. Since the frequencies of interest are outside of the optimum performance range of the FVC, substantial AC noise corresponding to the signal frequency leaks through. This is removed by splitting the signal and using the differential input capability of the digital oscilloscope. Due to the crude electronics in the data line, the differential input is critical to the success of the measurement.

The net effect of this circuitry is to produce positive DC level change at the scope for a corresponding increase in the mechanical frequency of the pyrolysis tube; the polarity of this change can be reversed by reversing the polarity of the coupling at the scope. Therefore, as material pyrolyzes from the end of vibrating tube, the frequency of the tube will increase and produce an increase in the DC level at the scope, Fig. 2-2

The mass calibration is performed quasi-dynamically. This is done by applying known masses to the end of the cantilevered tubes, supplying DC power to the mass feedback-loop, and recording the period of oscillation along with the amplified output of the FVC. "shrink tubing" of the kind used in the electronics industry provides convenient reference masses. Small lengths are cut and placed around the at center of the flat heating element. Heat from a hot-air-gun is applied to insure good adhesion of this 0.5 mm PVC tubing. Care is taken to avoid excessive heating which would inhibit later removal. Power is supplied to the mass measurement system and the period of oscillation is noted along with the FVC output. The applied mass is carefully removed and weighed on a micro-balance to the nearest hundredth of a milligram. The required calibration curve is generated by repeating this procedure for applied loadings ranging from zero to 2.5 mg.

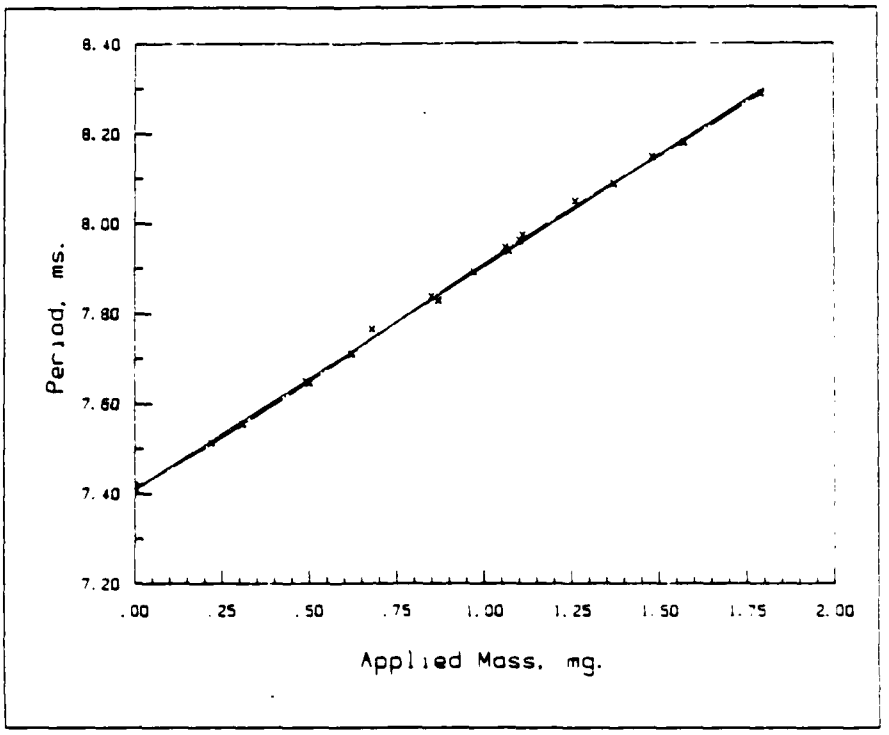


**Fig 3-7a. Period of Oscillation vs. Applied Mass.**

Representative calibration curves are given in Figs. 3-7a and 3-7b. A straight line, and for comparison a fifth order polynomial have been fit to this data. For all intents and purposes the calibration is linear. With properly designed electronics it could be made exactly linear. This is an important realization. The implication is that no calibration is necessary. Since we are not interested in the absolute mass, but only the relative change - $\alpha$, the fraction decomposed.

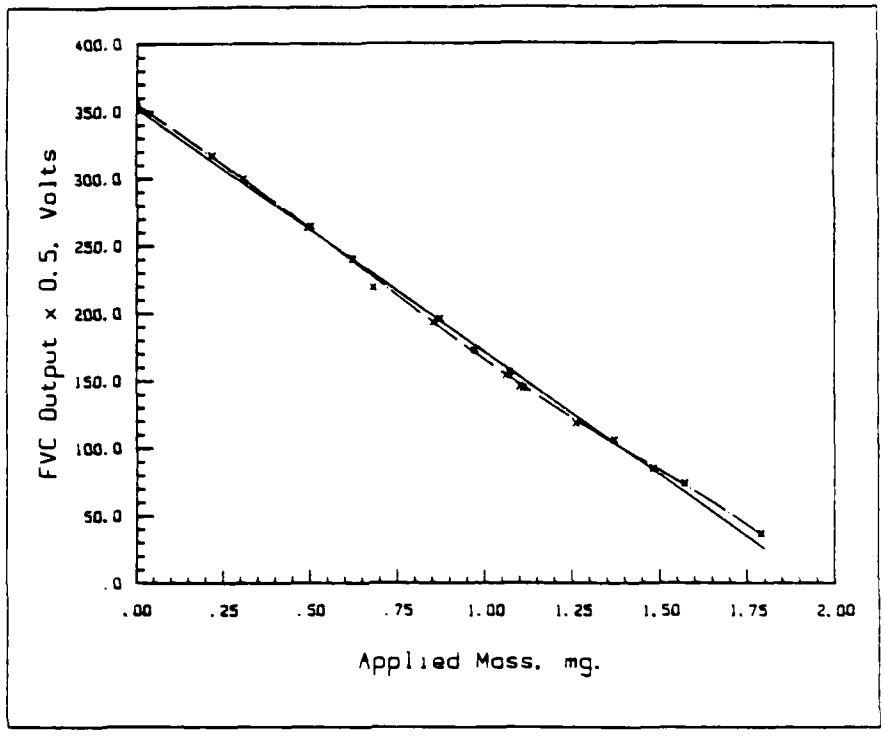


**Fig. 3-7b. Amplified FVC Output vs. Mass.**

Therefore, the change in period is directly proportional to the change in mass. This simplifies the measurements considerably. If this were not the case, it would be necessary to generate calibration curves for each new tube mounted, as well as curves for various length tubes.

### 3.3.2 Temperature Calibration

The pyrolysis tube tip contains a type-E thermocouple which has been fashioned according to the procedure outlined in Appendix A. This type of thermocouple was selected due to its large Seebeck coefficient and also because the type-E

materials are ferromagnetic alloys. The output is referenced to a battery powered electronic Type-E "ice-point" or compensator. This provides an output from which temperatures can be interpolated directly from the Type-E thermocouple tables. Interpolation is facilitated through the use of a ninth degree polynomial [48,49] which can accurately interpolate the table to within 0.5 °C. The output is in turn sent to amplifier #4, Fig. 3-4, which has been previously zeroed and configured: DC offset = 0; gain = 10; and bandwidth = 10 Hertz which strips any AC noise. The thermocouple is checked using the linear-furnace which contains an independent type-K thermocouple. This procedure is carried out at several temperatures bracketing the range of interest. This is done mainly to check for shorting of the thermocouple leads. Temperatures are compared at several points spanning the range of interest.

# CHAPTER IV

# EXPERIMENTAL METHODS AND PROCEDURES

## 4.1 Low Heating Rate Measurements

A series of pyrolysis measurements were carried out on HTPB and PBAN - polymers which are commonly used as binders in solid propellants. These materials were evaluated on both the TGA and VTGA at low heating rates; this was done, not so much to determine low rate kinetic constants, which may be found in the literature, but mainly to compare the performance of the two techniques. Due to the lack of detailed information on the physical/chemical nature of the polymer samples, it becomes necessary to perform both of these tests on identical samples in order to make a reasonable comparison of the two methods.

### 4.1.1 Thermogavimetric Analyses

All thermogravimetric analyses were performed on a Perkin-Elmer TGA-2 analyzer equipped with a system 7/4 controller. A diagram of the experimental layout is shown in Fig. 4-1. The main benefit derived from using the System 7/4 controller is that it permits an automatic temperature calibration under the direction of an internal microprocessor. The controller also allows the operator run samples

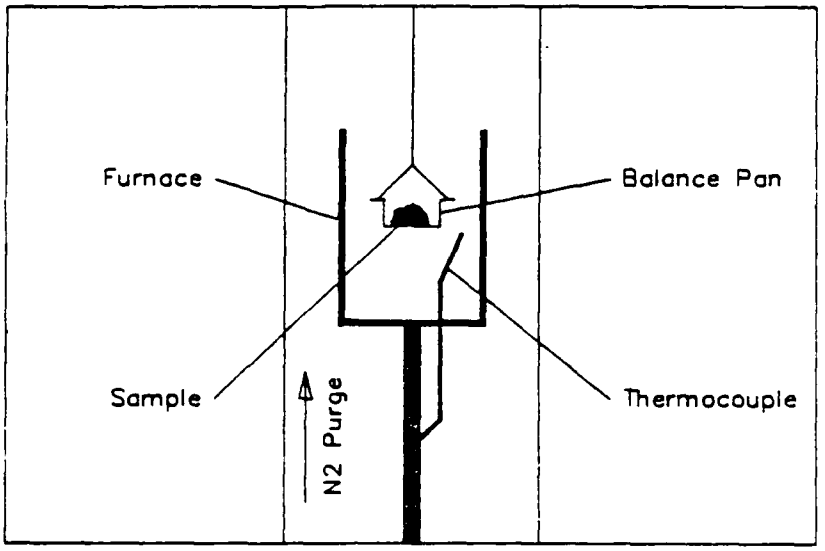


Fig. 4-1 Thermogravimetric Analyzer.

using linear heating programs at rates from 0 to 3.3 °C/s. During automatic calibration, the program temperature and the "apparent temperature" (the measured furnace temperature) are constrained to agree precisely at three predefined temperatures ( 300 °C, 450 °C and 600 °C were used in this work. ) This "apparent temperature" is really the temperature somewhere in the furnace and is not necessarily identical to the temperature in the sample pan. The temperatures in the sample pan were determined using Curie point standards. Small samples of ferromagnetic alloys were placed in the sample pan, the apparatus sealed, and operated under a

Nitrogen purge. A magnet was mounted slightly below furnace/sample pan; the magnetic force on the sample produces an apparent weight increase in the sample. When the furnace temperature approaches the Curie points of the materials in the pan, an apparent weight loss occurs, since at their respective Curie temperatures the materials become paramagnetic. Fig. 4-2 shows the result of this procedure.

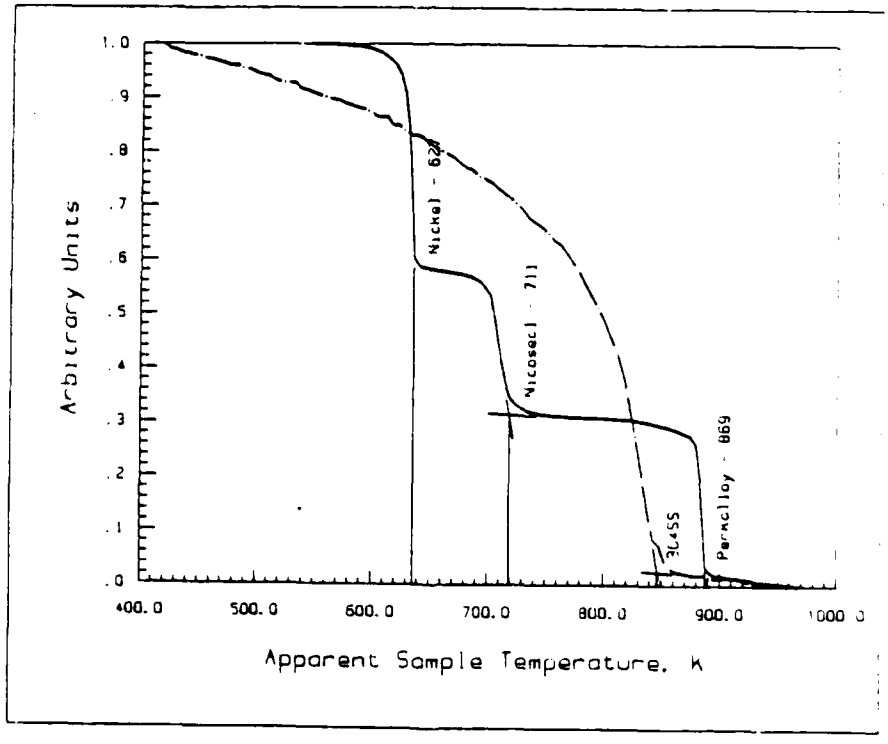


**Fig. 4-2. Curie-Point Temperature Calibration Curves**

The curve for 304 Stainless Steel, the material in the tips of the VTGA tubes, is also shown, and has a Curie tempera-

ture of 827 °K. This experiment should be repeated for each heating rate of interest, since the discrepancy between the apparent temperature and the true sample temperature becomes greater at higher heating rate. The temperatures in the TGA plots of Chapter V reflect corrections made by this procedure.

The maximum heating rate obtainable with this unit is 3.33 °C/s, but, to guarantee thermal equilibration between the sample, the sample pan, and the furnace, it is best to use heating rates on the order of 0.05 °C/s in practice.

The microbalance was calibrated, using weights of known mass, prior to each set of tests. A digital oscilloscope was used to acquire both mass and temperature data, rather than the usual strip-chart recorder. The mass data-line was amplified one-hundred times to permit good sensitivity for samples sizes of less than one milligram. Acquired data is stored on a floppy disk and is later transferred to microcomputer for analysis.

Two separate TGA analyses were performed on each of the polymers. These differed mainly in the sample preparation. In the first set, sample were cut from the solid polymer; these were "conditioned" in the TGA at 110 °C for several minutes to remove any moisture. Sample sizes were about 1.0 mg. The samples were subjected to a programmed linear temperature rise as is typical in TGA analyses. These results can be compared directly with those found in the

literature. Mindful of the somewhat different sample geometry and environment found in the VTGA apparatus, a second set of tests were performed to facilitate comparison of TGA data with VTGA data. In the VTGA tests, samples dissolved in a solvent, are "painted" on the small pre-oxidized metal strip at the end of the quartz tube; this procedure results in very thin samples. In a similar fashion, samples in the second set of TGA tests, were dissolved in the identical solvent, and coated on the same type of pre-oxidized metal strip. The strip plus the sample were then placed in the TGA pan. The metal strip was included to keep any catalytic effects due to the metal constant. What could not be nullified was the different convective environments to which samples were subjected in the two methods.

The polymeric samples were obtained commercially, the source and the details of which may be found in Appendix A. All test were conducted in a nitrogen atmosphere, and sufficient time was allow for the sample chamber to purge of entrapped air prior to commencing the test.

### 4.1.2 VTGA Analyses

These tests were performed in the apparatus described in Chapter III. Samples dissolved in appropriate solvents are "painted" on pre-oxidized metal strip. Care is taken to avoid any uneven coatings and to insure sample weight is identical from run-to-run. To determine sample weight, power is applied to the feedback loop, and the period

measured. Run-to-run sample weight is judged to be identical, if after allowing sufficient time for solvent evaporation, the period of oscillation is identical to the previous test. By comparing the periods of oscillation of the "loaded" and "unloaded" quartz tubes with calibration curves, like the one in Fig. 3-7a, estimates of initial sample weights can be made. Sample weights for most VTGA test were under 0.5 mg; the sample thickness is calculated estimated to be approximately 40 μm. This calculation was based upon the measured tip area, which is given in Table 3-1. The linear furnace, which has been preheated to 110 °C, is positioned around the sample and the sample is conditioned until all solvent is removed. This is indicated when the DC-level in the mass data-line (test point C in Fig. 3-6) becomes constant. The furnace mount is equipped with a graduated scale to permit identical positioning of the furnace from test-to-test. The system is "tuned" to achieve the optimum sinusoidal waveform at test point A by adjusting the DC-offset and gain controls on the feedback loop amplifier, amplifier #4. A plexiglass chamber is placed over the apparatus, and the entire enclosure is purged with nitrogen. The nitrogen purge gas is manually cut-off just prior to the onset of sample decomposition to prevent the gas flow from interfering with the measurements. As in the TGA test, the furnace is under linear programmed control by the TGA System 7/4 controller.

At the conclusion of the test the temperature is raised sufficiently, to remove any sample residue which remains, although it is sometimes difficult to remove carbonaceous deposits. This procedure is repeated for subsequent analyses; the same quartz tube and metal sample supports are reused in these tests. These tubes are surprisingly durable and can be reused on numerous samples; with care, thermocouple junction failure normally occurs before mechanical failure of the tube.

## 4.2 High-Heating-Rate Measurements

The high heating rate measurements used the Fischer Curie point pyrolyzer to rapidly heat the metal support on which the samples were coated. Procedures in these measurements were identical to those in the low rate VTGA tests except with regard to sample heating and the time required for solvent removal from the sample. Very little control over the heating rate was possible with the Curie point pyrolyzer used in this work. This is the principal drawback to the present instrument design. The heating rate is a strong function of the position of the induction coil with respect to the sample and it is not possible to precisely predict the actual value a priori. The coil used in this work was larger than the one supplied by the instrument manufacturer; the ID of the redesigned coil was 0.50 inches. This had more room for tube vibration. Heating rates

obtained with this device varied form about 30 °C/s to about 60 °C/s. Figure 4-2 contains an oscillograph showing both the mass and temperature data.

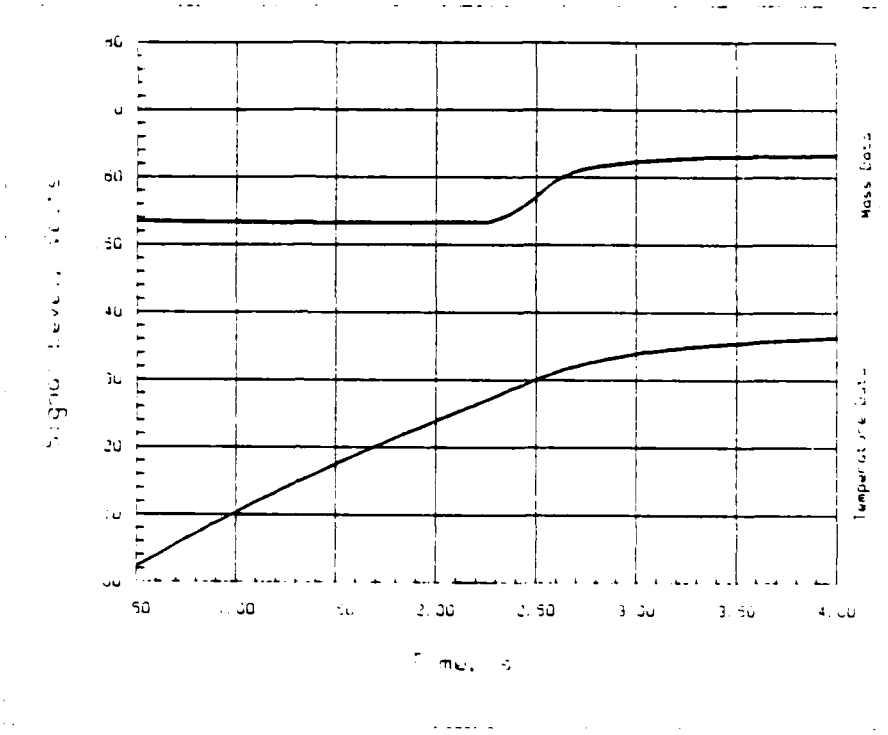

Fig. 4-3 High-Heating-Rate VTGA Output.

As can be seen, sample decomposition takes place near the Curie temperature of the 304SS; the sample was positioned by trial-and-error with respect to the induction coil in an attempt to avoid decomposition in the non-linear region near the Curie temperature. This was a laborious process.

Unfortunately, the Curie point pyrolyzers which are

commercially available have been designed to be used in connection with Gas Chromatography; they offer no way to "throttle" the heating rate, and pyrolysis time is limited to about 9 seconds. In addition, the only tube material readily available for construction of the "heating element" was 304SS steel, thus limiting the ultimate temperature which could be attained. These constraints all combined to seriously limit control over heating rates. In future work these constraints could be designed out of the system.

## 4.3 Data Analysis Procedures

4.3.1 TGA Data Analysis. Mass and temperature data acquired on the Oscilloscope is transferred to the microcomputer using Program 1, Appendix B; it is stored on disk in the form of Voltage vs. time in two separate files. This data is consolidated and scaled using Program 2. Program 4 reduces this scaled data by the algorithm outlined in Chapter II. Arrhenius parameters are extracted from this data by application of Program 5.

4.3.2 VTGA Data Analysis The Data analysis procedures used here are identical to those used in analyzing the TGA experiments, with the exception that raw data files are consolidated using Program 3, Appendix B, in place of Program 2, due to the different data scaling required in the TGA and VTGA data. A thermogram from such an analysis of HTPB is shown in Fig. 4-4. This figure contains four

separate decomposition curves run under identical conditions; precision is seen to be excellent.

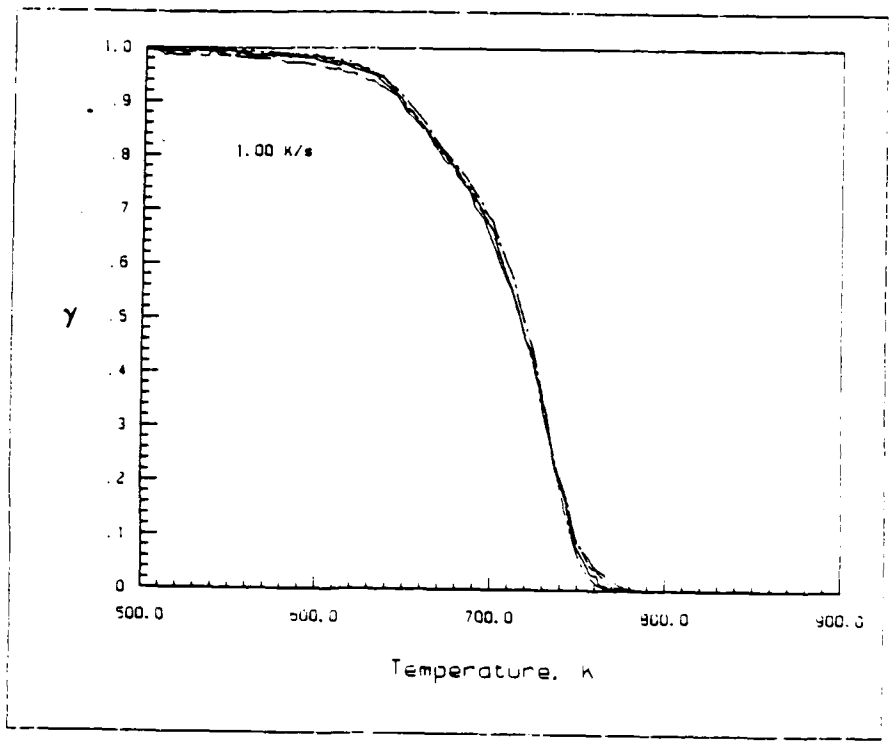


Fig. 4-4 Low-Heating-Rate VTGA Thermogram of HTPB

# CHAPTER V

# RESULTS AND DISCUSSION

## 5.1 Baseline Data

In order to obtain baseline data and to test the computational algorithms, the decomposition kinetics of PBAN and HTPB were measured in the TGA and computed. Thermograms for PBAN and HTPB are shown in Figures 5-1a and 5-1b, respectively, and the calculated kinetic parameters are given in Tables 5-1a and 5-1b. Global Arrhenius parameters for these polymers have been computed for $0.10 \leq \alpha \leq 0.30$; Arrhenius parameters have also been computed for $0.10 \leq \alpha \leq 0.90$ to facilitate comparison of the data with the literature. The thermograms shown in these figures are for heating rates varying from 0.05 °K/s to 3.3 °K/s (3 °K/min. to 200 °K/min.) as is indicated in the upper left-hand corner of each figure.

Several observations can be made concerning this data. Firstly, as usual, the decomposition shifts to higher temperatures as the heating rates are increased. (See Eqn. 2-4). Secondly, this shift is proportionally less at higher heating rates. For example, the difference in heating rate between curves a and b in both of these figures is 0.033

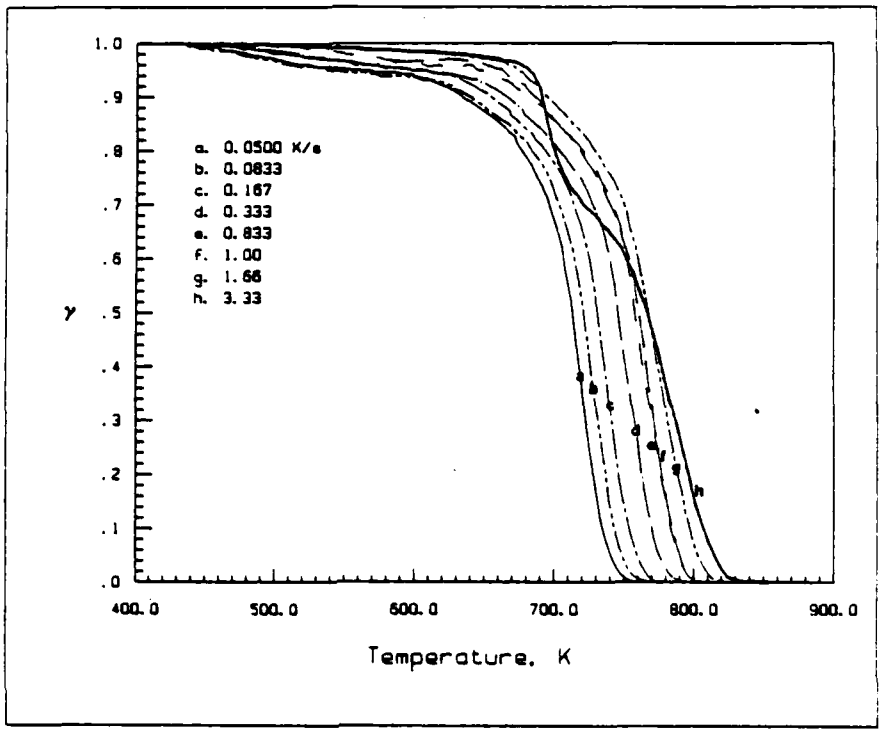


Fig. 5-1a. TGA Thermograms of PBAN - Bulk Sample.

°C/s, whereas, the difference in heating rate between curves g and h is around 1.67 °C/s. - over fifty times greater. Yet the shift in temperature is about the same. Thirdly, precision of the data appears to be quite good, and corresponding kinetic values in Tables 5-1a and 5-1b are in reasonable agreement with values from the literature, Table 5-1c, making some allowance for the expected polymer-to-polymer variability. Lastly, at heating rates of 3.33 °C/s, the bold lines in Figs. 5-1a and 5-1b, both PBAN and HTPB exhibit anomalies which could be interpreted as evidence of two

Table 5-1a. TGA Kinetic Results for PBAN - Bulk Sample

Ea : cal/mole
A : sec-1
β : °K/s
T : °K

| Item | ID | Material | Ea | A | n | β | $\alpha_o - \alpha_f$ | T Range | Analysis | Source |
|---|---|---|---|---|---|---|---|---|---|---|
| | | | | | | | 0.1≤α≤0.3 | | | |
| 1 | 240186-10 | PBAN | 11875 | 1.175E+0 | 0 | 0.0500 | 0.083-0.28 | 623-694 | CR | TGA |
| 2 | 240186-09 | PBAN | 11269 | 1.096E+0 | 0 | 0.0833 | 0.081-0.28 | 626-701 | CR | TGA |
| 3 | 240186-08 | PBAN | 13556 | 1.141E+1 | 0 | 0.1667 | 0.082-0.28 | 643-711 | CR | TGA |
| 4 | 240186-11 | PBAN | 13932 | 2.547E+1 | 0 | 0.3333 | 0.081-0.30 | 653-723 | CR | TGA |
| 5 | 240186-03 | PBAN | 17499 | 7.268E+1 | 0 | 0.8333 | 0.091-0.29 | 682-738 | CR | TGA |
| 6 | 240186-02 | PBAN | 15235 | 1.568E+2 | 0 | 1.0000 | 0.085-0.29 | 673-739 | CR | TGA |
| 7 | 240186-05 | PBAN | 17719 | 1.392E+3 | 0 | 1.6667 | 0.084-0.29 | 689-749 | CR | TGA |
| 8 | 240186-07 | PBAN | - | - | - | 3.3333 | - | | - | - |
| | | | | | | | 0.1≤α≤0.3 | | | |
| 9 | 240186-10 | PBAN | 16545 | 5.629E+1 | 0 | 0.0500 | 0.083-0.88 | 623-733 | CR | TGA |
| 10 | 240186-09 | PBAN | 15969 | 5.269E+1 | 0 | 0.0833 | 0.081-0.89 | 626-743 | CR | TGA |
| 11 | 240186-08 | PBAN | 17715 | 3.231E+2 | 0 | 0.1667 | 0.082-0.86 | 643-750 | CR | TGA |
| 12 | 240186-11 | PBAN | 17309 | 2.547E+1 | 0 | 0.3333 | 0.081-0.86 | 653-766 | CR | TGA |
| 13 | 240186-03 | PBAN | 20174 | 5.507E+3 | 0 | 0.8333 | 0.091-0.86 | 682-781 | CR | TGA |
| 14 | 240186-02 | PBAN | 19473 | 4.041E+3 | 0 | 1.0000 | 0.085-0.86 | 673-789 | CR | TGA |
| 15 | 240186-05 | PBAN | 21225 | 1.926E+4 | 0 | 1.6667 | 0.084-0.29 | 689-794 | CR | TGA |
| 16 | 240186-07 | PBAN | - | - | - | 3.3333 | - | | - | - |

competing chemical processes, which only become distinct at the higher heating rates. This would perhaps be more apparent if the derivative of these curve were shown.

Closer scrutiny suggests that the anomalies in the higher heating rate curves are in reality physical processes related to the geometry of the sample - most probably due to entrapment and escape of decomposition products or low

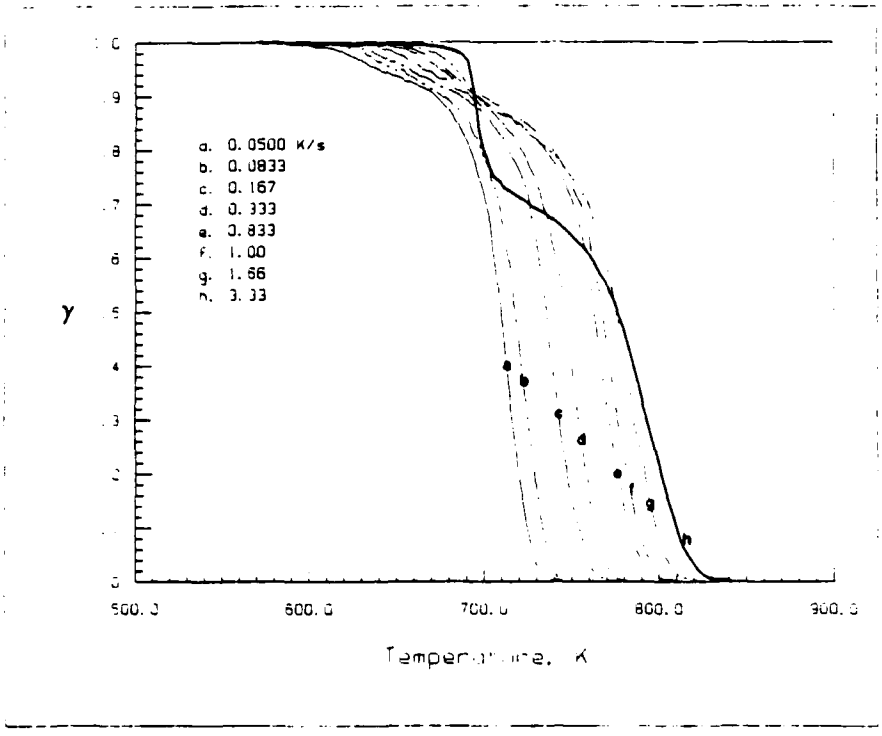


**Fig. 5-1b. TGA Thermograms of HTPB - Bulk Sample.**

molecular weight material in the interior of the sample. This conclusion was arrived at by repeating these test with samples in the form of thin films.

Figures 5-2a and 5-2b contain this data. The samples were deposited on small strips of pre-oxidized stainless steel in similar fashion to the VTGA sample preparation described in Chapter IV. This procedure also facilitates the comparison of the TGA data with the VTGA data. The corresponding kinetic data for these curves may be found in Tables 5-2a and 5-2b. It can be seen that no such anomalies

Table 5-1b. TGA Kinetic Results for HTPB - Bulk Sample

Ea : cal/mole
A : sec-1
β : °K-sec-1
T : °K

| Item | ID | Material | Ea | A | n | β | $\alpha_o - \alpha_f$ | T Range | Analysis | Source |
|---|---|---|---|---|---|---|---|---|---|---|
| | | | | | | | 0.1≤α≤0.3 | | | |
| 1 | 290186-09 | HTPB | 32188 | 5.534E+6 | 0 | 0.0500 | 0.10 -0.28 | 672-700 | CR | TGA |
| 2 | 290186-08 | HTPB | 29657 | 1.093E+6 | 0 | 0.0833 | 0.10 -0.30 | 675-708 | CR | TGA |
| 3 | 290186-06 | HTPB | 23729 | 1.649E+4 | 0 | 0.1667 | 0.10 -0.28 | 687-725 | CR | TGA |
| 4 | 290186-01 | HTPB | 21938 | 7.432E+3 | 0 | 0.3333 | 0.10 -0.28 | 692-732 | CR | TGA |
| 5 | 290186-02 | HTPB | 16102 | 1.952E+2 | 0 | 0.8333 | 0.10 -0.29 | 696-750 | CR | TGA |
| 6 | 290186-03 | HTPB | 16328 | 2.571E+2 | 0 | 1.0000 | 0.10 -0.29 | 698-753 | CR | TGA |
| 7 | 290186-04 | HTPB | 13624 | 4.891E+1 | 0 | 1.6667 | 0.10 -0.30 | 697-759 | CR | TGA |
| 8 | 290186-05 | HTPB | - | - | - | 3.3333 | - | - | - | - |
| | | | | | | | 0.1≤α≤0.3 | | | |
| 9 | 290186-09 | HTPB | 40770 | 3.794E+9 | 0 | 0.0500 | 0.10 -0.87 | 672-723 | CR | TGA |
| 10 | 290186-08 | HTPB | 37584 | 4.437E+8 | 0 | 0.0833 | 0.10 -0.87 | 675-732 | CR | TGA |
| 11 | 290186-06 | HTPB | 33732 | 2.908E+7 | 0 | 0.1667 | 0.10 -0.88 | 687-752 | CR | TGA |
| 12 | 290186-01 | HTPB | 30354 | 3.889E+6 | 0 | 0.3333 | 0.10 -0.89 | 692-763 | CR | TGA |
| 13 | 290186-02 | HTPB | 24851 | 1.289E+5 | 0 | 0.8333 | 0.10 -0.89 | 696-782 | CR | TGA |
| 14 | 290186-03 | HTPB | 24749 | 1.297E+3 | 0 | 1.0000 | 0.10 -0.90 | 698-788 | CR | TGA |
| 15 | 290186-04 | HTPB | 19845 | 6.273E+3 | 0 | 1.6667 | 0.10 -0.87 | 697-796 | CR | TGA |
| 16 | 290186-05 | HTPB | - | - | - | 3.3333 | - | | - | - |

exist in the thin film data! This suggests that this phenomenon is a function of sample geometry; most probably, at higher heating rates, trapped vapors in the interior of the sample can not diffuse to the surface with sufficient rapidity. Gases apparently escape all at once when the pressure within the sample rises to a sufficient level. The rate of decomposition becomes diffusion limited, at least in

Table 5-1c. Literature Values of Kinetic Constants

Ea : cal/mole
A : sec-1
β : °k-sec-1
T : °K

| Item | ID | Material | Ea | A | n | β | αo - αf | T Range | Analysis | Source |
|---|---|---|---|---|---|---|---|---|---|---|
| 1 | - | HTPB | 23228 | 3.85E+3 | 0 | 0.0167 | 0 - 1 | - | CR | TGA[50,Tbl 5] |
| 2 | - | HTPB | 26775 | 8.22E+4 | 0 | 0.0333 | 0 - 1 | - | CR | TGA[50,Tbl 5] |
| 3 | - | HTPB | 26132 | 9.11E+4 | 0 | 0.0833 | 0 - 1 | - | CR | TGA[50,Tbl 5] |
| 4 | - | HTPB | 28917 | 1.03E+6 | 0 | 0.1667 | 0 - 1 | - | CR | TGA[50,Tbl 5] |
| 5 | - | HTPB | 25632 | 1.39E+5 | 0 | 0.3333 | 0 - 1 | - | CR | TGA[50,Tbl 5] |
| 6 | - | HTPB | 22419 | 2.54E+4 | 0 | 0.8333 | 0 - 1 | - | CR | TGA[50,Tbl 5] |
| 7 | - | HTPB | 19516 | 7.44E+3 | 0 | 1.6667 | 0 - 1 | - | CR | TGA[50,Tbl 5] |
| 8 | - | CTPB | 28000 | 3.4 E+5 | | | 0 - 1 | - | | DSC[52,Tbl 1] |

the early stages. Thus the TGA is unable to adequately represent the thermal decomposition kinetics of these polymers even at rates as low as 3.33 °C/s when a bulk sample is employed.

It can also be seen that the decomposition temperatures of the samples in these figures and those in figures 5-1a and b are virtually identical. It should be mentioned in passing that it is doubtful if the temperature of the sample and the furnace are in equilibrium at heating rates much above 0.5 °C/s. This is why, in the most accurate work, TGA analyses are normally run at heating rates below this value.

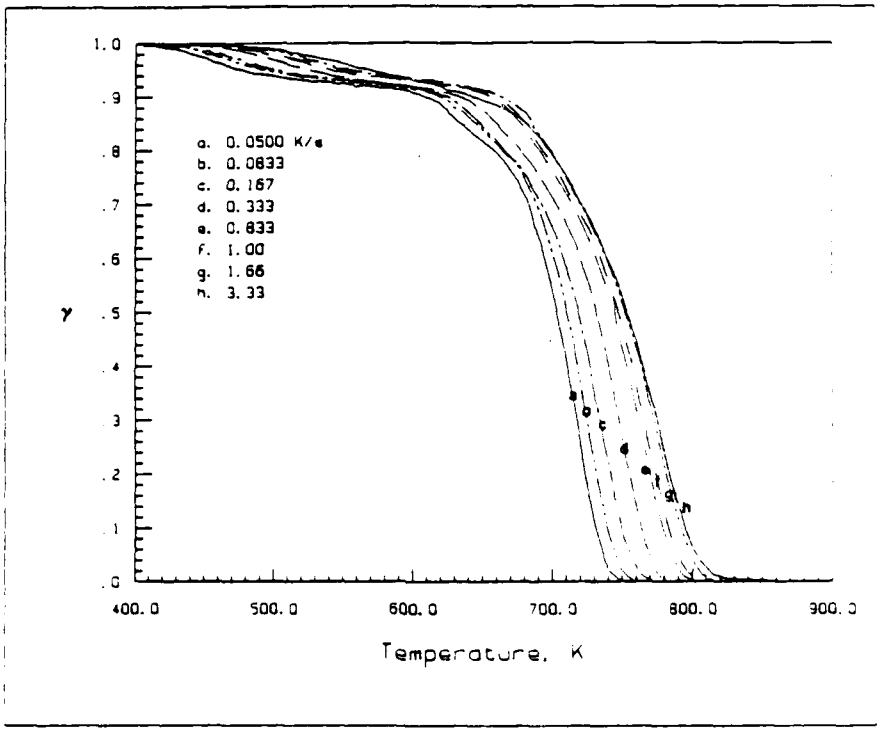


Fig. 5-2a. TGA Thermograms PBAN - Thin Films.

Table 5-2a. TGA Kinetic Results for PBAN - Thin Film.

Ea : cal/mole
A : sec-1
β : °K-sec-1
T : °K

| Item | ID | Material | Ea | A | n | β | $\alpha_o - \alpha_f$ | T Range | Analysis | Source |
|---|---|---|---|---|---|---|---|---|---|---|
| | | | | | | | 0.1≤α≤0.3 | | | |
| 1 | 160186-10 | PBAN | 9087 | 1.613E-1 | 0 | 0.0500 | 0.10 -0.29 | 608-682 | CR | TGA |
| 2 | 160186-09 | PBAN | 10026 | 5.242E-1 | 0 | 0.0833 | 0.10 -0.29 | 619-686 | CR | TGA |
| 3 | 160186-08 | PBAN | 11062 | 2.385E+0 | 0 | 0.1667 | 0.10 -0.30 | 622-692 | CR | TGA |
| 4 | 160186-11 | PBAN | 11535 | 5.927E+0 | 0 | 0.3333 | 0.10 -0.29 | 632-700 | CR | TGA |
| 5 | 160186-03 | PBAN | 15412 | 2.488E+2 | 0 | 0.8333 | 0.10 -0.29 | 657-711 | CR | TGA |
| 6 | 160186-02 | PBAN | 15911 | 4.159E+2 | 0 | 1.0000 | 0.10 -0.29 | 660-714 | CR | TGA |
| 7 | 160186-01 | PBAN | 15709 | 3.522E+2 | 0 | 1.0000 | 0.10 -0.29 | 661-715 | CR | TGA |
| 8 | 160186-05 | PBAN | 16397 | 9.219E+2 | 0 | 1.6667 | 0.10 -0.29 | 662-717 | CR | TGA |
| 9 | 160186-07 | PBAN | 17009 | 3.522E+2 | 0 | 3.3333 | 0.10 -0.29 | 642-718 | - | - |
| | | | | | | | 0.1≤α≤0.9 | | | |
| 10 | 160186-10 | PBAN | 13060 | 4.802E+0 | 0 | 0.0500 | 0.10 -0.90 | 608-730 | CR | TGA |
| 11 | 160186-09 | PBAN | 13957 | 1.429E+1 | 0 | 0.0833 | 0.10 -0.90 | 619-739 | CR | TGA |
| 12 | 160186-08 | PBAN | 13326 | 1.593E+1 | 0 | 0.1667 | 0.10 -0.88 | 622-748 | CR | TGA |
| 13 | 160186-11 | PBAN | 13552 | 3.132E+1 | 0 | 0.3333 | 0.10 -0.86 | 632-763 | CR | TGA |
| 14 | 160186-03 | PBAN | 15359 | 2.419E+2 | 0 | 0.8333 | 0.10 -0.86 | 657-775 | CR | TGA |
| 15 | 160186-02 | PBAN | 15462 | 2.972E+2 | 0 | 1.0000 | 0.10 -0.89 | 660-782 | CR | TGA |
| 16 | 160186-01 | PBAN | 15674 | 3.481E+2 | 0 | 1.0000 | 0.10 -0.86 | 661-778 | CR | TGA |
| 17 | 160186-05 | PBAN | 15419 | 4.392E+2 | 0 | 1.6667 | 0.10 -0.87 | 662-788 | CR | TGA |
| 18 | 160186-07 | PBAN | 16132 | 1.178E+2 | 0 | 3.3333 | 0.10 -0.87 | 642-792 | - | - |

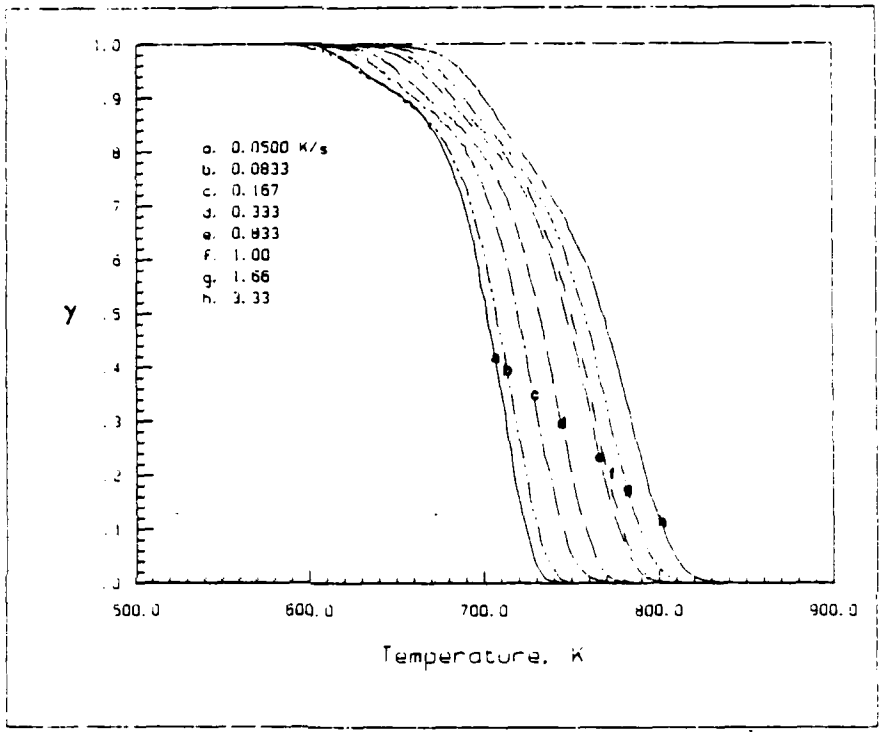


Fig. 5-2b. TGA Thermograms HTPB - Thin Films.

Table 5-2b. TGA Kinetic Results for HTPB - Thin Film.

Ea : cal/mole
A : sec-1
β : °K-sec-1
T : °K

| Item | ID | Material | Ea | A | n | β | $\alpha_o - \alpha_f$ | T Range | Analysis | Source |
|---|---|---|---|---|---|---|---|---|---|---|
| | | | | | | | 0.1≤α≤0.3 | | | |
| 1 | 310186-02 | HTPB | 25418 | 4.919E+4 | 0 | 0.0500 | 0.10 -0.29 | 654-688 | CR | TGA |
| 2 | 310186-03 | HTPB | 20902 | 2.257E+3 | 0 | 0.0833 | 0.11 -0.29 | 654-692 | CR | TGA |
| 3 | 310186-01 | HTPB | 19474 | 1.1937+3 | 0 | 0.1667 | 0.10 -0.29 | 661-702 | CR | TGA |
| 4 | 310186-04 | HTPB | 18313 | 8.073E+2 | 0 | 0.3333 | 0.10 -0.29 | 669-714 | CR | TGA |
| 5 | 310186-05 | HTPB | 18196 | 1.511E+3 | 0 | 0.8333 | 0.10 -0.29 | 679-726 | CR | TGA |
| 6 | 310186-07 | HTPB | 18627 | 2.356E+3 | 0 | 1.0000 | 0.10 -0.29 | 683-728 | CR | TGA |
| 7 | 310186-09 | HTPB | 19773 | 8.408E+3 | 0 | 1.6667 | 0.10 -0.30 | 689-734 | CR | TGA |
| 8 | 310186-10 | HTPB | 23117 | 1.643E+5 | 0 | 3.3333 | 0.10 -0.30 | 700-741 | CR | TGA |
| | | | | | | | 0.1≤α≤0.3 | | | |
| 9 | 310186-02 | HTPB | 29385 | 1.116E+6 | 0 | 0.0500 | 0.10 -0.88 | 654-722 | CR | TGA |
| 10 | 310186-03 | HTPB | 26164 | 1.437E+5 | 0 | 0.0833 | 0.11 -0.90 | 654-731 | CR | TGA |
| 11 | 310186-01 | HTPB | 24361 | 5.452E+4 | 0 | 0.1667 | 0.10 -0.90 | 661-744 | CR | TGA |
| 12 | 310186-04 | HTPB | 22820 | 2.634E+4 | 0 | 0.3333 | 0.10 -0.89 | 669-757 | CR | TGA |
| 13 | 310186-05 | HTPB | 20715 | 1.037E+4 | 0 | 0.8333 | 0.10 -0.90 | 679-777 | CR | TGA |
| 14 | 310186-07 | HTPB | 21125 | 1.573E+4 | 0 | 1.0000 | 0.10 -0.88 | 683-778 | CR | TGA |
| 15 | 310186-09 | HTPB | 20428 | 1.385E+4 | 0 | 1.6667 | 0.10 -0.89 | 689-787 | CR | TGA |
| 16 | 310186-10 | HTPB | 20051 | 1.725E+4 | - | 3.3333 | 0.10 -0.90 | 700-802 | CR | TGA |

## 5.2 Low-Heating-Rate VTGA Data

In order to demonstrate that the VTGA was a functional thermogravimetric analyzer, a series of thermal decomposi-tions experiments were performed on PBAN and HTPB at low heating rates; in this work every effort was expended to insure that conditions matched those found in the previous thin-film TGA experiments.

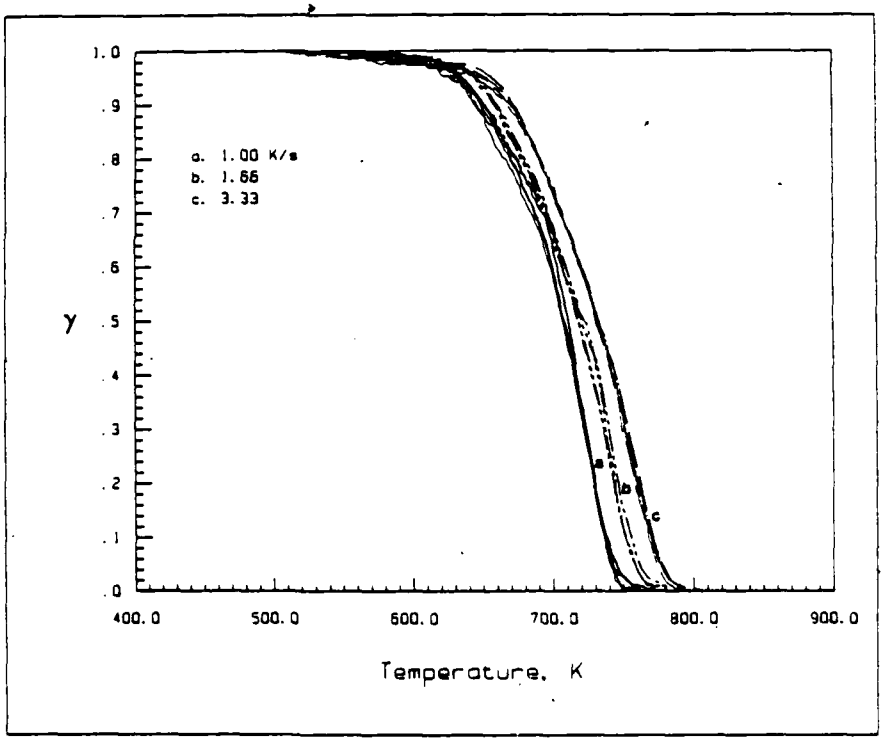


**Fig. 5-3a. VTGA Thermograms of PBAN**

It must be recognized that low-heating-rate VTGA experiments are similar to, but not identical with, the thin-film TGA tests. Samples in the VTGA are subjected to a

much different convective environment during sample pyrolysis. Data from these experiments is presented in Figs. 5-3a and 5-3b and the corresponding Arrhenius data may be found in Tables 5-3a and 5-3b.

In this low-heating-rate VTGA work, four decomposition experiments were run at each of three heating rates. The curves have the same overall appearance as those found in Figures 5-2 and display the same dependence upon heating rate as found in the earlier TGA work. The precision in these VTGA curves is excellent! Note, however, that the temperature range over which the decompositions occur, at any heating rate, is about 20 °C lower than found in the corresponding TGA data. This was found to be the case in all VTGA experiments in this work. It is believed that this is the result of the different convective environments in the two experiments.

Both PBAN and HTPB polymers decompose <u>via</u> a random depolymerization mechanism, producing products which are both liquids and gases. Providing of course that the decomposition is not diffusion limited, gases formed upon decomposition immediate leave the sample, and consequently produce an immediately weight loss. However, this is not necessarily the case with liquids. Liquids formed during decomposition in the TGA can remain on the sample or in the sample pan and evaporate at some later time.

Table 5-3a. VTGA Kinetic Results for PBAN - Low Rate.

Ea : cal/mole
A : sec-1
β : °K-sec-1
T : °K

| Item | ID | Material | Ea | A | n | β | $\alpha_o - \alpha_f$ | T Range | Analysis | Source |
|---|---|---|---|---|---|---|---|---|---|---|
| | | | | | | | 0.1≤α≤ 0.3 | | | |
| 1 | 130286-01 | PBAN | 19994 | 1.714E+4 | 0 | 1.0000 | 0.10 -0.29 | 646-686 | CR | TGA |
| 2 | 130286-02 | PBAN | 20740 | 2.825E+4 | 0 | 1.0000 | 0.10 -0.30 | 650-692 | CR | TGA |
| 3 | 130286-03 | PBAN | 20928 | 3.971E+4 | 0 | 1.0000 | 0.10 -0.29 | 644-682 | CR | TGA |
| 4 | 130286-04 | PBAN | 21966 | 8.128E+4 | 0 | 1.0000 | 0.10 -0.30 | 650-687 | CR | TGA |
| 5 | 130286-05 | PBAN | 23639 | 4.035E+5 | 0 | 1.6667 | 0.10 -0.30 | 658-693 | CR | TGA |
| 6 | 130286-06 | PBAN | 23732 | 3.999E+5 | 0 | 1.6667 | 0.10 -0.29 | 662-695 | CR | TGA |
| 7 | 130286-07 | PBAN | 24410 | 7.105E+5 | 0 | 1.6667 | 0.10 -0.29 | 660-693 | CR | TGA |
| 8 | 130286-08 | PBAN | 20704 | 4.384E+4 | 0 | 1.6667 | 0.10 -0.29 | 652-691 | CR | TGA |
| 9 | 130286-09 | PBAN | 25875 | 3.106E+6 | 0 | 3.3333 | 0.10 -0.29 | 669-706 | CR | TGA |
| 10 | 130286-10 | PBAN | 26704 | 5.730E+6 | 0 | 3.3333 | 0.10 -0.30 | 674-706 | CR | TGA |
| 11 | 130286-11 | PBAN | 26424 | 4.762E+6 | 0 | 3.3333 | 0.11 -0.29 | 673-701 | CR | TGA |
| 12 | 130286-12 | PBAN | 24705 | 1.322E+6 | 0 | 3.3333 | 0.10 -0.29 | 668-701 | CR | TGA |
| | | | | | | | 0.1≤α≤0.9 | | | |
| 13 | 130286-01 | PBAN | 20239 | 2.103E+4 | 0 | 1.0000 | 0.10 -0.89 | 636-735 | CR | TGA |
| 14 | 130286-02 | PBAN | 21263 | 4.273E+4 | 0 | 1.0000 | 0.10 -0.89 | 650-735 | CR | TGA |
| 15 | 130286-03 | PBAN | 18750 | 6.967E+3 | 0 | 1.0000 | 0.10 -0.89 | 644-737 | CR | TGA |
| 16 | 130286-04 | PBAN | 20123 | 1.992E+4 | 0 | 1.0000 | 0.10 -0.89 | 650-736 | CR | TGA |
| 17 | 130286-05 | PBAN | 19353 | 1.424E+4 | 0 | 1.6667 | 0.10 -0.88 | 658-749 | CR | TGA |
| 18 | 130286-06 | PBAN | 19029 | 1.039E+4 | 0 | 1.6667 | 0.10 -0.89 | 662-755 | CR | TGA |
| 19 | 130286-07 | PBAN | 19826 | 2.000E+4 | 0 | 1.6667 | 0.10 -0.89 | 660-750 | CR | TGA |
| 20 | 130286-08 | PBAN | 17362 | 3.165E+3 | 0 | 1.6667 | 0.10 -0.88 | 669-768 | CR | TGA |
| 12 | 130286-09 | PBAN | 19240 | 1.926E+4 | 0 | 3.3333 | 0.10 -0.88 | 669-768 | CR | TGA |
| 22 | 130286-10 | PBAN | 18487 | 1.083E+4 | 0 | 3.3333 | 0.11 -0.88 | 674-769 | CR | TGA |
| 23 | 130286-11 | PBAN | 18557 | 1.168E+4 | 0 | 3.3333 | 0.11 -0.89 | 673-769 | CR | TGA |
| 24 | 130286-12 | PBAN | 19069 | 1.781E+4 | 0 | 3.3333 | 0.10 -0.87 | 666-765 | CR | TGA |

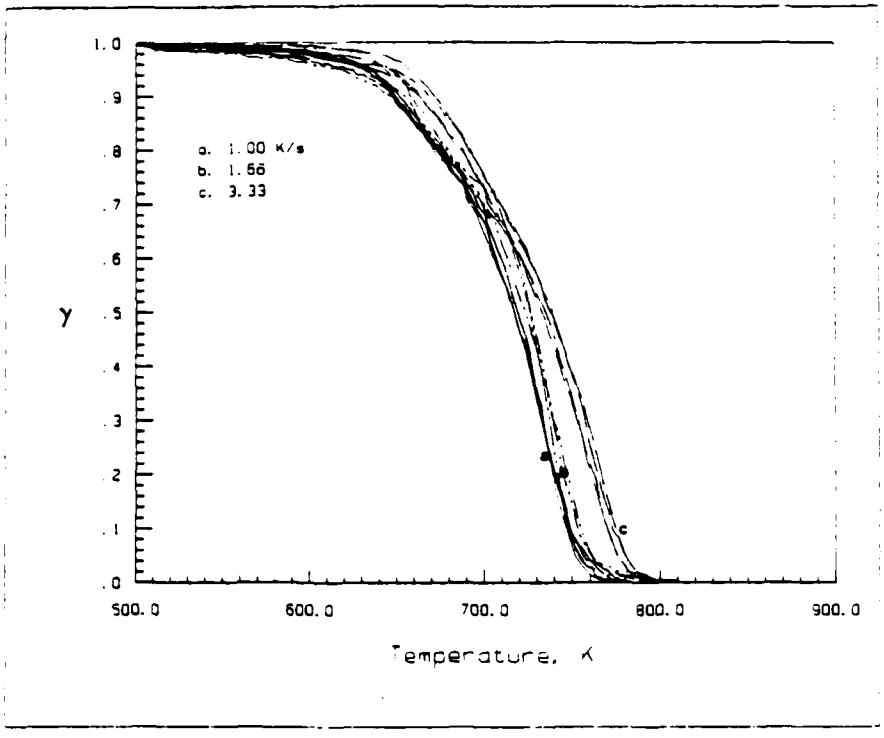


Fig. 5-3b. VTGA Thermograms of HTPB.

Table 5-3b. VTGA Kinetic Results for HTPB - Deposited on 304SS from Toluene

Ea : cal/mole
A : sec-1
β : °K-sec-1
T : °K

| Item | ID | Material | Ea | A | n | β | $\alpha_o - \alpha_f$ | T Range | Analysis | Source |
|---|---|---|---|---|---|---|---|---|---|---|
| | | | | | | | $0.1 \leq \alpha \leq 0.3$ | | | |
| 1 | 090286-13 | HTPB | 18510 | 4.887E+3 | 0 | 1.0000 | 0.10 -0.30 | 647-690 | CR | VTGA |
| 2 | 090286-14 | HTPB | 17703 | 2.560E+3 | 0 | 1.0000 | 0.11 -0.29 | 650-692 | CR | VTGA |
| 3 | 090286-15 | HTPB | 18442 | 4.342E+3 | 0 | 1.0000 | 0.10 -0.29 | 652-694 | CR | VTGA |
| 4 | 090286-16 | HTPB | 17109 | 1.651E+3 | 0 | 1.0000 | 0.11 -0.29 | 648-691 | CR | VTGA |
| 5 | 090286-01 | HTPB | 16901 | 2.487E+3 | 0 | 1.6667 | 0.10 -0.30 | 642-690 | CR | VTGA |
| 6 | 090286-02 | HTPB | 20815 | 4.822E+4 | 0 | 1.6667 | 0.10 -0.30 | 650-693 | CR | VTGA |
| 7 | 090286-03 | HTPB | 18153 | 6.405E+3 | 0 | 1.6667 | 0.10 -0.30 | 643-689 | CR | VTGA |
| 8 | 090286-04 | HTPB | 18337 | 8.919E+3 | 0 | 1.6667 | 0.10 -0.30 | 638-683 | CR | VTGA |
| 9 | 090286-05 | HTPB | 17741 | 7.340E+3 | 0 | 3.3333 | 0.10 -0.29 | 652-700 | CR | VTGA |
| 10 | 090286-06 | HTPB | 18178 | 1.032E+4 | 0 | 3.3333 | 0.11 -0.28 | 654-697 | CR | VTGA |
| 11 | 090286-07 | HTPB | 15573 | 1.445E+3 | 0 | 3.3333 | 0.10 -0.29 | 646-698 | CR | VTGA |
| 12 | 090286-08 | HTPB | 22254 | 2.263E+5 | 0 | 3.3333 | 0.10 -0.29 | 662-699 | CR | VTGA |
| | | | | | | | $0.1 \leq \alpha \leq 0.9$ | | | |
| 13 | 090286-13 | HTPB | 17922 | 3.092E+3 | 0 | 1.0000 | 0.10 -0.87 | 647-744 | CR | VTGA |
| 14 | 090286-14 | HTPB | 18025 | 3.333E+3 | 0 | 1.0000 | 0.11 -0.90 | 650-745 | CR | VTGA |
| 15 | 090286-15 | HTPB | 18371 | 4.127E+3 | 0 | 1.0000 | 0.10 -0.87 | 652-746 | CR | VTGA |
| 16 | 090286-16 | HTPB | 17198 | 1.784E+3 | 0 | 1.0000 | 0.11 -0.89 | 648-746 | CR | VTGA |
| 17 | 090286-01 | HTPB | 16271 | 1.511E+3 | 0 | 1.6667 | 0.10 -0.89 | 642-747 | CR | VTGA |
| 18 | 090286-02 | HTPB | 17507 | 3.512E+3 | 0 | 1.6667 | 0.10 -0.88 | 650-752 | CR | VTGA |
| 19 | 090286-03 | HTPB | 16060 | 1.209E+3 | 0 | 1.6667 | 0.10 -0.90 | 643-754 | CR | VTGA |
| 20 | 090286-04 | HTPB | 15883 | 1.207E+3 | 0 | 1.6667 | 0.10 -0.89 | 638-747 | CR | VTGA |
| 12 | 090286-05 | HTPB | 15020 | 8.676E+2 | 0 | 3.3333 | 0.10 -0.89 | 652-773 | CR | VTGA |
| 22 | 090286-06 | HTPB | 15716 | 1.524E+3 | 0 | 3.3333 | 0.11 -0.90 | 654-770 | CR | VTGA |
| 23 | 090286-07 | HTPB | 13834 | 3.663E+2 | 0 | 3.3333 | 0.11 -0.87 | 646-770 | CR | VTGA |
| 24 | 090286-08 | HTPB | 15864 | 1.570E+3 | 0 | 3.3333 | 0.10 -0.88 | 662-772 | CR | VTGA |

Thus even though the sample has decomposed, there is no apparent weight loss until the sample is at a higher temperature. In addition, liquids formed can condense on cooler parts of the apparatus and obscure the results; this was actually observed in the decomposition of these polymers, particularly with PBAN. In the VTGA, on the other hand, liquids formed during decomposition would vaporize much more readily, due the much greater convective environment in which the sample pyrolyzes.

In Table 5-3a are the calculated Arrhenius parameters for PBAN obtained with the VTGA. This data shows fair agreement with that obtained in the thin-film TGA work. Global energies of activation are slightly higher than in the TGA work, this may illustrate that evaporation is a significant factor in the TGA decomposition of PBAN. Results for HTPB, Table 5-3b, are in excellent agreement with the thin-film TGA work. Global energies of activation are graphically presented in Figures 5-4a and 5-5b for both the low-heating-rate TGA and VTGA work; data points for the VTGA results in these figures represent the average of four distinct experiments.

Given the precision in the VTGA curves and the ability to measure reasonable values of Arrhenius parameters for these polymers, the claim is made that this device is indeed a functioning thermogravimetric analyzer possessing some distinct advantages over the conventional methods. These

advantages include: small sample size, ≈0.5 mg; samples are thin films in contact with a good heat sink, minimizing thermal irregularities with in the sample; sample temperatures are measured directly; condensation on the cooler parts of the instrument would not significantly affect results; results are independent of buoyancy and vapor pressure effects in the sample pan, and elevated heating rates are possible.

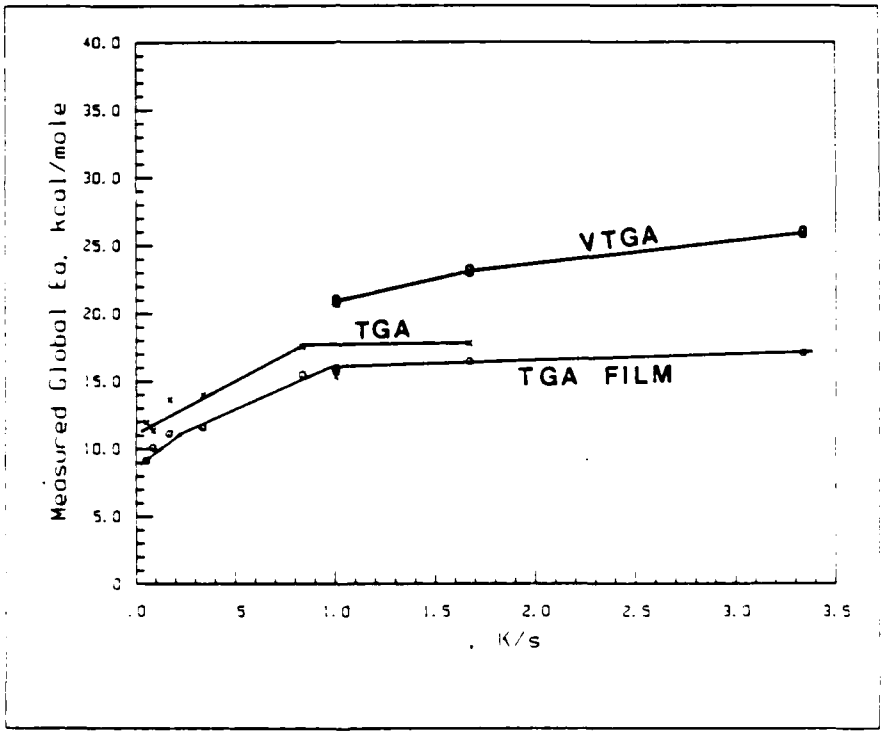


Fig. 5-4a. Low-Heating-Rate Global Ea's for PBAN.

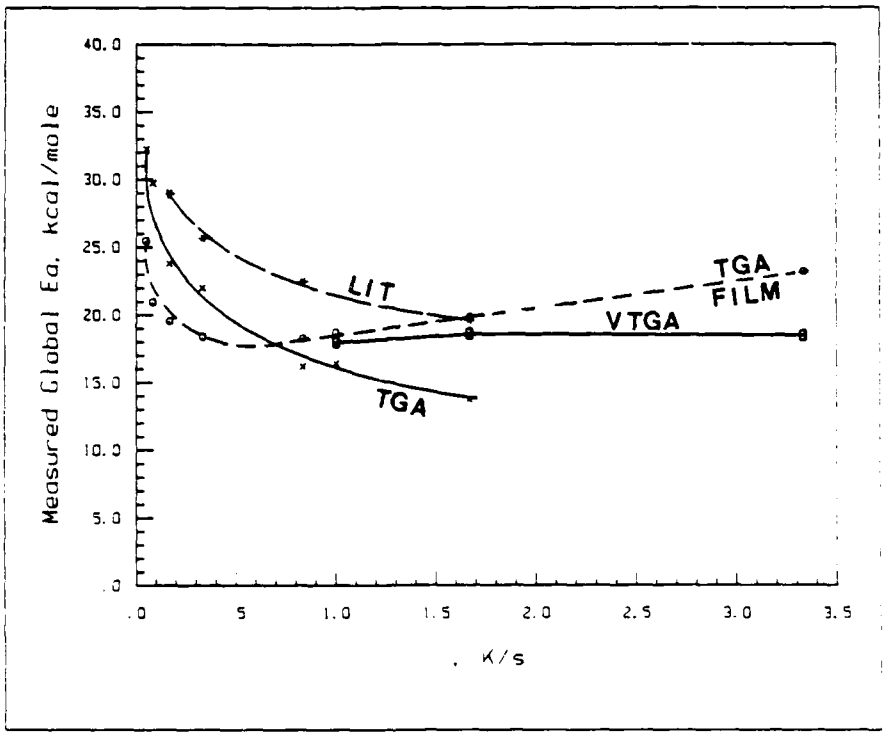


Fig. 5-4b. Low-Heating-Rate Global Ea's for HTPB.

## 5.3 High-Heating-Rate Results

### 5.3.1 PBAN

A series of pyrolysis experiments were conducted on PBAN at increased heating rates. Heating rates varied from around 20 °K/s to 60 °K/s. It is worth mentioning again that very little control over the heating rate was possible with the induction heating unit used in this work, and the upper temperature limit was restricted to values below about

830 °K. The upper bound on the temperature was mainly imposed by the availability of materials for heating element fabrication. (The only available ferromagnetic fine gauge tubing available at the time was 304 stainless steel.)

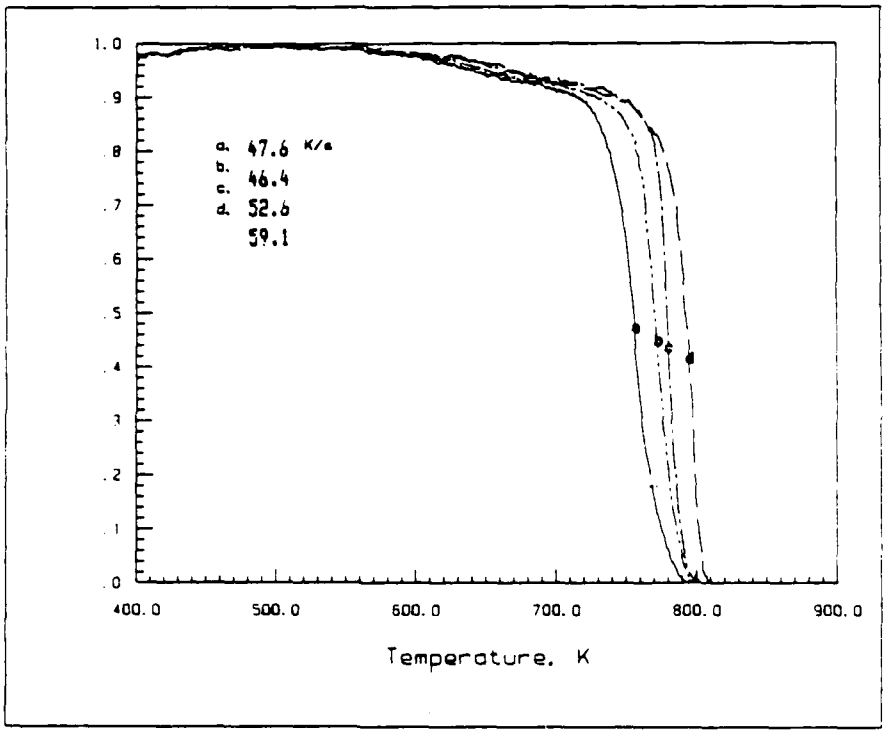


**Fig. 5-5. VTGA Thermograms of PBAN - High-Heating-Rate.**

Figure 5-5 contains typical results for the decomposition of PBAN. Sample sizes were between 0.25 mg and 0.50 mg which of course were applied as a thin film to both sides of the strip - about 0.125 mg to 0.25 mg per side. Heating rates are over an order of magnitude greater than those presented in the previous section.

Comparing the data in this figure with that of Figs. 5-2a and 5-3a, several differences are apparent. The temperature range of the decomposition has shifted to slightly higher values, and this range has become narrower. This implies a higher rate of decomposition as can be seen by the steepness of the curves. This translation to higher

Table 5-4. VTGA Kinetic Results for PBAN - High Rate.

Ea : cal/mole
A : sec-1
β : °K-sec-1
T : °K

| Item | ID | Material | Ea | A | n | β | αo - αf | T Range | Analysis | Source |
|---|---|---|---|---|---|---|---|---|---|---|
| | | | | | | | 0.1≤α≤ 0.3 | | | |
| 1 | 190286-10 | PBAN | 33366 | 2.457E+9 | 0 | 47.6 | 0.10 -0.29 | 714-745 | CR | VTGA |
| 2 | 190286-09 | PBAN | 26496 | 1.055E+7 | 0 | 46.4 | 0.10 -0.30 | 728-763 | CR | VTGA |
| 3 | 190286-13 | PBAN | 25013 | 3.040E+6 | 0 | 52.6 | 0.10 -0.29 | 740-775 | CR | VTGA |
| 4 | 190286-11 | PBAN | 24072 | 9.447E+6 | 0 | 59.1 | 0.10 -0.28 | 743-784 | CR | VTGA |

temperatures is more pronounced in the early stages of the pyrolysis, and pyrolysis at these higher heating rates occurs over a much narrower temperature range. The kinetic constants for PBAN are presented in Table 5-4. The global Ea's for PBAN presented in the previous section were about 25 kcal/mole with A's of about $10^{8}$; the values presented in

Table 5-5 are for all intents and purposes the same. This coupled with the similar shaped pyrolysis curves would suggest that about the same physical/chemical processes are occurring at these elevated heating rates as are occurring at the lower rates.

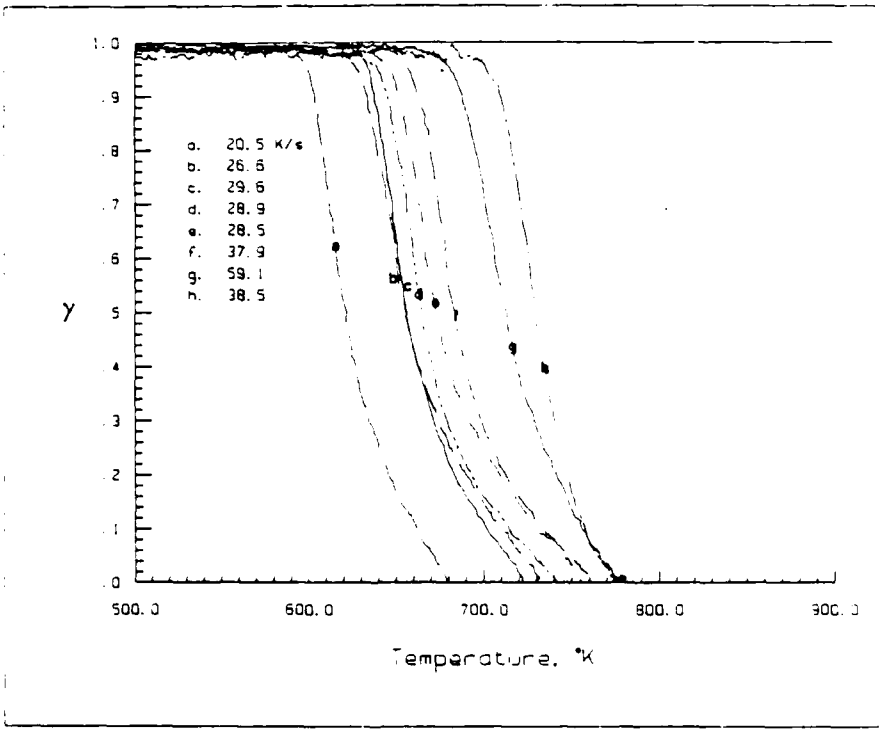


Fig. 5-6. VTGA Thermogram of HTPB - High-Heating-Rate.

### 5.3.2 HTPB.

Fig. 5-6 contains the results of the high heating rate experiments on HTPB. As with PBAN, sample sizes are between 0.25 mg and 0.50mg. These were deposited on the pre-oxidized heating element from a solution of the polymer in Toluene. There are very obvious differences between thermograms in this figure and those found in figures 5-2b and 5-3b. Not only are the overall shapes different, but the decomposition has shifted to slightly lower temperatures. Comparing these curves with those in Fig. 5-3b shows that with the exception of curve a the onset of the decomposition is at about the

Table 5-5. VTGA Kinetic Results for HTPB - High Heating Rate.

Ea : cal/mole
A : sec-1
β : °K-sec-1
T : °K

| Item | ID | Material | Ea | A | n | β | $\alpha_o - \alpha_f$ | T Range | Analysis | Source |
|---|---|---|---|---|---|---|---|---|---|---|
| | | | | | | | 0.15≤α≤ 0.3 | | | |
| 1 | 170286-16 | HTPB | 89601 | 7.564E+31 | 0 | 20.5 | 0.10 -0.30 | 604-612 | CR | VTGA |
| 2 | 170286-19 | HTPB | 89643 | 2.803E+23 | 0 | 26.6 | 0.10 -0.29 | 634-645 | CR | VTGA |
| 3 | 190286-02 | HTPB | 92850 | 8.321E+27 | 0 | 29.6 | 0.11 -0.30 | 638-648 | CR | VTGA |
| 4 | 190286-03 | HTPB | 79153 | 1.975E+26 | 0 | 28.9 | 0.10 -0.29 | 645-656 | CR | VTGA |
| 5 | 170286-20 | HTPB | 78499 | 5.922E+25 | 0 | 28.5 | 0.1' -0.29 | 652-662 | CR | VTGA |
| 6 | 170286-17 | HTPB | 84412 | 2.483E+27 | 0 | 37.9 | 0.11 -0.30 | 663-674 | CR | VTGA |
| 7 | 170286-18 | HTPB | 71930 | 2.974E+22 | 0 | 49.7 | 0.11 -0.29 | 689-701 | CR | VTGA |
| 8 | 190286-06 | HTPB | 98880 | 1.088E+30 | 0 | 38.5 | 0.11 -0.28 | 710-720 | CR | VTGA |

temperature, but the rates are significantly higher.

The lower portion of the curves are much more protracted, possibly, but not necessarily, indicating a shift in the apparent order of the decomposition. (See Fig. 2-3a.) With but one exception there is a trend to higher temperatures as heating rate to the sample is increased. Examination of the calculated kinetic parameters presented in Table 5-6 shows that there has been a dramatic change in the global Arrhenius values. Ea's have increase from below 20 kcal/mole to around 80 kcal/mole. All this would indicate a radical shift in decomposition mechanism. These values are startlingly high compared to the previous results, and to the high-rate data in the literature. In mitigation, it must be remembered that bond energies in HTPB are around 80 kcal/mole; if the global energy of activation is interpreted in terms of the weakest bond in the molecule, then these values do not seem as unrealistic. These larger values could also be explained in terms of the finding of Gontkovskaya, et al. [31], discussed in Chapter I. In this work the authors solved rate expressions with heat transfer for the cases where the decomposition proceeded via several parallel reactions. They showed that an increase in heating rate promotes the course of the reaction along the path with the highest activation energy. Real-time chemical analysis of the decomposition products would be necessary in order to draw any meaningful conclusions as to the details of the processes which are occurring.

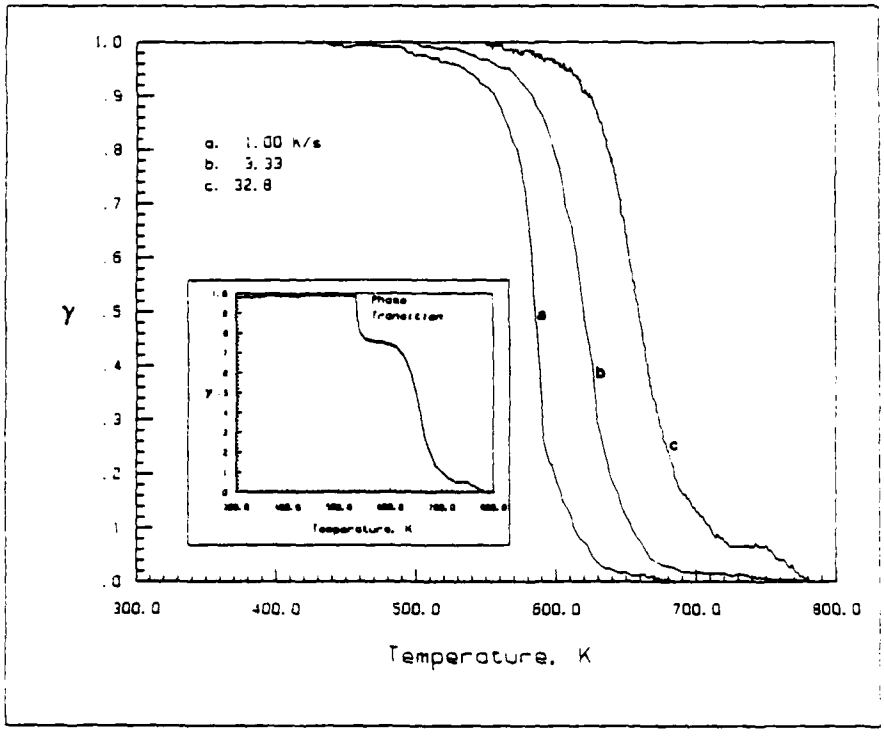


Fig. 5-7a. VTGA Thermogram of AP.

### 5.3.3 AP

The VTGA was designed to measure pyrolysis data on polymers. It was felt that crystalline materials would not adhere to the heating elements during rapid heating. Several runs were made on ammonium perchlorate to demonstrate this. Surprisingly, it was possible to make kinetic measurements on this material using both the linear furnace and the induction furnace. Sample size was again between 0.25 and 0.50 mg only in this case it was deposited on the metal strip from an acetone solution. Many applications of the solution were required to build up a sufficient quantity of sample. Several pyrolysis curves are shown in Fig 5-7a. Curves a and b were obtained with the linear furnace while curve c was obtained with the induction furnace. The inset in Fig 5-7a shows curve c as it was recorded. The abrupt weight loss at 545 °K corresponds to the temperature of the crystalline phase change in AP; apparently this is sufficiently violent to loosen some of the AP which was affixed to the heating element. Normalizing this pyrolysis curve produces curve c in the main figure. Corresponding kinetic data may be found in Table 5-6. A comparison of this data with the literature values given in the lower portion of the table is shown in Fig. 5-7b. (The numbers in Fig. 5-7b refer to item numbers in Table 5-6.) It is well known that the Ea of AP is strongly dependent upon the temperature of the decomposition, the data in this figure is presented as a

function of temperature, where the box represents the VTGA data in Table 5-6, items 1 through 3.

Table 5-6. VTGA Kinetic Results for AP - Deposited on 304SS from Acetone

Ea : cal/mole
A : sec-1
β : °K-sec-1
T : °K

| Item | ID | Material | Ea | A | n | β | αo - αf | T Range | Analysis | Source |
|---|---|---|---|---|---|---|---|---|---|---|
| | | | | | | | 0.1≤α≤ 0.3 | | | |
| 1 | 130286-13 | AP | 26168 | 8.953E+7 | 0 | 1.00 | 0.11 -0.28 | 558-578 | CR | VTGA |
| 2 | 130286-15 | AP | 28172 | 5.506E+8 | 0 | 3.3 | 0.10 -0.25 | 584-604 | CR | VTGA |
| 3 | 190286-15 | AP | 36145 | 7.016E+11 | 0 | 32.8 | 0.10 -0.29 | 652-694 | CR | VTGA |
| 4 | | AP(90μm) | ≈30000* | - | 1 | 0.16-0.3 | ≈0 - 1 | 613-683 | DSM | TGA[54] |
| 5 | | AP(90μm) | 56000β | - | 1 | - | ≈0 - 1 | 673-713 | DSM | TGA[54] |
| 6 | | AP | 25100 | - | 1.2 | - | 0.0 - 0.2 | 523-573 | AE | G [55] |
| 7 | | AP(80μm) | 46700 | - | 2 | - | 0 - 1 ? | 643-673 | CC | G [55] |
| 8 | | AP(56μm) | 35700 | - | 2 | - | 0 - 1 ? | 643-673 | CC | G [55] |
| 9 | | AP(28μm) | 31000 | - | 2 | - | 0 - 1 ? | 643-673 | CC | G [55] |
| 10 | | AP | 33490 | 8.950E+10 | 3 | - | 0 - 1 ? | - | AE | G [55] |

* Actual Values for in temperature range were reported as "slightly less than 30 kcal/mole.
β Pre-decomposed on DSC to investigate high tempera'ure region.

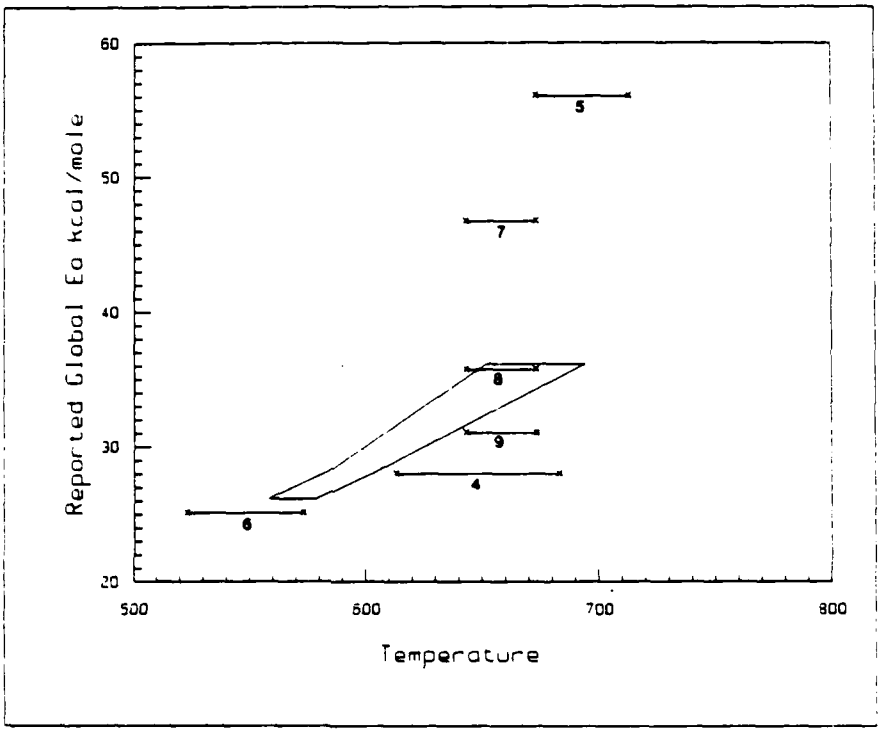


Fig. 5-7b. VTGA and Literature Results for AP.

# CHAPTER VI

# CONCLUDING REMARKS AND SUGGESTIONS

## 6.1 General Remarks

In the previous chapter it was demonstrated that it is possible to make a mass measurement of a sample during rapid pyrolysis at heating rates up to 60 °C/s. Pyrolysis curves so obtained, agreed well with curves obtained using a conventional TGA. The precision demonstrated in Figs. 5-3a and 5-3b is excellent. Kinetic values are in reasonable agreement with the TGA and the literature. With a better inductive heating unit and data-line frequency response, it should be possible to attain rates of several hundreds of degrees per second. Nevertheless, given the serious limitations in the current induction heater, results obtained at the these higher heating rates are fairly good - at least reasonable. Moreover, the work demonstrates that using vibration to make sensitive mass measurements is feasible. As far as is known to the author, this is the first device which will make continuous mass and temperature measurements on sub-milligrams sample at heating rates above about 3.3 °C/s.

## 6.2 The Method - Advantages and Disadvantages

VTGA apparatus has several advantages over existing TGA equipment. However, in its present form, there are also some glaring design deficiencies which need to be re-worked in order to have a routinely usable instrument at heating rates of 100 °C/s or better. It is believed that by correcting some of the design deficiencies, the most important of which is the high-heating-rate control and frequency of the data-line, the instrument would be capable of routine analyses at heating rates of 100 °C/s. Thermal decomposition experiments at heating rates, which would be relevant to solid propellant combustion, would of course require a new experimental approach using high-energy lasers of 1000 Watts or more to heat the sample.

### 6.2.1 Advantages

The instrument has several clear advantages for the thermal analysis of polymers over the traditional TGA which uses the double-beam balance. In TGA's, buoyancy and convection can affect the most sensitive mass measurements; this would be particularly true of energetic materials which give considerable off-gassing during decomposition. It has been shown [53] that significant pressures of pyrolysis products exist within the weighing pan during decomposition. Moreover, condensation of pyrolysis products on the cooler parts of the balance mechanism can effect overall results. This would be a minor concern in the VTGA. Rapid-off

gassing would still affect the motion of the tube to some degree, but, this would occur only at the highest rates.

Conventional TGA's, suffer from problems in the accuracy with which they can measure temperature. The sample is not in contact with the heat source nor is it in contact with the thermocouple. This results in considerable thermal inertia and limits heating rates to very low values. Moreover, due to exo- and endo-thermal processes taking place within the sample, the actual sample temperature may be significantly different than the indicated temperature; this has been shown to be critical in the analysis of results [31]. Since the samples in the VTGA are thin films, this is not expected to be as great a problem; these films are in intimate contact with the heat source and the thermocouple. This heating element/thermocouple is a good heat sink - thermal gradients across the sample will not be as significant. Thin film samples also reduce the problem of diffusion of subsurface gaseous products to the exterior. The relative importance of each these limitations are pointed out in Ref. [53].

### 6.2.2 Deficiencies

The present design of the apparatus is far from optimum. Improvements can be made to the laser, and signal conditioning and data lines; major improvements need to be made to the heater control system.

**The Laser.** Low mW lasers, like the one used in the

VTGA frequency detection system, are mainly used for alignment of optical systems, with the result that the quality of the emitted light is often poor. It may contain considerable 60 cycle noise, particularly if a low quality power supply is used. The photocell can not differentiate between noise in the light source and the signal generated by the oscillation of the tube. The presence of noise requires oscillation of the tubes at amplitudes greater than 1 mm. To a certain extent it impacts on the sensitivity of the measurement; also, the higher the amplitude the more pronounced is convection in the area of the sample. By switching to a higher quality laser during this work, it was possible to determine the period of oscillation to another decimal place. Presumably, better quality lasers would further improve results.

**Signal Conditioning and Data Acquisition.** Time resolution of the apparatus could be improved by going to higher frequencies, shortening the tube is of course the simplest way of doing this. As the sample volatilizes, the amplitude decreases, and frequency increases. At times, the amplitude decreases sufficiently, such that the S/N ratio in the feedback loop is high enough to cause the motion of the tube to stop. For this and other reasons it is desirable to maintain the amplitude constant during the test. This indicates the need for a servo-loop as indicated by the dashed box in Fig. 3-4. This servo-system would increase

the emf to the main feedback-loop when a decrease in RMS voltage was detected in the circuit. It would function in much the same way as does a radio which maintains constant volume as the automobile travels into areas of varying signal strength.

The FVC currently used, operates at 0 to 10 volts for an input of 0 to 10000 Hertz; thus, at 160 Hertz, we are operating on the outer limits of its performance range. This necessitates the use of extensive filtering of the signal and the use of a differential input at the scope, Fig 3-6; both of these seriously limit the frequency response of the mass data-line. It would be much more desirable to replace this with a frequency to voltage converter operating at 0 -10 Volts over 0 -1000 Hertz, or better still, a zero crossing detector/counter combination.

**Heater Control.** The principal limitation of the VTGA is in heating rate control at high heating rates and the ultimate temperature attainable. Improvement to the heating rate control would require the construction of an induction heating unit which permitted a variable power output to the induction coil and longer heating times. (The one used in this work was limited to 9 s.) A temperature-heating rate servo-loop to linearize and control the heating rate would go a long way to improve the results. In subsequent work in this area, small ferromagnetic tubes should be manufactured so that heating-element/thermocouple combinations can be

fabricated which are capable attaining higher temperatures.

## 6.3 Suggested Work.

### 6.3.1 Experimental

A very interesting experiment would be the modification of Baer's and Hedge's rapid pyrolysis experiment [10] to include the feedback-loop/mass measuring system used in present work. Their experiment is briefly described in Chapter I. Baer was able to rapidly heat thin films of polymer which were mounted on a thin metal strip which also served as a heating element. This heating element was fixed between two supports and heating was accomplished by passing a strong electric current through the strip. Mass measurements were made discontinuously by "quenching" the sample with a cold blast of air and weighing the strip. Sample temperatures were measured using an infrared radiometer "looking" at the back side of the heating element rather than at the sample itself; this eliminates the problem of radiation absorption by pyrolysis products. Radiometers are available with 8 μs response times, a significant improvement over the thermocouple (3 ms). (A similar radiometric temperature measurement scheme could be used with the present quartz tube arrangement.) If Baer's 25 μm thick heating element were mounted in such a way that it could vibrate, introduction of the feedback-loop system used in the present work would make a continuous mass measurement

possible. Moreover, with this arrangement it should be possible to obtain higher frequencies of vibration than with a cantilevered tube, and hence, obtain better time resolution. The frequency of vibration would depend upon the tension in the vibrating metal ribbon. The tension of course would have to be kept constant; this difficulty has apparently been overcome by Gast and Jokobs [43,44]. Such an arrangement could effectively be implemented at pressure. And heating rates up to several hundreds of °C/s would not be unreasonable with such an arrangement.

### 6.3.2 Theoretical.

In the linear pyrolysis experiments reviewed in Chapter I, reported values for global energies of activation for HTPB and PBAN are between 10 and 17 kcal/mole. The bond energies for the weakest bonds in these molecules are, however, closer to 80 kcal/mole. The relatively low values for Ea have been attributed to evaporation being the rate limiting step at the higher heating rates. (It was pointed out in Chapter I that evaporation could be expressed in terms of an Arrhenius type expression, Eqn. 1-9.) This argument has also been used by Chaiken [27] to explain the shift to lower values of Ea when PMMA is decomposed at higher heat fluxes. It would be interesting to determine if this shift to lower values has a plausible theoretical foundation.

In Chapter I, the work of Gontkovskaya, et al. [30,32]

was described wherein they analyzed the kinetics of decomposition with heat transfer for a material decomposing via two parallel reactions. Numerical solutions to the differential equations showed that higher heating rates promoted the process with the higher activation energy! This result would seem to be at odds with the explanation of Chaiken and others.

In related papers they analyze and numerically solve the case of sequential reactions. [32,33] In a similar fashion, the decomposition/vaporization of a polymer can be described as a sequential processes, Eqn. 6-1:

$$P \xrightarrow{k_1} n_1 \xrightarrow{k_2} n_2 \qquad (6\text{-}1)$$

where, n1 is the condensed phase decomposition product of the polymer, P, and n2 is the product of vaporization of n1. $k_1$ and $k_2$ are the rate constants for the decomposition and vaporization, respectively. The following equations would describe the process:

$$\frac{dp_1}{dt} = -A_1 e^{-E_1/RT} p_1 \qquad (6\text{-}2)$$

$$\frac{d\eta_1}{dt} = - R_2 + A_1 e^{-E_1/RT} \rho_1 \qquad (6\text{-}3)$$

$$c\rho \frac{dT}{dt} = Q_1 A_1 e^{-E_1/RT} \rho_1 + R_2 \Delta H_v - \alpha \frac{S}{V} (T - T_s) \qquad (6\text{-}4)$$

with the initial conditions,

$$\beta = dT/dt, \quad T = T_s = T_i, \quad \rho_1 = 1, \quad \eta_1 = 0 \qquad (6\text{-}5)$$

where $R_2$ is the rate of vaporization of n1, given by the non-dimensional form of Eqn. 1-9. It would be interesting to see if the numerical solution to this set of differential equations, for plausible values of the various parameters, would yield situations where vaporization would be the rate limiting condition. Reasonable values for some parameters may be found in [12] and [15].

## 6.4 Conclusions

1. Global Arrhenius parameters are in general not constants and must be empirically determined - this is particularly true for complex substances such as polymers.

2. Arrhenius parameters used in kinetic and combustion models must be empirically determined under conditions

similar to those over which the model is to be used and considered valid.

3. Global kinetic parameters can be strong functions of the experimental conditions, for example, heating rate, pressure, and temperature; calculations which determine Arrhenius parameters from experimental data, should make this determination over as narrow a range in these condition as is possible.

4. In order to obtain the maximum benefit from high-heat-flux experiments, numerical techniques for the smoothing of thermal analysis data, and for the integration of the rate expression over finite limits, need to be developed.

5. An algorithm which uses only the early stages of decomposition for determination of Arrhenius parameters necessarily requires fewer assumptions as to the details of the decomposition; no assumption as to reaction order is necessary.

6. Global reaction order is an empirical parameter dependent upon the details of the experiment.

7. Construction of a thermogravimetric analyzer which uses vibration (VTGA) to measure small changes mass of thin polymer films is feasible. Moreover, it is possible to construct such a device where the sample is in contact with the thermocouple. Such a device is not impaired by effects such as buoyancy, condensation of products, and to a certain

extent, sample off-gassing.

8. The VTGA developed in this work is capable of measuring the decomposition kinetics of thin polymer films, at heating rates up to 3.33 °C/s, with a precision and accuracy at least as good, and probably better, than a conventional TGA.

9. The present VTGA design can measure decomposition kinetics of polymer films at heating rates in the range of 20 - 60 °C/s. ; major redesign of the induction heater and FVC will be necessary to precisely and accurately represent the high-high-heat flux kinetics of polymers at varied and reproducible heating rates. Such a redesign should provide for programmable heating rates - not necessarily linear. Redesign should permit operation at heating rates in excess of 100 °C/s.

10. Over the small variations in mass used in the VTGA, the calibration is essentially linear; this greatly simplifies the use of this device.

11. The TGA could not successfully determine kinetic constants for bulk samples of HTPB and PBAN at heating rates 3.3 °C/s. At heating rates above this value it is likely that the decomposition in bulk samples is diffusion controlled. It is also doubtful that thermal equilibrium exists in the TGA test cell even at this low rate.

12. Data indicates that PBAN is likely to decompose via the same mechanism at heating rates of 0.5 °C/s - 3.3

°C/s as it does at heating rates of 40 - 60 °C.

13. Data indicates that there is a change the controlling mechanism or the path in the decomposition of HTPB when heating rates are changed from values around 1 °C/s to values of about 40 °C/s.

14. It is possible to determine kinetic parameters of crystalline materials in a VTGA-type apparatus.

# APPENDIX A

## EQUIPMENT, INSTRUMENTATION, AND MATERIALS

### Equipment and Instrumentation.

Item.

1. IBM-Personal Computer

Manufacturer: IBM Corporation

Configuration: 515K Ram Total; two 360K Floppy disk drives; Quadboard II Expansion Board, w/ two Serial Ports, Clock, 256K Ram; Amdek 300A Monitor; Hercules Color Card w/Parrallel Port; HP 7470A Digital Plotter; Okidata 92P Printer.

2. Nicolet 4094 Digital Osciloscope

Manufacturer: Nicolet Instrument Corporation
5225-2 Verona Road
Madison, WI 53711

Configuration: Model 4562 two-channel plug-in, up to two MHertz sampling rate both channels; single Floppy Diskette Drive; RS-232 Computer Interface.

3. Vibration Exciter (Mini-Shaker), Type 4810

Manufacturer: Brel & Kjaer
DK-2850 Naerum, Denmark

Specifications: Force rating 10 Newton Sine Peak; Frequency range 10 Hz to 18 kHz; Max. bare table acceleration 56g; First axial resonance above 18 kHz.; Max. displacement 6 mm.

4. Neff Model 122 DC Amplifier

Manufacturer: NEFF Instrument Corporation

1088 East Hamilton Road
Duarte, California 91010

a. Configuration: without bandpass filter.

b. Configuration: with bandpass filter.

5. DC Power Supplies

Manufacturer: Hewlett-Packard Co.
1501 Page Mill Road
Palo Alto, CA 94304

a. Specifications: HP 6215A, 0 - 30V, 0 -500 mA.

b. Specifications: HP 6228B Dual Power Supply, 0 - 50 V, 0 - 1 A.

c. Specifications: HP Harrison 6204B, 0 - 4 V, 0 - .3 A; 0 - 20 V, 0 - .6 A

6. Laser

Manufacturer: Uniphase, Inc.

Configuration: Model 1101
Max-Power 1 mW, Beam Diameter 0.63 mm
Power Supply, External Type, Model 1201-1

7. Optical Bench and Mounts

Manufacturer: Ealing Corporation
Pleasant Street
South Natic, Mass. 01760

a. Specifications: Model 22-6894, 1 meter.

b. Specifications: Model 22-6837, 1/4 meter.

8. Curie Point Pyrolyzer

Manufacturer: Fischer
5309 Meckenheim/b. Bonn
Insustriepark Kottenforst

Specifications: Model 0310, 1.2 MHertz, 2000 W output, 382 Oe. coil Field Strength.

9. Electronic Compensator ("Ice Point")

Manufacturer: Omega Engineering
One Omega Drive
Box 4047
Stamford, CT 06907

Specifications: Model LXCJ-E, Type-E(Chromel-Constantan).

Configuration: Self-Powered by Battery

10. Electronic Digital Balance

Manufacturer: Mettler Instrument Corporation
Box 71
Hightstown, NJ 08502

Specifications: Model AE-160, Range 0 - 162g, Reproducibility S.D. .1 mg., Linearity +/- .2 mg., Readability .1 mg.

11. Thermocouples

Manufacturer: Omega Engineering
One Omega Drive
Box 4047
Stamford, CT 06907

Specifications: Type E, Chromel SPCH-001, Constantan SPCR-001

12. Thermogravimetric Analyzer

Manufacturer: Perkin-Elmer Corp.
Instrument Division
Norwalk, Connecticut 06856
203-762-1000

Specifications: TGA-2 and System 7/4 Controler
Maximum Programmable Heating Rate 200°C/min
Temperature Range: Ambient - 1040°C

13. Frequency Meter

Manufacturer: John Fluke Mfc. Co Inc.
P. O. Box 43210
Mountain Lake Terr., WA 98043
206-744-2211

Specifications: Model 1900A Multi-Counter

14. Photodiode Support

Manufacturer: Brinkman Instruments Inc.
Cantiague Road
Westbury, NY 11590
516-334-7500

Specifications: Model RP-IV Micro-manipulator

15. Photodiode.

Manufacturer: TRW, Inc.

Specifications: Photo-transistor, TRW-OP802W

16. Frequency-to-Voltage Converter

Manufacturer: In-House Built Unit

Specifications: Unit designed around Teledyne-Philbrick 4710 low drift 100kHz F/V Converter. Output set to yield 0-10 Volts for 0-1kc.

Supplier: Teledyne-Philbrick

## Materials

Item.

1. Quarts Tubes

Manufacturer: Vitro Dynamics Inc.
114 Beach Street
Rockaway, New Jersey 07866

Specifications: Convenience Vials.

2. Steel Tubbing

Manufacturer: Small Parts Inc.
6901 N.E. Third Avenue
P.O. Box 381736
Miami, Florida 33238-1736
305-715-0856

Specifications: 304 Stainless Steel, Hypodermic Tubbing
304 Stainless Steel, Thin Wall Tubing

3. Polymers

Manufacturer: Scientific Polymer Products, Inc.
6265 Dean Parkway
Ontario, N. Y. 14519
716-265-0413

Specifications: PBAN
Acrylonitrile/butadiene Copolymer
Acrylonitrile Content 21%
Average Mooney Viscosity 55
Density 0.95
Soluble in MEK, Toluene, THF

HTPB
Polybutadiene, cis and trans
9% Vinyl 1.2
Nominal M.W. 200,000
Nominal M.N. 96,000
Density 0.90
Tg - 95°
Solubility Parameter 8.38
$n_{D25}$ = 1.5178
Soluble in THF, aliphatic, cycloaliphatic, and aromatic hydrocarbons.

## Preparations and Fabrications

### 1. Composite Pyrolysis Tubes

The quartz pyrolysis tubes are actually composite tubes formed by cementing a metal tube of smaller outside diameter to the end of the quartz tube. This metal tip serves several purposes: it mainly functions as a support upon which to coat the polymer samples, however, it also provides a convenient point of attachment for thermocouple leads, and is consequently an excellent medium for heat transfer between the sample and the thermocouple. In cases where induction heating is employed, it can also function as a heating element - the metal is ferromagnetic and is fabricated from 304 stainless steel tubing.

To construct one of these pyrolysis tubes, a 3 cm length of stainless steel tubing is cut from tubing stock with a typical O.D. of 0.013 inches and an I.D. of 0.007 inches. Cutting is performed using a hand grinder equipped with a very thin grinding wheel; this is used so as not to collapse the tube ends. These ends are polished with the grinder, if necessary, to remove sharp edges and to insure that the tube is open at both ends. One lead of one-mil thermocouple wire is inserted through the tube ( a hypodermic cleaning wire is often helpful to drag the wire through the tube). In a similar fashion, the second lead is also inserted. The respective leads are marked with tape for later identification, and the leads are cut leaving about six inches of both leads extending from this tube section. The tube is placed between two pieces of hardened tool-steel; about a millimeter of the tube on the side with the long thermocouple leads is allowed to protrude outside. This is the serve as a "stem" which will later be inserted into the quartz tube. The edges of these tool-steel pieces have been sanded to a rounded edge so as not to cut the stainless steel tube section. This assembly is placed in a 30,000 lb. press and pressed for a short time. The resulting piece, when removed, resembles a spatula blade with the thermocouple leads extending from the stem. The flattened end of the "spatula" is trimmed the desired length. The "stem" inserted into the end of a quartz tube of slightly larger I. D. routing one lead of the thermocouple through the center of the quartz tube. The stem is cemented in place using a 2000 °F ceramic cement; the remaining lead is spirally wound around the outside of the tube and secured at the opposite end with a small piece of shrink tubing. The thermocouple is checked for continuity and the entire assembly is mounted in the experimental apparatus and the thermocouple leads are soldered in place. Where ferromagnetism is not important

lighter metal tubing, such as aluminum could be used.

Note: One of the most difficult tasks of the project was to find a method to make these metal tips complete with thermocouples. Several other methods were attempted but with out success. For example, ferromagnetic materials were chemically deposited on a gold substrate on the tip of the quartz tube. The gold was sputtered coated on the tip. The materials so formed, did not heat well in the induction heater and thermocouples could not be readily applied. Welding the thermocouples proved difficult and welds would not hold. Clearly if a method can be found to apply low weight ferromagnetic materials to quartz tubes or ribbons, and thermocouples could be attached or temperatures measured with a radiometer, the sensitivity of the method would be greatly enhanced. A large penalty is paid in sensitivity by the necessity of using the rather heavy (about 7 mg) stainless steel tube for the heating elements.

# APPENDIX B

## COMPUTER PROGRAMS

**Program 1.** This program, written in MS-BASIC, transfers data from memory of a Nicolet 4094 Digital Oscilloscope to an IBM-PC/XT/AT; temporary files and data are stored on Drive C:. Data transmission rate is 9600 BAUD via an RS-232 interface; data transmission requires the use of a nul-modem since both the oscilloscope and the computer are configured as data terminal equipment. Data is stored in an ASCII file in two columns - time and volts.

```
2 '****************** IBM-PC - NICOLET DATA TRANSFER PROGRAM ********************
3 '*****************************************************************************
4 '**   Author: Robert J. Powers, Aerospace Engineering Dept., Georgia Tech
5 '
6 '******************************** MAIN PROGRAM ********************************
7 '** CONFIGURATION, IBM-PC : RS-232C PORT SET UP A COM PORT 1
8 '** CONFIGURATION, NICOLET: RS- 232C ADDRESS 30 (ASCII CHARACTER N);
9 '**                        DATA TRANSMISSION RATE 9600 BAUD
10 '
15 DIM TIT$(4),N$(11),W(8,4)
20 OPT = 0
40 CLS :LOCATE 1,25
50 COLOR 0,7
60 PRINT "IBM-PC - Nicolet";
70 COLOR 7,0
80 PRINT " Data Transfer Program"
90 PRINT:LOCATE 3,37:PRINT "Version 1.00":PRINT
100 PRINT "
110 PRINT "
120 PRINT "                    1. Initialize Data Transfer (C)(B)
130 PRINT "
140 PRINT "                    2. Nicolet Disk Storage and Retrieval (R)(S)(U)
150 PRINT "
160 PRINT "                    3. Display Waveform Data in Nicolet Memory (W)
170 PRINT "
200 PRINT "                    4. Transfer Data in Nicolet Memory to PC (D)(N)
210 PRINT "
220 PRINT "                    5. Add Title to Waveforms in Nicolet Memory (T)
230 PRINT "
```

```
240 PRINT "     ╔                6. Exit to System                                  ╗"
250 PRINT "     ╚═══════════════════════════════════════════════════════════════╝"
260 PRINT "
270 LOCATE 24,1
280 INPUT "Select Option: ",OPT
290 CLS
300 IF OPT = 1 THEN GOSUB 350
310 IF OPT = 2 THEN GOSUB 560
320 IF OPT = 3 THEN GOSUB 2000
325 IF OPT = 4 THEN GOSUB 5000
330 IF OPT = 5 THEN GOSUB 1590
335 IF OPT = 6 THEN SYSTEM
336 LOCATE 24,1:PRINT "                                                    ";
340 GOTO 20
345 END
346 '
347 '
348 '
350 '************************ INITIALIZATION SUBROUTINE ************************
360 '***************************************************************************
410 CLS
420 OPEN "COM1:9600,N,8,1,LF" AS #1
425 CTRLA$ = CHR$(1)
430 PRINT #1, CTRLA$;"N";
440 PRINT #1,"C,4,2,13,10"
480 CLOSE #1
482 OPEN "COM1:9600,N,8,1,LF" AS #1
484 PRINT #1,"B"
486 INPUT #1,E$
488 CLOSE #1
490 E = VAL(E$)
500 IF E <> 0 GOTO 530
510 PRINT "                              Initialization Successfull !"
515 LOCATE 24,1:INPUT "Press Return to Continue",DUM
520 GOTO 550
530 PRINT "                  Initialization Error Detected !  Error Code = ";
540 PRINT E$
545 LOCATE 24,1:INPUT "Press Return to Continue",DUM
550 RETURN
560 '********************** NICOLET DISK ACCESS SUBROUTINE **********************
565 '***************************************************************************
570 CLS
580 LOCATE 1,30
590 COLOR 0,7
600 PRINT " Nicolet Disk Access "
610 COLOR 7,0
620 PRINT "
630 PRINT "        ┌──────────────────────┬──────────────────────┐"
640 PRINT "        │ Memory Section #     │ Memory Section       │"
650 PRINT "        ├──────────────────────┼──────────────────────┤"
660 PRINT "        │          0           │ All                  │"
670 PRINT "        │          1           │ 01                   │"
```

```
670 PRINT "          ┌──────────┬──────────┐          "
680 PRINT "          │    2     │    Q2    │          "
690 PRINT "          │    3     │    Q3    │          "
700 PRINT "          │    4     │    Q4    │          "
710 PRINT "          │    5     │    H1    │          "
720 PRINT "          │    6     │    H2    │          "
730 LOCATE 14,56: PRINT "          └──────────┴──────────┘          ":LOCATE 14,13
740 LINE INPUT; "Select Mode (R = Recall, S = Store, E = End): "; MODE$
750 IF MODE$ = "R" THEN GOTO 780
760 IF MODE$ = "S" THEN GOTO 960
770 IF MODE$ = "E" THEN GOTO 1290 ELSE GOTO 730
780 OPEN "COM1:9600,N,8,1,LF" AS #1
790 LOCATE 14,61
800 COLOR 16,7
810 PRINT " RECALL "
820 COLOR 7,0
830 LOCATE 24,1
840 INPUT; "Enter -- Track #, Memory Section:  ", RN,MS
850 N$ = STR$(RN)
860 S$ = STR$(MS)
870 R$ = "R" + "," + "0" + "," + N$ + "," + S$
880 PRINT #1,R$
890 LINE INPUT #1,E$
900 CLOSE #1
910 LOCATE 24,1
920 PRINT "                                          ":LOCATE 24,1
930 LINE INPUT; "More ? "; DUM$
940 IF DUM$ = "y" OR DUM$ = "Y" OR DUM$ = "YES" OR DUM$ = "yes" THEN GOTO 730
950 GOTO 1290
960 OPEN "COM1:9600,N,8,1,LF" AS #1
970 LOCATE 14,61
980 COLOR 16,7
990 PRINT " STORE "
1000 COLOR 7,0
1010 LOCATE 24,1
1020 INPUT; "Enter -- Memory Section, Track Number #:  ",MS,TN
1030 N$ = STR$(TN)
1040 S$ = STR$(MS)
1050 R$ = "S,0,"+N$+","+S$
1060 PRINT #1,R$
1070 INPUT #1,E$
1080 CLOSE #1
1090 IF E$ = "02" THEN 1100 ELSE GOTO 1250
1100 LOCATE 24,1
1110 PRINT "                                          ";
1120 LOCATE 24,1
1130 BEEP
1140 PRINT "Track"::PRINT N$;:PRINT " is write protected!";
1150 LINE INPUT;"  Unprotect and Retry (Y or N)? ",DUM$
1160 IF DUM$ = "y" OR DUM$ = "Y" THEN GOTO 1170 ELSE GOTO 1250
1170 OPEN "COM1:9600,N,8,1,LF" AS #1
```

```
1180 PRINT #1,"U,0,"+N$+S$
1190 INPUT #1,E$
1200 PRINT #1,R$
1210 INPUT #1,E$
1220 CLOSE #1
1230 GOTO 1090
1240 LOCATE 24,1
1250 LOCATE 24,1:PRINT "                                                              ":
     :LOCATE 24,1
1260 LINE INPUT: "More ? ":DUM$
1270 IF DUM$ = "y" OR DUM$ = "Y" OR DUM$ = "YES" OR DUM$ = "yes" THEN GOTO 730 ELSE GOTO 1290
1280 IF DUM$ = "y" OR DUM$ = "Y" THEN GOTO 1170 ELSE GOTO 1250
1290 RETURN
1300 '********************** WAVEFORM DATA SUBROUTINE ************************
1305 '*****************************************************************************
1307 FOR I = 1 TO 8
1309 FOR J = 1 TO 4
1310 W(I,J) = 0
1312 NEXT J
1315 NEXT I
1320 OPEN "COM1:9600,N,8,1,LF" AS #1
1330 PRINT #1,"W"
1340 INPUT #1,E$
1350 INPUT #1,W1
1360 FOR J = 1 TO W1
1370 FOR I = 1 TO 8
1380 INPUT #1,W(I,J)
1390 NEXT I
1400 NEXT J
1410 CLOSE #1
1420 LOCATE 2,1
1430 PRINT "
1440 PRINT "      Waveform Number
1450 PRINT "      Extra Data
1460 PRINT "      Number of Data Points
1470 PRINT "      Normalization Set Number
1480 PRINT "      Normalization Step
1490 PRINT "      Channel Number
1500 PRINT "      Retain Reference Status
1510 PRINT "      Title Number
1520 PRINT "
1530 FOR I = 1 TO 8
1540 LOCATE I+2,43
1545 COLOR 15,0
1550 PRINT USING "#######":W(I,1):W(I,2):W(I,3):W(I,4)
1555 COLOR 7,0
1560 NEXT I
1570 RETURN
1580 '********************** DISPLAY TITLING SUBROUTINE ************************
1585 '*****************************************************************************
1590 CLS
```

```
1600 LOCATE 1,32
1610 COLOR 0,7
1620 PRINT "Display Titling"
1630 COLOR 7,0
1640 PRINT
1650 PRINT "
1660 PRINT "
1670 PRINT "
1680 PRINT "
1690 PRINT "
1700 PRINT "
1710 PRINT "
1720 PRINT "
1730 LOCATE 14,30
1740 PRINT "  "
1750 LOCATE 15,30
1760 PRINT "                                ";
1770 LOCATE 17,30
1780 PRINT "                                ";
1790 LOCATE 15,13
1800 INPUT "Enter -- Title #: ",TN
1810 LOCATE 17,13
1820 PRINT "Enter -- Title  : "
1830 LOCATE 16,30
1840 PRINT " ┌──────────────────────────────┐"
1850 LOCATE 17,32
1860 INPUT "",T$
1870 OPEN "COM1:9600,N,8,1,LF" AS #1
1880 D$ = STR$(TN)
1890 PRINT #1, "T,1,"+MID$(D$,2,1)
1900 INPUT #1,E
1910 PRINT #1, USING "\                              \";T$
1920 INPUT #1,E
1930 CLOSE #1
1940 LOCATE 24,14
1950 PRINT "            ";
1960 LOCATE 24,1
1970 LINE INPUT ;"More Titles ? ";DUM$
1980 IF DUM$ = "y" OR DUM$ = "Y" OR DUM$ = "YES" OR DUM$ = "yes" THEN GOTO 1730
1990 RETURN
2000 LOCATE 1,23
2010 COLOR 0,7
2020 PRINT " Data for Waveforms Currently in Memory "
2030 COLOR 7,0
2040 LOCATE 5,1
2050 GOSUB 1300
2060 LOCATE 24,1
2070 INPUT "Press Return to Continue",DUM
2080 RETURN
5000 '********************** DATA TRANSFER SUBROUTINE **********************
5010 '*************************************************************************
```

| Title # | Memory Section |
|---|---|
| 1 | Q1,H1,ALL |
| 2 | Q2,H2 |
| 3 | Q3 |
| 4 | Q4 |

```
5020 '
5030 '****************************************** DISPLAY CURRENT WAVEFORM DATA
5040 CLS
5050 LOCATE 1,35
5060 COLOR 0,15
5070 PRINT " Data Transfer "
5080 LOCATE 1,1
5090 COLOR 7,0
5100 GOSUB 1300
5110 LOCATE 2,7
5120 COLOR 0,7
5130 PRINT " Current Wavefora Data "
5140 COLOR 7,0
5150 OPEN "COM1:9600,N,8,1,LF" AS #1
5160 FOR I = 1 TO 4
5170 I$ = STR$(I)
5180 PRINT #1,"T,0," + I$
5190 INPUT #1,E$
5200 INPUT #1,TIT$(I)
5210 NEXT I
5220 CLOSE #1
5230 LOCATE 12,1
5240 PRINT "
5250 PRINT "
5260 PRINT "
5270 PRINT "
5280 PRINT "
5290 PRINT "
5292 LOCATE 18,1
5293 PRINT "
5294 PRINT "
5295 PRINT "
5296 PRINT "
5300 LOCATE 12,6:COLOR 0,7:PRINT " Title # ";
5310 LOCATE 12,26: PRINT " Titles ": COLOR 7,0
5320 FOR I = 1 TO 4
5330 LOCATE 12 + I,8
5340 TIT$(I) = LEFT$(TIT$(I),32)
5350 PRINT " ";:PRINT I;: PRINT ".  ";:COLOR 15,0:PRINT TIT$(I):COLOR 7,0
5360 NEXT I
5370 LOCATE 12,57:PRINT "═══════════"
5375 LOCATE 13,52:PRINT "Waveform #:  "
5376 LOCATE 13,66:PRINT "Org:       "
5380 LOCATE 14,52:PRINT "Start:";:PRINT "       End:      "
5390 LOCATE 15,52: PRINT "Step:             "
5400 LOCATE 16,52:PRINT "Total Pts:        "
5405 LOCATE 18,10:COLOR 0,7:PRINT " Transfer Status ":COLOR 7,0
5406 LOCATE 19,10:PRINT "Status:";:LOCATE 19,32:PRINT "#:";:LOCATE 19,38:PRINT "To: "
     ;:LOCATE 19,55:PRINT "Origin: "
5407 LOCATE 20,10:PRINT "Start: ";:LOCATE 20,25:PRINT "End: ";:LOCATE 20,40:PRINT "Step: ";
     :LOCATE 20,55:PRINT "Total Pts: "
```

```
5410 '********************************************** SETUP FOR DATA TRANSFER
5420 OPEN "COM1:9600,N,8,1,LF" AS #1
5430 LOCATE 24,1
5440 LINE INPUT; "Select Option (T = Transfer; E = Exit): ", DUM$
5450 IF DUM$ = "T" OR DUM$ = "t" THEN GOTO 5460 ELSE CLOSE:RETURN
5460 LOCATE 24,1:PRINT "                                                                    ";
5470 LOCATE 24,1: LINE INPUT; "Enter -- Target File Name: ", FILE$
5480 FILENAME$ = "C:TEMP.RAW"
5490 TARGET$ = FILE$
5500 LOCATE 24,1:PRINT "                                                                    ";
5510 LOCATE 12,57: COLOR 0,7:PRINT "To: "+TARGET$:COLOR 7,0
5520 LOCATE 24,1:INPUT; "Enter -- Waveform #: ",NUM
5521 LOCATE 13,63:COLOR 15,0:PRINT NUM:COLOR 7,0
5525 LOCATE 24,1:PRINT "                                                                    ";
5526 LOCATE 24,1: LINE INPUT; "Select Origin (N = Normal; R = Reset): ",ORIG$
5528 IF ORIG$ = "R" OR ORIG$ = "r" THEN NUMERICS$ = "Reset" ELSE NUMERICS$ = "Normal"
5529 LOCATE 13,71:PRINT "      ":LOCATE 13,71:COLOR 15,0:PRINT NUMERICS$:COLOR 7,0
5530 '********************************************** RETRIEVE NORMALIZATION DATA
5540 SET$ = STR$( W(4,NUM) )
5550 PRINT #1, "N," + SET$
5560 INPUT #1,E$
5570 FOR I = 1 TO 11
5580 INPUT #1,N$(I)
5600 NEXT I
5610 INPUT #1,E$
5620 '************************************ CALCULATE NORMALIZATION PARAMETERS
5630 VNORM  = VAL( N$(5) )
5640 HNORM  = VAL( N$(6) )
5650 VZERO  = VAL( N$(7) )
5660 HZERU  = VAL( N$(8) )
5670 HZERL  = VAL( N$(9) )
5680 RVZERO = VAL( N$(10))
5690 RHZERO = VAL( N$(11))
5700 HZERT  = ( HZERU * 65536! ) + HZERL
5710 '********************************************** SPECIFY DATA TRANSFER LIMITS
5720 LOCATE 24,1:PRINT "                                                                    ";
5730 LOCATE 24,1:LINE INPUT; "Enter -- Starting Point # (C = Cursor Position): ",SRT$
5740 IF SRT$ = "c" OR SRT$ = "C" THEN 5750 ELSE 5840
5750 LOCATE 24,1:PRINT "                                                                    ";
5760 PRINT #1, "M,14"
5770 INPUT #1,E
5780 INPUT #1,E
5790 INPUT #1,VPOS
5800 INPUT #1,E
5810 VPOS = VPOS - 49664!
5820 SRT = VPOS/(15872/W(3,NUM))
5825 SRT = INT(SRT)
5830 GOTO 5850
5840 SRT = VAL(SRT$)
5845 SRT = INT(SRT)
5850 LOCATE 14,58:COLOR 15,0:PRINT SRT:COLOR 7,0
```

```
5860 LOCATE 24,1:PRINT '                                                              ";
5870 LOCATE 24,1:LINE INPUT; "Enter -- End Point (C = Cursor Position): ",ENDS$
5880 IF ENDS$ = "C" OR ENDS$ = "c" THEN 5890 ELSE 5980
5890 LOCATE 24,1:PRINT "                                                              ";
5900 PRINT #1, "M,14"
5910 INPUT #1,E
5920 INPUT #1,E
5930 INPUT #1,VPOS
5940 INPUT #1,E
5950 VPOS = VPOS - 49664!
5960 ENDS = VPOS / (15872 / W(3,NUM))
5965 ENDS = INT(ENDS)
5970 GOTO 5990
5980 ENDS = VAL(ENDS$)
5985 ENDS = INT(ENDS)
5990 LOCATE 14,70:COLOR 15,0:PRINT ENDS;:COLOR 7,0
6000 LOCATE 24,1:PRINT "                                                              ";
6010 LOCATE 24,1:INPUT; "Enter -- Step Size: ",STP
6011 LOCATE 15,57:COLOR 15,0:PRINT STP:COLOR 7,0
6012 TOT = INT(((ENDS - SRT) / STP)+1)
6014 LOCATE 16,62:COLOR 15,0:PRINT TOT:COLOR 7,0
6020 LOCATE 24,1:PRINT "                                                              ";
6030 LOCATE 24,1
6040 LINE INPUT; "Enter -- A to Abort; C/R to Continue: "; DUM$
6050 IF DUM$ = "a" OR DUM$ = "A" THEN :CLOSE:GOTO 5370
6054 COLOR 23,0
6055 LOCATE 19,18:PRINT "Transfering "
6058 COLOR 7,0:LOCATE 19,34:PRINT "  ":LOCATE 19,34:COLOR 15,0:PRINT NUM:COLOR 7,0
6059 LOCATE 19,42:PRINT "           "
6070 LOCATE 19,42:COLOR 15,0:PRINT TARGET$:LOCATE 19,63:PRINT "      ":LOCATE 19,63
     :PRINT NUMERICS$
6076 LOCATE 20,16:PRINT "       ":LOCATE 20,16: PRINT SRT
6077 LOCATE 20,29:PRINT "       ":LOCATE 20,29: PRINT ENDS
6078 LOCATE 20,45:PRINT "       ":LOCATE 20,45: PRINT STP
6079 LOCATE 20,65:PRINT "       ":LOCATE 20,65: PRINT TOT
6080 COLOR 7,0
6082 '********************************************** PREPARE FOR DATA TRANSFER
6090 XOFF$ = CHR$(19): XON$=CHR$(17)
6100 OPEN FILENAME$ FOR OUTPUT AS 2
6110 WN$ = STR$(NUM)
6120 ST$ = STR$(SRT)
6130 TPTS$ = STR$(TOT)
6140 SEP$ = STR$(STP)
6150 '************************************* SEND STRING TO BEGIN DATA TRANSFER
6160 PRINT #1,"D,0," + WN$ +","+ ST$ +","+ TPTS$ +","+SEP$
6170 INPUT #1,E
6180 '******************************************** XOFF/XON HANDSHAKING ROUTINE
6190 WHILE NOT EOF(1)
6200 COUNT = 0
6210 WHILE LOC(1) < 20  AND COUNT < 10
6220 COUNT = COUNT + 1
```

```
6230 WEND
6240 PRINT #1,CHR$(XOFF$)
6250 WHILE NOT EOF(1)
6260 D$ = INPUT$(LOC(1),#1)
6370 PRINT #2,D$;
6380 WEND
6390 PRINT #1,CHR$(XON$)
6400 WEND
6410 CLOSE #2
6420 '************************************************** NORMALIZATION ROUTIN
6425 OPEN FILENAME$ FOR INPUT AS 2
7000 OPEN TARGET$ FOR OUTPUT AS 3
7060 POINTNUM = SRT
7070 FOR I = 1 TO TOT
7080 INPUT #2,D$
7090 D = VAL(D$)
7094 IF NUMERICS$ = "Reset" THEN GOTO 7115
7100 TIME =  ( POINTNUM -  HZERT) * HNORM
7110 VOLTAGE = (D - VZERO) * VNORM
7114 GOTO 7120
7115 TIME = ( POINTNUM - RHZERO) * HNORM
7116 VOLTAGE = ( D - RVZERO ) * VNORM
7120 PRINT #3, USING "##.####^^^^";TIME;
7130 PRINT #3, "   ";
7140 PRINT #3, USING "##.####^^^^";VOLTAGE
7150 POINTNUM = POINTNUM + STP
7160 NEXT I
7170 CLOSE #3
7180 CLOSE #2:LOCATE 24,1:PRINT "                                                                    ";
7190 KILL FILENAME$
7200 CLOSE #1
7210 LOCATE 19,18:COLOR 15,0:PRINT "Complete !    ":COLOR 7,0
7220 LOCATE 24,1:LINE INPUT; "More ? ",DUM$
7230 IF DUM$ = "YES" OR DUM$ = "yes" OR DUM$ = "Y" OR DUM$ = "y" THEN LOCATE 19,18
     :COLOR 15,0:PRINT "Previous       ":COLOR 7,0:GOTO 5370
7240 RETURN
```

**Program 2.** Program 2 consolidates and scales raw TGA data files. The two data files, mass and temperature, transferred using Program 1 are converted into a single file containing mass and temperature data. The program computes $\alpha$, $\tau$, and $1/T$.

```
      PROGRAM TGA
C *** ***************************************************************************
C     This program converts and consolidates raw TGA data, acquired on a      *
C     digital oscilloscope, and produces a file containing mass, fraction     *
C     remaining, or fraction decomposed, as a function of time, or            *
C     temperature.                                          Version 31 Jan 86 *
C *** ***************************************************************************

      INTEGER      FLAG, FLAG1
      REAL         MTIME,MASS,MASS0,LMASS,OMALFA
      CHARACTER*14 FNOUT,FNMASS,FNTDEGC
      CHARACTER*14 DUMMY

      CALL CLEAR

      FLAG         = 0
      FLAG1        = 0

      WRITE(*,'(A,//)') ' * TGA:  Nicolet Mass-Temperature Data Conversi
     1on and Consolidation - 31Jan86 *'
      WRITE(*,'(A\)') ' Enter Mass Data File Name: '
      READ(*,'(A)') FNMASS
      WRITE(*,'(A\)') ' Enter Mass Scale Factor: '
      READ(*,*) SFMASS
      WRITE(*,'(A\)') ' Enter Temperature Data File Name: '
      READ(*,'(A)') FNTDEGC
      WRITE(*,'(A\)') ' Enter Temperature Scale Factor: '
      READ(*,*) SFTEMP
      WRITE(*,'(A\)') ' Enter Output  File Name: '
      READ(*,'(A)') FNOUT


      OPEN(3,FILE=FNOUT, STATUS = 'NEW' )
   50 OPEN(1,FILE=FNMASS,STATUS = 'OLD')
      OPEN(2,FILE=FNTDEGC,STATUS = 'OLD')


  100 READ(1,*,END=200) MTIME,MASS
      READ(2,*) TTIME,TDEGC

      MASS         = MASS * SFMASS
      TDEGC        = TDEGC * 1.E+3

      IF(TTIME .NE. MTIME) THEN
```

```
      WRITE(*,'(A)') ' WARNING *** TIME MISSMATCH  '
      ENDIF

      IF (FLAG  .EQ. 0) THEN
      MASS0       = MASS
      FLAG        = 1
      ENDIF

      IF(FLAG1 .EQ. 1) THEN
      ALFA        = (MASS0 - MASS) / (TOTAL)
      OMALFA      = 1. - ALFA
      TDEGK       = TDEGC + 273.15
      WRITE(3,105) TTIME,TDEGK,MASS,ALFA,OMALFA
  105 FORMAT(1X,F7.2,3X,F7.2,3X,F9.4,3X,F12.7,3X,F12.7)
      ENDIF

      GOTO 100

  200 IF(FLAG1 .EQ. 0) THEN
      LMASS       = MASS
      TOTAL       = MASS0 - LMASS
      FLAG1       = 1
      CLOSE(1)
      CLOSE(2)
      GOTO 50
      ENDIF

      CLOSE(1)
      CLOSE(2)
      CLOSE(3)

      STOP 'NORMAL Program Termination'

      END
```

**Program 3.** Program 3 consolidates and scales raw VTGA data files. The two data files, mass and temperature, transferred using Program 1 are converted into a single file containing mass and temperature data. The program computes $\alpha$, $\tau$, and $1/T$. Voltage readings from the temperature data file are converted to Temperature using a ninth-degree polynomial from Ref. [ ].

```
      PROGRAM VTGA
* *** ************************************************************************
*     This program converts VTGA millivolt readings to fraction decomposed,  *
*     α, and temperature.  The conversions are based on the assumptions that *
*     the VTGA mass calibration is linear and that thermocouple outputs      *
*     correspond to the type-E tables.  R. J. Powers  Version: 9Feb86        *
* *** ************************************************************************

      INTEGER      PTNO, I
      REAL         MTIME,TTIME,TIME,MVOLTS,MTVOLTS,MVOLT0,MVOLT1,ALFA
      REAL         DELTA
      CHARACTER*14 FNOUT,FNMASS,FNTEMP

      CALL CLEAR
      WRITE(*,'(A)') ' * VTGA Mass-Temperature Data Conversion and Conso
     lidation-9Feb86*'

      WRITE(*,*)
      WRITE(*,*)

* *** Initialization ***
      WRITE(*,'(A\)') ' Enter Mass Data File Name <fname.ext> : '
      READ(*,'(A)') FNMASS
      WRITE(*,'(A\)') ' Enter Temperature Data File Name <fname.ext> : '
      READ(*,'(A)') FNTEMP
      WRITE(*,'(A\)') ' Enter Output  File Name <fname.ext> : '
      READ(*,'(A)') FNOUT
      WRITE(*,'(A\)') ' Enter Thermocouple Amplification Factor: '
      READ(*,*) AMPFACT

      OPEN(3,FILE=FNOUT, STATUS = 'NEW' )
      OPEN(1,FILE=FNMASS,STATUS = 'OLD')
      OPEN(2,FILE=FNTEMP,STATUS = 'OLD')

* *** Find Max-Min Values of the Mass Voltage Values ***
      READ(1,*) MTIME,MVOLTS
      MVOLT0      = MVOLTS
      MVOLT1      = MVOLTS
      I           = 1

   40 READ(1,*,END=50) MTIME, MVOLTS
```

```
      IF( MVOLTS .LT. MVOLT0 ) MVOLT0 = MVOLTS
      IF( MVOLTS .GT. MVOLT1 ) MVOLT1 = MVOLTS
      I           = I + 1
      GOTO 40

*  *** Number of Data Points and Mass Voltage Change
   50 PTNO        = I
      DELTA       = MVOLT1 - MVOLT0
      CLOSE(1)
      OPEN(1,FILE=FNMASS,STATUS = 'OLD')

*  *** Read Voltages and Convert to Alfa, Gamma, and Temperature
      DO 100     I = 1, PTNO
      READ(1,*) MTIME, MVOLTS
      READ(2,*) TTIME, TVOLTS

      IF(TTIME .NE. MTIME) THEN
      WRITE(*,'(A)') ' WARNING *** TIME MISSMATCH  '
      ELSE
      TIME        = TTIME
      ENDIF

*     Convert mVolt Readings to Alfa, Gamma, And Temperature
      ALFA        = ( MVOLTS -  MVOLT0 ) / DELTA
      GAMMA       = 1.0 - ALFA
      CALL TEMP(TVOLTS,AMPFACT,MTVOLTS,TDEGC)
      TDEGK     = TDEGC + 273.15
*  *** Send Output to Data File ***
      WRITE(3,90) TIME,MTVOLTS,TDEGC,TDEGK,MVOLTS,ALFA,GAMMA
   90 FORMAT(1X,F9.2,2X,F9.4,2X,F7.2,2X,F7.2,2X,1PE12.4,2X,0PF10.6,
     1       2X,F10.6)
  100 CONTINUE

      CLOSE(1)
      CLOSE(2)
      CLOSE(3)

      STOP 'NORMAL Prograa Terainatian'
      END

      SUBROUTINE TEMP(TEMPVOLTS,AMPFACT,MVOLTS,TDEGC)
*  *** ***************************************************************************
*     This Subroutine converts VOLTS from a type-E thermocouple and returns    *
*     mVolts (MVOLTS) and temperatrue in Deg. C. (TDEGC); an amplification     *
*     factor (AMPFACT) must also be supplied.                                  *
*****************************************************************************
      REAL MVOLTS
      DIMENSION A(10)

*  *** Polynomial Coefficients
      DATA A /0.,104967248.,17189.45282,-282639.0850,12695339.5,-448703084
```

```
1.0,1.108e6D+10,-1.76807D+11,1.71842D+12,-9.19278D+12,2.0e132D+13/

 MVOLTS       = (TEMPVOLTS/AMPFACT) * (1.0E+3)
 X            = TEMPVOLTS/AMPFACT

 TDEGC = (A(1) + X*(A(2) + X*(A(3) + X*(A(4) + X*(A(5) + X*(A(6) +
1X *(A(7) + X*(A(8) + X*(A(9) + A(10)*X)))))))))

 RETURN
 END
```

**Program 4.** This program operates on the output data file of Program 2 or 3 and converts these into "Coats & Redfern coordinates" from which Arrhenius parameters may be extracted using Program 5.

```
      PROGRAM CR
C *** ***************************************************************************
C     The following program reduces TGA data using the algorithm of Coats &  *
C     Redfern. [35,42] Required inputs are Temperature, T, and the fraction   *
C     decomposed, α. Outputs are: data point number, input data, the C&R      *
C     coordinates, and the zero order ordinate.  R. J. Powers Version 29JAN86 *
C *** ***************************************************************************


      REAL*8       T,ALFA,ALFA1,ALFA2,COLUMN,X,Y,N,Z
      INTEGER      NN,ACOL,TCOL,NCOL
      CHARACTER*14 FNDATA,FNOUT
      DIMENSION    T(1000),ALFA(1000),COLUMN(12),X(1000),Y(1000),Z(1000)
      DATA         NN /0/

      CALL CLEAR

      WRITE(*,'(A,//)') ' *** Coats and Redfern Kinetic Analysis - 31Jan
     186 *** '
      WRITE(*,'(A\)') ' Enter Input Data File Name:  '
      READ(*,'(A)') FNDATA
      WRITE(*,'(A\)') ' Enter Reaction Order:  '
      READ(*,*) N
      WRITE(*,'(A\)') ' Enter - # columns, T column, alfa column: '
      READ(*,*) NCOL,TCOL,ACOL
      WRITE(*,'(A\)') ' Enter Initial α: '
      READ(*,*) ALFA1
      WRITE(*,'(A\)') ' Enter  Final  α: '
      READ(*,*) ALFA2
      WRITE(*,'(A\)') ' Enter Output File Name:  '
      READ(*,'(A)') FNOUT

      OPEN(3,FILE = FNDATA, STATUS = 'OLD')
      OPEN(4,FILE = FNOUT, STATUS = 'NEW')

      I            = 1
  608 READ(3,*,END = 700) (COLUMN(J), J = 1, NCOL)
      IF (COLUMN(ACOL) .LE. ALFA1 .OR. COLUMN(ACOL) .GE. ALFA2) GOTO 608
      NN           = NN + 1
      ALFA(I)      = COLUMN(ACOL)
      T(I)         = COLUMN(TCOL)
      I            = I + 1
      GOTO 608

  700 CONTINUE
```

```
      IF( N .EQ. 1.D0 ) THEN
      CALL ORDER1( T,ALFA,NN, X,Y,Z )
      ELSE
      CALL ORDERN( T,ALFA,NN,N,  X,Y,Z )
      ENDIF

      WRITE(*,77) NN,ALFA1,ALFA2
   77 FORMAT(1X,/,I4,' Data Points Read between α = ',F6.3,' and α = ',
     1F6.3,/)
      DO 35 I = 1,NN
      WRITE(4,37) I,T(I),ALFA(I),X(I),Y(I),Z(I)
   37 FORMAT(1X,I3,4X,F7.2,4X,F8.3,4X,1PD12.4,4X,1PD12.4,4X,1PD12.4)
   35 CONTINUE

      CLOSE(3)
      CLOSE(4)
      STOP ' NORMAL Program Termination'
      END

      SUBROUTINE ORDER1( T,ALFA,NN, X,Y,Z )
*** ****************************************************************************
*          Variable List                                                       *
*              X         = First order C&R abscissa                            *
*              Y         = First order C&R ordinate                            *
*              Z         = Zero order C&R ordinate                             *
*** ****************************************************************************
      REAL*8       T,ALFA,X,Y,Z
      DIMENSION    T(1000),ALFA(1000),X(1000),Y(1000),Z(1000)

      DO 10    I = 1,NN
      Y(I)       = DLOG( ( -DLOG(1.D0 - ALFA(I)) ) / (T(I)** 2.D0)  )
      X(I)       = 1.D0 / T(I)
      Z(I)       = DLOG( ALFA(I) / ( T(I)**2.D0 ) )
   10 CONTINUE

      RETURN
      END


      SUBROUTINE ORDERN( T,ALFA,NN,N, X,Y,Z )
*** ****************************************************************************
*          Variable List                                                       *
*              X         = Nth order C&R abscissa                              *
*              Y         = Nth order C&R ordinate                              *
*              Z         = Zero order C&R ordinate                             *
*** ****************************************************************************
      REAL*8       T,ALFA,X,Y,N,Z
      DIMENSION    T(1000),ALFA(1000),X(1000),Y(1000),Z(1000)
```

```
      DO 10      I = 1,NN
      Y(I)    = DLOG(   ( 1.D0 - ( (1.D0 - ALFA(I)) ** (1.D0 - N) )  )
     1                / (( 1.D0 - N ) * ( T(I) ** 2.D0 ))              )
      X(I)         = 1.D0 / T(I)
      Z(I)         = DLOG( ALFA(I) / ( T(I)**2.D0 ) )
   10 CONTINUE

      RETURN
      END
```

**Program 5.** This program calculates Arrhenius parameters from the output of Program 4.

```
      PROGRAM CREA
C *** ****************************************************************
C     This program calculates global Arrhenius parameters from C&R    *
C     data by fitting a least squares line to the values.             *
C     Input data are the recriprocal of the temperature and the C&R   *
C     ordinate. Outputs are the global activation energy, pre-        *
C     exponential, and the corrolation coefficient for the fit.       *
C                                                                     *
C     Author: R. J. Powers                          Version:  1 Feb 86 *
C *** ****************************************************************

      REAL*8       COLUMN,X,Y,RATE,E,A,M,B,R,TRUNC,ALPHA1,ALPHA2,A1,A2
      REAL*8       XTEN,XSTART,XEND,YSTART,YEND,LEN,T1,T2
      INTEGER      ACOL,XCOL,YCOL,NCOL,NUM
      CHARACTER*1  REPLY
      CHARACTER*14 FNDATA,FNOUT
      DIMENSION    COLUMN(12),X(500),Y(500)
      CALL CLEAR

      WRITE(*,'(A,//)') ' *** Coats and Redfern: Arrhenius Parameters -
     11Feb86 ***'

      WRITE(*,'(A\)') ' Enter Input Data File Name:  '
      READ(*,'(A)') FNDATA
      WRITE(*,'(A\)') ' Enter Heating Rate (°K/sec):  '
      READ(*,*) RATE
      WRITE(*,'(A\)') ' Enter - # columns, α col, 1/T col(1/°K), C&R ord
     1 col: '
      READ(*,*) NCOL,ACOL,XCOL,YCOL
      WRITE(*,'(A\)') ' Enter Initial α : '
      READ(*,*) ALPHA1
      WRITE(*,'(A\)') ' Enter Final α :  '
      READ(*,*) ALPHA2

      OPEN(3,FILE = FNDATA, STATUS = 'OLD')

      I            = 0
  700 READ(3,*,END=701) (COLUMN(J), J = 1, NCOL)
      IF ( COLUMN(ACOL) .LT. ALPHA1 .OR. COLUMN(ACOL) .GT. ALPHA2 )
     1   GOTO 700

      I            = I + 1
      IF(I .EQ. 1) A1 = COLUMN(ACOL)
      IF(I .EQ. 1) T1 = COLUMN(2)
      X(I)         = COLUMN(XCOL)
      Y(I)         = COLUMN(YCOL)
      A2           = COLUMN(ACOL)
```

```
      T2          = COLUMN(2)
      GOTO 700

  701 NUM         = I
      WRITE(*,38) NUM,A1,A2
   38 FORMAT(1X,/,I3,' Data Points Read between α = ',F7.3,' and α = ',
     1       F7.3)
      WRITE(*,39) T1,T2
   39 FORMAT(1X,  3X,'                          T = ',F7.1,' and T = ',
     1       F7.1,/)
      CALL LINFIT(X,Y,NUM, M,B,R)

      E           = M * (-1.987D0)
      TRUNC       = ( 1.D0 - ( (2.D0 * 1.987 * (1.D0/X(NUM))) / E ) )
      A           = DEXP(B) * RATE * E  / ( 1.987D0 * TRUNC )

      WRITE(*,800) E
  800 FORMAT(1X,'E = ',2PD12.4)
      WRITE(*,810) A
  810 FORMAT(1X,'A = ',1PD12.4)
      WRITE(*,820) R
  820 FORMAT(1X,'R = ',1PD12.4)

      WRITE(*,'(/,A\)') ' Generate This Line (Y/N) ? '
      READ(*,'(A)') REPLY
      IF( REPLY .EQ. 'y' .OR. REPLY .EQ. 'Y' ) THEN
      WRITE(*,'(A\)') ' Enter Output File Name (fname.ext): '
      READ(*,'(A)') FNOUT
      OPEN(5,FILE=FNOUT,STATUS='NEW')

      XTEN        = 0.0D0
      WRITE(*,'(A\)') ' Enter Extension Factor (%): '
      READ(*,*) XTEN

      XTEN        = XTEN /1.0D2
      LEN         = DABS( X(NUM) - X(1))
      XSTART      = DMIN1( X(NUM), X(1) )
      XEND        = DMAX1( X(NUM), X(1) )
      XSTART      = XSTART - ( LEN * XTEN )
      XEND        = XEND   + ( LEN * XTEN )
      YSTART      = B + ( M * XSTART )
      YEND        = B + ( M * XEND   )
      WRITE(5,17) XSTART, YSTART
      WRITE(5,17) XEND,YEND
   17 FORMAT(1X,1PE11.4,5X,E11.4)
      CLOSE(5)
      ENDIF


      CLOSE(3)
      STOP ' NORMAL Termination'
```

```
      END


      SUBROUTINE LINFIT(X,Y,NN, M,B,R)
*  ***  ********************************************************************
*     The following subroutine fits the best straight line to a given  *
*     set of "NN" data points. Input data is contained in arrays X and *
*     Y; the outputs are the slope, the Y-intercept, and the           *
*     correlation coefficient - M,B,R respectively.                    *
*                                                                      *
*          Variable List                                               *
*                                                                      *
*              R         = Correlation Coefficient                     *
*              B         = Intercept                                   *
*              M         = Slope                                       *
*              SUMX      = Sum of X                                    *
*              SUMY      = Sum of Y                                    *
*              SUMXY     = Sum of X*Y                                  *
*              SUMX2     = Sum of X**2                                 *
*              SUMY2     = Sum of Y**2                                 *
*                                                                      *
*  ***  ********************************************************************

      REAL*8 X,Y,M,B,R,DUMY,SUMX,SUMY,SUMX2,SUMY2,SUMXY,A
      INTEGER NN
      DIMENSION X(500),Y(500)

      SUMX      = 0.0D0
      SUMY      = 0.0D0
      SUMXY     = 0.0D0
      SUMX2     = 0.0D0
      SUMY2     = 0.0D0

      DO 100 I  =1,NN
      SUMX      = SUMX + X(I)
      SUMY      = SUMY + Y(I)
      SUMX2     = SUMX2 + ( X(I) * X(I) )
      SUMY2     = SUMY2 + ( Y(I) * Y(I) )
      SUMXY     = SUMXY + ( X(I) * Y(I) )
  100 CONTINUE

      DUMY      = DBLE(NN)
      A         = SUMX2 * DUMY - (SUMX * SUMX)
      B         = (SUMX2 * SUMY - SUMX * SUMXY ) / A
      M         = (SUMXY * DUMY - SUMX*SUMY )/ A
      R         = (B * SUMY + M * SUMXY - SUMY * SUMY /DUMY)/
     1            (SUMY2 - (SUMY * SUMY/DUMY))

      RETURN
      END
```

## REFERENCE LIST

1. Hermance, C. F., "A Model of Composite Propellant Combustion Including Surface Heterogeneity and Heat Generation," AIAA J., 4(9), 1966, pp. 1629 - 1637.

2. Glick, R.L., "On the Statistical Analysis of Composite Solid Propellant Combustion," AIAA J., 12(3), 1976, pp. 384-385.

3. Cohen, N. S., Price, C. F., and Strand, L. D., "Analytical Model of the Combustion of Multicomponent Solid Propellant Combustion Based on Multiple Flames," AIAA J., Paper 77-927, July, 1977.

4. Beckstead, M. W., Derr, R. L., and Price, C. F., "A Model of Composite Solid Propellant Combustion Based on Multiple Flames," AIAA J., 8(12), 1970, pp. 2200 - 2207.

5. Flanagan, J. E. and Oberg, C. L., "A Modified Two Stage Flame Model of Steady-State Composite Solid Propellant Combustion," Report 59-017, Rocketdyne Div., Rockewell International Corp., Canoga Park, Calif., Sept 1970.

6. Cohen, N. S., "Review of Composite Burn Rate Modeling," AIAA J., 18(3), 1980, pp. 277 - 293.

7. Lengelle, G., "Thermal Degradation Kinetics and Surface Pyrolysis of Vinyl Polymers," AIAA J., 8(11), 1970, pp. 1989 - 1996.

8. Wilfong, R. E., Penner, S. S., Daniels, F., "An Hypothesis for Propellant Burning," J. Phys. Chem., 54, 1950, pp. 863 - 872.

9. Houser, T. J., "Kinetics of Polymer Pyrolysis from Surface Regression Rates," J. Chem. Phys., Vol. 45, No. 3, 1966, pp. 1031 - 1037.

10. Baer, A. D., Hedges, J. H., Seader, J. D., Jayakar, K. M., Wojcik, L. H., "Polymer Pyrolysis over a Wide Range of Heating Rates," AIAA J., 15(10), 1977, pp. 1398 - 1404.

11. Sabadell, A. J., Wenograd, A. J., and Summerfield, M., "Measurement of Temperature Profiles through Solid Propellant Flames Using Fine Thermocouples," AIAA J., 3(9), 1965, pp. 1580 - 1584.

12. Fenimore, C. P. , and Martin, F. J., "Burning of Polymers", The Mechanisms of Pyrolysis, Oxidation, and Burning of Organic Materials, Nat. Bur. Standards Spec. Pub. 357, 1972, pp. 159 - 170.

13. Williams, F. A., Combustion Theory, Benjamin/Cummings Pub. Co, Menlo Park, 1985.

14. Bouck, L. S., Baer, A. D., and Ryan, N. W., "Pyrolysis and Oxidation of Polymers at High Heating Rates," Fourteenth Symposium (International) on Combustion, The Combustion Institute, Pittsburgh, Pa., 1973, pp. 1139 - 11499.

15. Farre-Ruis, F. and Guichon, G., "On the Conditions of Flash Pyrolysis of Polymers as used in Pyrolysis-Gas Chromatography," Anal. Chem., 40(6), 1968, pp. 998 -1000.

16. Wall, L. A., "Pyrolysis of Polymers," The Mechanisms of Pyrolysis, Oxidation, and Burning of Organic Materials, Nat. Bur. Standards Spec. Pub. 357, 1972, pp. 47 - 60.

17. Madorsky, S. L., Thermal Degradation of Organic Polymers, Interscience, New York, 1964, pp. 293 - 303.

18. Baer, A. D., "Pyrolysis of Polymer Films in Air at High Temperatures and at High Heating Rates," J. of Fire & Flammability, 12(7), 1981, pp. 214 - 228.

19. Kohn, S., "Experimental Techniques of Studying Pyrolysis of High Polymers Subjected to Rapid Heating," (Translation from: La Recherche Aeronautique, 88, 1962),NASA-TT F-11,283, 1967, pp. 1 - 22.

20. Hedges, J. H., Baer, A. D., and Ryan, N. W., "Pyrolysis and Ignition of Polymers under Approximated Fire Conditions," Seventeenth Symposium (International) on Combustion, The Combustion Institute, 1978, pp. 1173 - 1181.

21. Shannon, L. J., and Erickson, J. E., "Thermal Decomposition of Composite Solid Propellant Binders," Sixth ICRPG Combustion Conference, CPIA Publication No. 192, 1969, pp. 519 - 530.

22. McAlevy III, R. F., Lee, S. Y., and Smith, W. H., "Linear Pyrolysis of Polymethylmethacrylate," J. AIAA, Vol. 6, No. 6, 1968, pp. 1137 -1142.

23. Coates, R. L., "Linear Pyrolysis Rate Measurements of Propellant Constituents," J. AIAA, Vol. 3, No. 7, 1965, pp. 1257 - 1261.

24. Mc Alevy III, R. F., and Blazowski, W. S., "The Surface Pyrolysis Boundary Condition for the Combustion of Polymers," The Mechanisms of Pyrolysis, Oxidation, and Burning of Organic Materials, Nat. Bur. Standards Spec. Pubb. 357, 1972, pp. 185 - 192.

25. Cohen, N. S., Fleming, R. W., and Derr, R. L., "Role of Binders in Solid Propellant Combustion," AIAA J., Vol. 12, No. 2, 1974, pp. 212 - 218.

26. Schultz, R. D., and Dekker, A. O., " ," Fifth Symposium (International) on Combustion, Reinhold Pub. Corp., New York, 1955, pp. 260 - 267.

27. Barsh, M. K., Andersen, W. H., Bills, K. W., Moe, B., and Schultz, R. D., "Improved Instrument for the Measurement of Linear Pyrolysis Rates of Solids," Rev. of Sci. Instru., Vol. 29, No. 5, 1958, pp. 392 - 395.

28. Chaiken, R. F., Andersen, W. H., Barsh, M. K., Mishuck, E., Moe, G., and Schultz, R. D., "Kinetics of the Surface Degradation of Polymethylmethacrylate," J. of Chem. Phys., Vol. 32, No. 1, 1960, pp. 141 - 146.

29. Blazowski, W. S., Cole, R. B., and McAlevy III, R. F., "Linear Pyrolysis of Various Polymers Under Combustion Conditions," Fire and Explosion, ( ), pp. 1177 - 1186.

30. Hansel, J. G., and McAlevy III, R. F., "Energetics and Chemical Kinetics of Polystyrene Surface Degradation in Inert and Chemically Reactive Environments," AIAA J., Vol. 4, No. 5, 1966, pp. 841 - 848.

31. Gontkovskaya, V. T., Ozerkovskaya, N. I., Barzykin, V. V., and Pestrikov, S. V., "Special Characteristics of Nonisothermal Processes in Systems with Parallel Reactions with Linear Heating," Fizika Goreniya i Vzryva, Vol. 14, No. 6, 1978, pp. 92 -96, (Translated Plenum Pub. Co. 00010-5082/78/1406-0776)

32. Gontkovskaya, V. T., Ozerkovskaya, N. I., Barzykin, V. V., and Pestrikov, S. V., "Progress of Sequential Reactions Under linear Heating Conditions," Fizika Goreniya i Vzryva, Vol. 16, No. 1, 1980, pp. 63 -68. ( Translated Plenum Pub. Co. 0010-5082/80/1601-0058 )

33. Gontkovskaya, V. T., Kolpakov, V. A., "Nonisothermal Processes in a System with Serial and Parallel Reactions Under Conditions of Linear Heating," Fizika Gorenia i Vzryva, Vol. 8, No. 3, 1982, pp. 63 - 68. ( Translated

Pleenum Pub. Co. 0010-5082/82/1803-0315 )

34. Rogers, R. N., "Differential Scanning Calorimetric Determination of Kinetic Constants of Systems that Melt with Decomposition," Thermochemica Acta, 3, 1972, pp. 437 - 447.

35. Coats, A. W. and Redfern, J. P., "Kinetic Parameters from Thermogravimetric Data," Nature, 201(1), 1964, pp. 68 - 69.

36. Tang, T. B., "Kinetic Functions Can Not be Determined from Analysis of Dynamic Data," Thermochimica Acta, 58, 1982, pp. 373 - 377.

37. Flyn, J. H., and Wall, L. A., "General Treatment of the Thermogravimetry of Polymers," J. Research Nat. Bur. Standards - A Physics and Chemistry, 70a(6), 1966, pp. 487 - 523.

38. Rainville, E. D., Special Functions, Macmillan, New York, 1960.

39. Reich, L. and Stivala, S. S., "Kinetic Parameters from Thermogravimetric Curves," Thermochimica Acta, 24, 1978, pp. 9 - 16.

40. Reich, L. and Stivala, S. S., "Computer Determined Kinetic Parameters from TG Curves," Thermochimica Acta, 36, 1980, pp. 103 - 105.

41. House Jr., J. E., "A General Iterative Method for Obtaining Kinetic Parameters from TG Data," Thermochemica Acta, 57, 1982, pp. 47 - 55.

42. Earnst, C. M., "Modern Thermogravimetry," Analytical Chemistry, 56(13), 1984, pp. 4471A - 1486A.

43. Gast, Th. and Jakobs, H., "A Measuring Method for the Simultaneous Observation of Mass and Heat Capacity with the Aid of Vibrations," Proceedings of the Second European Symposium on Thermal Analysis, ed D. Dollimore, Hayyden, London, 1981.

44. Gast, Th. and Jakobs, H., "Gedanken zur Gleichzeitigen Beobachtung von Masse - und Enthalpieanderungen mit Hilfe von Schwingungen," Acta Imeko, 1973, pp. 303 -310.

45. Oertli, Ch., Buhler, Ch., and Simon, W., "Curie Point Pyrolysis Gas Chromatography Using Ferromagnetic Tubes as Sample Supports," Chromatographia, 6(12), 1973, pp. 499 -

502.

46. Lehrle, R. S., "Micropyrolysis Gas-Liquid Chromatography," Laboratory Practice, 17(6), 1967, pp. 696 - 717.

47. Barlow, A., and Lehrle, R. S., Robb, J. C., and Sunderland, D., "PMMA Degradation, Kinetics and Mechanisms in the Temperature Range 340 C to 460 C," Polymer, 8, 1967, pp. 537 - 545.

48. American Society for Testing and Materials, Manual on the Use of Thermocouples in Temperature Measurement, STP 470B, ASTM, Baltimore, 1982.

49. Omega, Temperature Measurement Handbook and Encyclopedia, Omega Engineering Inc., Stamford, CT, 1985, p. T-12.

50. Ninan, K. N. and Krishnan, "Thermal Decomposition Kinetics of Polybutadiene Binders," J. Spacecraft, 19, No. 1, 1982, pp. 92 -94.

51. Price, E. W., "Comment on 'Thermal Decomposition of Polybutadiene Binders'," J. Spacecraft, Vol. 20., No. 3, 1983, p. 320.

52. Strahle, W. C. and Varney, M. M., "Thermal Decomposition Studies of Some Solid Propellant Binders," Combustion & Flame, 16, 1971, pp. 1 - 8.

53. Coats, A. W., and Redfern, A. W., "Thermogravimetric Analysis," Analyst, Vol. 88, 1963, pp. 906 - 924.

54. Waesche, R. H. W., "Research Investigation of the Decomposition of Composite Solid Propellants," United Aircraft Corp. Rept. G910476-24, 1968.

55. Solymosi, F., Structure and Stability of Salts of Halogen Oxyacids in the Solid Phase, John Wiley & Sons, New York, 1977.

56. Buhler Ch. and Simon W., "Curie Point Pyrolysis Gas Chromatography," J. Chromatographic Sci., 8(6), 1970, pp. 323 - 329.

57. Davies, J. and Simpson, P., Induction Heating Handbook, Mc Graw-Hill, Maidenhead, 1979.

58. Simon, W. and Gaiacobbo, H.,, "Thermal Fragmentation and Determination of the Structure of Organic Compounds," Angew. Chem. internat. edit., 4(11), 1965, pp. 938 - 943.

59. Coats, A. W., and Redfern, J. P., "Kinetic Parameters from Thermogravimetric Data II," Polymer Letters, Vol. 3., 1965, pp. 917 - 920.

# VITA

Robert J. Powers was born in Brooklyn, New York on the 25th of July, 1947. His secondary schooling was at La Salle Academy in Manhattan, after which he went on to earn a Bachelor of Science degree in Chemistry from the University of Dayton. Upon graduation in 1970, he joined the United States Air Force with whom he served for nine and one-half years. During that time he was attached to the United States Air Force Armament Laboratory, at Eglin AFB, Florida, where he held the positions of R&D Propellant Chemist, and subsequently Acting Chief of the Interior Ballistics Laboratory. He joined the Georgia Institute of Technology in the Fall of 1980 and earned a Master of Science in Aerospace Engineering in the Spring of 1982. He has recently accepted a position as a Principal Scientist with Atlantic Research Corporation of Alexandria, Virginia, where he hopes to pursue a career in rocketry and solid propellant technology. Mr. Powers is currently a chemist in the United States Air Force Reserves where he holds the rank of Major. He is married to Virginia McSherry of Tulsa, Oklahoma, and is the proud father of Erin, and Ryan.

*COMBUSTION AND FLAME* 63: 381-413 (1986)



# Combustion of Ammonium Perchlorate-Polymer Sandwiches

**E. W. PRICE, J. K. SAMBAMURTHI, R. K. SIGMAN, and R. R. PANYAM**

*School of Aerospace Engineering, Georgia Institute of Technology, Atlanta, GA 30332*

A series of experimental studies of combustion of sandwiches is reported, and the results are used to develop a relatively detailed qualitative model for the combustion zone microstructure.

## INTRODUCTION

The combustion of composite solid rocket propellants takes place in a thin region close to the surface of the propellant. The thickness of this region is dictated by the necessity to transfer heat back to the solid at a rate sufficient to maintain the rate of pyrolysis at the surface required in applications of the propellant. This in turn dictates that the scale of heterogeneity (usually set by oxidizer particle size) be small enough for fuel and oxidizer vapors to mix in the thin region near the surface. In practice, the dimensional scale turns out to be of order 100 $\mu$m, a scale encompassing an intricate flame complex (e.g., Ref. [1]). Experimental observation on such a dimensional scale is virtually impossible, a circumstance that has led to a rather speculative quality of research and literature on combustion mechanisms. The situation is further complicated by the uncertain relevance of flame theory when applied to such small, geometrically and chemically complicated flame systems.

A strategy to alleviate some of the experimental difficulties of observation is to study combustion of geometrically simple systems such as the oxidizer-binder sandwich. By edge burning these laminate structures, the combustion zone often conforms to a two-dimensional steady state configuration, hopefully amenable to more meaningful observation and theoretical interpretation. If this goal is achieved, then at least some aspects of the more complex propellant combustion problem can be clarified. Unfortunately, the microcombustion zone is still substantially inaccessible to experimental observation, even in the geometrically simple systems, so the strategies for research are still less direct than would be desired, and results correspondingly more speculative. One exception to the limitations of spatial resolution in measurements is the quench-burning experiment, which permits leisurely study of the surface of a quenched sample under high magnification (Fig. 1). Such experiments typically interrupt burning very abruptly by rapid depressurization of the combustor. While some artifacts are produced by the quench event, the details of the burning surface microstructure are largely preserved and can be used in combination with other information to infer combustion zone structure.

The sandwich approach has been used by many investigators (e.g., Powling [2], Highto-



0010-2180/86/$03.50

Appendix B

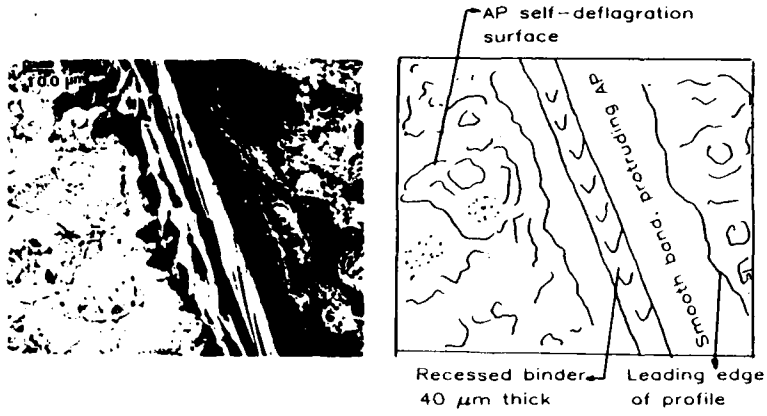


Fig 1 Surface of a quenched "sandwich" of AP-PBAN-AP laminae (region of surface near binder lamina)

wer and Price [3, 4], Boggs et al. [5], Netzer et al. [6, 7], Nadaud [8], Ermolaev et al. [9]). It has become evident in recent work [10, 11] that relevance to propellant combustion requires that binder laminae in sandwiches be very thin (to avoid anomalous effects such as binder melt flow that would not occur with high solids AP-HC binder propellants). It is also important that interpretation of results address observations near enough to the oxidizer-binder interfaces to correspond to situations possible on propellant surfaces (where the surfaces of exposed oxidizer particles are typically 100 μm across). In hindsight, these considerations may seem obvious, but a significant amount of published work on sandwiches of propellant ingredients has addressed either situations or aspects of results that were only marginally relevant to conventional propellants. The present studies, involving sandwiches of ammonium perchlorate and typical hydrocarbon binders, used primarily sandwiches with binder laminae of 10–100 μm thickness.

Earlier tests [3, 5, 10, 11] had shown certain critical features of quenched thin binder sandwiches of interest, which are summarized here so they can be used in interpretation of results:

1. The larger features of surface profiles are shown in Fig. 2 (see Refs. [10–12]). The figure shows that the AP self-deflagration is slower than the propagation in the

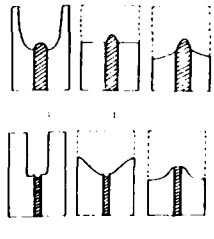

Fig 2 Surface profiles of AP polymer sandwiches a–c, 150 μm binder, d–f, 50 μm binder a, d 0.7 MPa, b, e 3.5 MPa, c, f 10 MPa

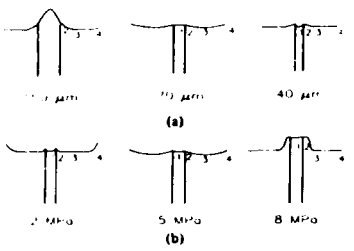


Fig. 3 Details of surface profiles in the region near the lamina interface planes. (a) Effect of binder thickness at 5 MPa. (b) Effect of pressure for 70 μm binder lamina.

"sandwich" region at low pressures (Fig. 2a,d,e), and that the AP self-deflagration leads the burning front at the high end of the pressure range tested (e.g., 8.5-14 MPa), implying that the oxidizer-fuel (O-F) flame is important to steady state burning at low pressure. The figure also shows that thick binder laminae tend to protrude above the adjoining AP, indicating that the central parts of the thick laminae depend for their pyrolysis upon heat flow from outer regions of the O-F flame. Protruding binders usually show evidence of softening, melting, and flow of melt over onto the AP surface.

2. The details in the vicinity of the binder lamina are shown in Fig. 3. Part a shows the trend with binder thickness at 5 MPa. Part b shows the trend with pressure (for a binder thickness of 50-70 μm). Figure 1 shows certain features of surface quality that are persistent in varying degree for all tested conditions on AP-hydrocarbon binder sandwiches with thin binder laminae, described further below (see Refs. [3-5, 10-17]).
3. All test samples from tests above 2 MPa exhibited regions of the AP surface ("distant" from the binder lamina) with the characteristic surface qualities of AP self-deflagration (Fig. 1), including flaky residue of a surface melt layer, and larger scale surface patterns of ridges and depressions (e.g., Refs. [3-5, 10-19]).
4. All thin-binder test samples showed (Fig. 3a,b) the binder lamina to be recessed relative to the region of the oxidizer laminae immediately adjoining the binder [3-5, 10-12] (binder lamina thickness less than 40 μm).
5. All test samples showed a region of the AP lamina centered 25-75 μm out from the binder interface plane that was the leading edge of the AP surface regression, i.e., the AP closer to the binder protruded [10-12] (Figs. 1, 3).
6. The surface of the AP in the protruding region adjoining the binder showed a distinctive, relatively smooth quality, with no flake relic of the AP melt (Fig. 1). This "smooth band" adjoining the oxidizer-binder interface was evident even with a binder (polysulfide) that pyrolized without evidence of a melt state [10-12], suggesting that the smooth surface is not due to the binder melt flows commonly observed in thick-binder sandwiches [3, 5, 6, 16, 17].

The present studies pursue the investigation of sandwich burning in further detail, with the goal of establishing a correct description of the flame complex. It is reemphasized that direct measurements of the flame are precluded by the "smallness" and complexity of the reaction region. A correct description depends on a process of inference from systematic observations of global combustion behavior (e.g., burning rate); measurable combustion zone microstructure (quenched samples); independent information about ingredient decomposition and combustion; and basic flame theory. In the following, several new investigations of sandwich burning are described, and the results are combined with the above sources of information and the previous results summarized in 1-6 above. The result is a relatively detailed *description of the combustion zone*. In the interest of brevity, the experiments and results of the

present studies are first summarized below with a minimum of discussion, and with frequent reference to other sources for details.

## EXPERIMENTAL PROCEDURE

The experiments will be described in sequence in very brief form. This will be followed by descriptions of preparation of test samples and test procedure.

### The Experiments

1. *Interrupted burning tests* on sandwiches with laminae of uniform thickness, to determine the nature of the burning surface [10-12, 15]. In these tests, the samples were quenched by rapid depressurization and the burned surfaces were examined in a scanning electron microscope (SEM). The test variables were test pressure, polymer lamina thickness, and substitution of other materials for the polymers (e.g., mica, gold, and a blend of polymer and fine ammonium perchlorate powder). The effect of these variables on the burning surface profile and surface quality provide indirect evidence of what is happening to the flame structure.
2. *Burning rate of sandwiches* as a function of binder thickness and pressure [18]. In these tests, PBAN laminae of particularly uniform thickness were used, and burning rate was measured by combustion photography.
3. *Deflagration limits* of AP-polymer sandwiches [10, 11, 15, 20, 21]. Constant pressure tests were run on sandwiches with "tapered" polymer laminae. Samples were ignited along the thick-binder edges of the sandwiches, and burning proceeded with progressive decrease in binder thickness. At test pressures below the AP self-deflagration limit, the samples spontaneously quenched before complete burnout, and the thickness of the binder at the quench surface was measured in the SEM. Tests were run over the pressure range 0.1-2.4 MPa, with HTPB, PBAN, and polysulfide binder.
4. *Effect of oxidizer particle size on propellant burning rate.* A family of propellants was prepared and burning rate determined over a pressure range. The propellants were formulated to test the relevance of a "sandwich-based" concept (regarding combustion zone structure) to the propellant burning situation. The propellants used bimodal oxidizer particle size distribution, with the size of the fine component being nominally 18, 49, and 82 μm. Burning rates were determined by combustion cinemicrophotography.

### Test Samples

*Sandwich samples* were prepared by methods and to sizes described previously [10, 15, 18]. Ammonium perchlorate laminae were prepared from Kerr-McGee high purity AP (nominal 100 μm particles). The powder was pressed at 210 MPa for a minimum of 20 min in a stainless steel die, yielding laminae 1.3 mm thick. Most sandwiches were made by bonding two laminae together with the polymeric binder. Thickness of the binder was controlled with spacer shims. Two types of polymer sandwiches were used. Plane-parallel laminae were used on burning rate tests and depressurization quench tests. "Tapered" polymer laminae [10, 11, 15, 21] used in spontaneous quench tests were prepared by using a spacer shim in one edge of the laminate only. Light pressure during curing resulted in the thin edge of the binder lamina of such samples being less than 10 μm thick.

In order to assure that no extraneous combustion effects would result from unsuspected characteristics of the pressed AP laminae, their self-deflagration was compared with that of single crystal samples. The quenched surface characteristics were similar to those of single crystals, except for somewhat greater irregularity in surface pattern. Burning rates were close to those reported by Boggs for single crystals [14, 19]. Samples were prepared with different AP particle size, and with reduced compaction pressures (131 and 61 MPa), and used in quench-burning tests on sandwiches. No effect was evident in the characteristics or profiles of

quenched surfaces. Some concern that fuel species might migrate into the surface layers of the AP laminae before testing was allayed by these results.

Sandwich samples were also made in which the *binder* (fuel) *lamina was either omitted or replaced by a sheet of mica or gold* [20, 21]. The objective was to clarify the mechanistic effects of the binder lamina. Efforts to dry-press these "binderless" sandwiches to assure good thermal and physical contact between laminae were unsuccessful, so the dry sandwich laminae were held together during tests by light pressure from a metal clip. While the test results suggest that contact between laminae was not perfectly uniform, burning behavior was fairly regular.

Sandwich samples were also made in which the fuel lamina was a *mixture of binder and 10 μm AP* [20, 21]. These were plane-parallel samples for use in depressurization quench tests. Samples were made with several "binder" laminae thicknesses, and in AP-binder mix mass ratios of 1 : 1 and 7 : 3. The mix was prepared by hand stirring for 20 min, followed by settling in a vacuum for 15 min to remove air bubbles. Sandwiches were then prepared in the same way as with pure binder laminae. Table I shows the binder thickness-mix mass ratios actually tested.

The experiments with *bimodal propellant samples* called for a series of formulations in which a relatively coarse fraction of AP (400 μm) was combined with a relatively fine fraction (i.e., bimodal AP size distribution). The series of propellants called for a graduated sequence of particle sizes of the fine component of the AP. For the intended purpose it was desirable to have a narrow size distribution within each size mode, and it was judged that the fine component mean sizes should be in the range 20–100 μm (see Discussion). These specifications were not fully achievable from available resources; accordingly, propellants were prepared with less ideal specifications as described in the following. Commercial high purity AP was available in a nominal size of 400 μm. This material was

**TABLE I**

**Test Conditions for Sandwich Tests with AP-Filled binder Laminae (10 μm AP, lamina thickness approximately 80 μm, unless noted otherwise)**

| Serial No. | Variable | Pressure 1.4 MPa (200 psi) | 4.2 MPa (600 psi) | 6.9 MPa (1000 psi) |
|---|---|---|---|---|
| 1 | Control-PBAN binder | × | × | × |
| 2 | 1/1 AP/PBAN | × | × | × |
| 3 | 7/3 AP/PBAN | × | × | × |
| 4 | Control-HTPB binder | × | × | × |
| 5 | 1/1 AP/HTPB | × | × | × |
| 6 | 7/3 AP/PBAN lamina 40 μm thick | | | × |
| 7 | 7/3AP/PBAN lamina 140 μm thick | | | × |
| 8 | 7/3AP/PBAN lamina 65 μm thick | | | × |

screened to limit its size variability to a range of 425–355 μm. Finer components were prepared in nominal sizes of 17.5, 49.0, and 82.5 μm by screening ground high purity AP. These nominal size designations are simply the midpoints of the size ranges, established by the screen mesh sizes used, which were 37 mesh pass for nominal 17.5 μm; 45 and 53 mesh for nominal 49.0 μm; and 75 and 90 mesh for nominal 82.5 μm. No attempt was made to quantify the size distributions within these sized samples, because the objective of the experiment required only demonstration of a specific qualitative difference in burning rate behavior of the propellants. The propellants were prepared by hand-mixing 4 g batches in an open beaker. The AP, monomer, and curing agent were measured in amounts that yielded 71% 400 μm AP, 16.5% fine component AP, and 12.5% PBAN binder. After 15 min of mixing, the mixture was placed under vacuum at room temperature for 30 min. The mixture was then transferred to rectangular molds of dimensions 50 mm × 12 mm × 2.5 mm and hand pressed by tapping the mixture for 20–30 min with a 1 cm diameter cylindrical Teflon stick. The samples were then cured in an oven at 72°C for 7 days. The cured propellants

were cut into rectangular samples (10 mm × 6 mm × 2.0 mm) for burning rate tests.

### Test Procedures

Experimental methods in the present work are mostly routine and reported elsewhere [10–12, 15, 18, 20, 21]. Sandwich samples were nominally 10 × 6 × 2.8 mm; they were mounted on a pedestal in a nitrogen-filled high pressure vessel and ignited on the top (6 × 2.8 mm) edge by an electrically heated wire. Propellant samples were 10 × 6 × 1.6 mm, mounted and ignited in a similar manner to the sandwiches. For combustion photography, a flushed windowed pressure vessel was used, with illumination of the sample from outside. For quench tests, a nonflushed pressure vessel was used that is equipped with pressure-release burst diaphragms. Characterization of samples after tests (quench tests) consisted primarily of surface quality, surface profile, and dimensional details as revealed in the scanning electron microscope. The thickness of the binder lamina of quenched samples, as reported in the Results, was measured in the SEM. In all tests on plane-parallel sandwiches where the lamina thickness of the entire sample was needed, the edges of the sample were examined before the test in an optical microscope or SEM to provide an estimate of average thickness and to disqualify samples with nonuniform thickness. This was particularly important in tests on burning rate, because rate is sensitive to thickness and there is no quenched sandwich to measure after the test. Variation of edge thicknesses of a binder laminae of more than ± 5 μm disqualified samples for burning rate tests; with care in sample preparation, this led to a rejection rate of about 50%.

Burning rates of both sandwiches and propellant samples were measured by projection of the motion pictures and measurement of timing marks and burning surface recession. This permitted any instances of uneven burning to be recognized and excluded from the rate data. Thirty percent of all tests were run in duplicate to monitor reproducibility; the test conditions for duplicate tests were selected randomly before any testing. For duplicate samples that burned evenly (most samples), no significant differences in rate were obtained.

## RESULTS

The experimental results are summarized in the following; because several separate investigations are covered, results of each investigation are accompanied by some interpretation as needed to explain why the tests were run. Then in a subsequent section, the interpretations are enlarged and combined to provide a qualitative description of the processes of sandwich burning.

### Surface Profiles and Burning Surface-Binder Substitutes

The persistence of the smooth band and protrusion of AP at the AP-binder interfaces was noted in earlier work and in the Introduction (Figs. 1, 3), and observed also in the present work. This effect was attributed in an earlier report [20, 21] to the effect of lateral heat flow from the oxidizer to the endothermic binder. Tests with other materials substituted for the binder were run to test this postulate. The choice of mica was made because it is a nonburning material with low thermal conductivity. The choice of gold was made because it is a nonburning material with high thermal conductivity. Presumably, the effect of lateral heat flow would remain with a gold lamina, and would be absent with a mica lamina. The tests with two AP laminae in direct contact were run as a control to test the effect of dry contact with no intervening lamina. The test results are typified by the examples in Fig. 4. Part a is from a control test with a 100 μm thick lamina of PBAN. Part b shows the details of the sandwich surface from a 4.2 MPa test on a sandwich with a mica lamina in place of the binder (the right side of the picture is the somewhat delaminated side of the protruding mica lamina; the AP surface on the left is in the region normally occupied by the smooth band). The detail shown in this figure is typical of the interface region in these "mica" tests. It is also typical of the self-deflagration of AP, normally exhibited on the

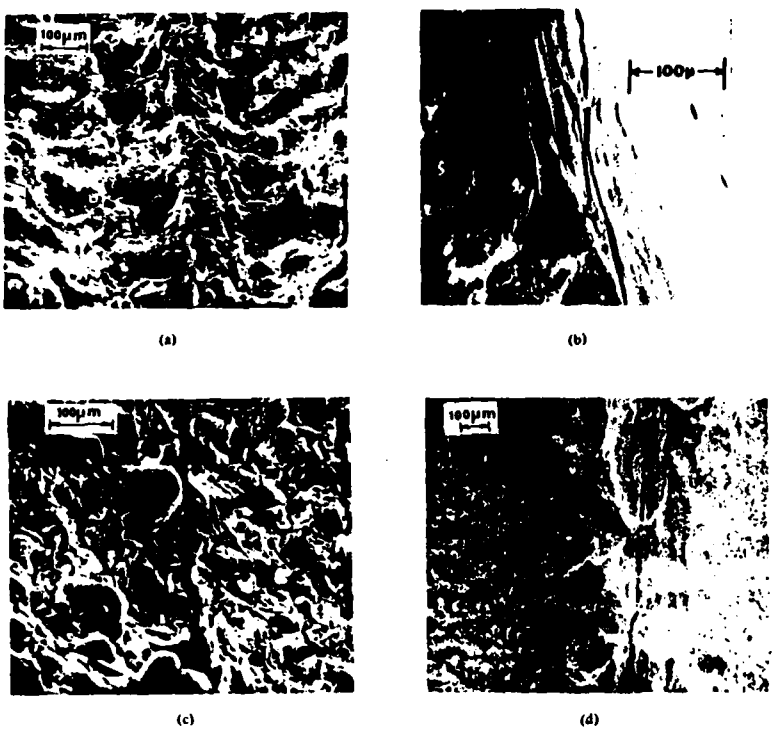


Fig. 4 Sandwiches with substitutions for binder lamina (pressure 4.2 MPa). (a) PBAN binder, approximately 100 μm. (b) Mica lamina. (c) No lamina (2 AP slabs, initially in contact). (d) Gold lamina.

AP laminae of sandwiches only at surface sites further from the interface. With mica laminae there was no smooth band and no protrusion of AP in the interface region.

Part c of Fig. 4 shows the quenched surface of a sample consisting simply of two AP laminae held together during burning by a metal clip. The figure shows the characteristics of simple AP deflagration, uninterrupted up to the interface plane. Under high magnification it was evident that the surfaces of the two slabs were together during burning; surface patterns near adjoining edges are correlated, and the edges show some matched features indicative of sepa-

ration of a contiguous surface layer that is liquid during burning. There is no protrusion of the AP laminae in the interface region. Separation of the two laminae, visible in the example, occurs during handling after the test.

Part d of Fig. 4 shows the quenched surface of an AP sandwich in which the binder lamina was replaced by a 15 $\mu$m layer of gold. Such samples consistently showed retarded burning (protruding AP) in the vicinity of the gold lamina, and a relatively smooth surface there. This behavior was not as uniform along the lamina as with a binder lamina, but was predominant. The nonuniformity is attributed to the difficulty in achieving uniform thermal contact between dry laminae.

It is stressed that the "smooth band" phenomenon described here is not a manifestation of the binder melt flow reported in many earlier studies. With thin-binder sandwiches used in the present studies, melt flow is minimal [10–12, 15] and available results show that the smooth band is present even with a nonmelting polysulfide binder [10] and with the gold lamina. The combined results are very strong evidence that the smooth band and protruding AP near the contact planes of conventional thin-binder sandwiches are caused by lateral heat flow into the binder lamina, with some corresponding modification of the AP decomposition–deflagration in the smooth band region. This conclusion is in contrast to that of Boggs [5], and of the present authors in early reports [15], who attributed smooth bands to binder melt flow (most investigators agree on the presence of melt flow with thick-binder laminae; most investigators have not done extensive testing with the thin-binder laminae studied here).

In addition to the above tests designed specifically to explore the cause of the smooth band and AP protrusion adjoining the contact surfaces, many other tests are reported here that were run for other purposes. In all cases where a pure binder lamina was used, the features 1–6 of the profiles and quenched surfaces as described in the Introduction were evident in a manner consistent with the trends described here.

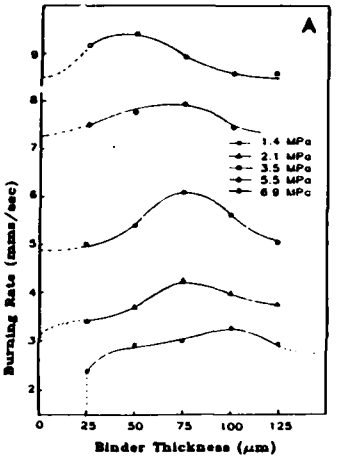


Fig. 5 . Burning rate of AP-PBAN sandwiches. A). Rate versus binder lamina thickness (data points are experimental measurements)

### Burning Rate of Sandwiches

The results of the sandwich burning rate tests [18] are shown in Fig. 5a. At large binder thickness the rate appears to approach a limit at each pressure (the limit is of only peripheral interest in the present study). As binder thickness is reduced, the burning rate increases to a maximum at a thickness of 65–85 $\mu$m, and then decreases for thinner binder. At pressures above the AP self-deflagration limit, the AP rate is approached as the binder thickness goes to zero. At lower pressure, decreasing binder thickness leads to a quench limit (measured in the "tapered" sandwich tests; see broken curve, lower left, Fig. 5a). The enhancement in burning rate by the binder lamina is strongest in the intermediate pressure range. Under conditions of rate enhancement (over the AP rate), the combustion front burns down the sample and leaves a trailing oxidizer profile that is V-shaped (Fig. 2e) when the test is above the AP self-deflagration limit, and U-shaped (Fig. 2d) below the AP self-deflagration limit. It was noted earlier [10–

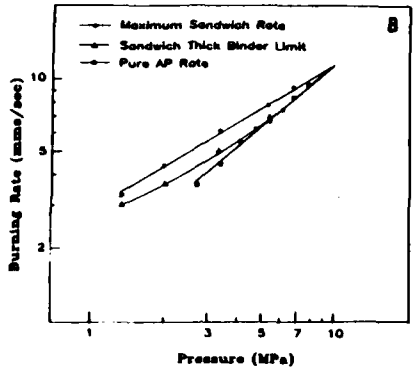


Fig. 5b. Rate versus pressure (data points are cross-plot points from curves in Fig. 5a).

.12 15, 20, 21] and in Fig. 2c, f that at higher pressures the AP self-deflagration *leads* the sandwich burning front, so it may be concluded that the family of curves in Fig. 5a would consist *of horizontal lines at pressures much higher than* reported in the figure. A partial cross plot of the curves in Fig. 5a as burning rate versus pressure is shown in Fig. 5b. This figure shows the AP self-deflagration rate (lower curve); the conditions for maximum sandwich rate (top curve); and the "thick slab limit," i.e., asymptotic rate for thick binder (middle curve). By extrapola*tion of the curve of maximum sandwich rate, the* enhancement in rate over the AP rate is seen to go to zero around 10 MPa. The thick slab rate is seen to approach the AP rate at about 5 MPa. In summary,

1. AP does not burn below 2 MPa, but sandwiches burn down to about atmospheric pressure unless the binder is too thin.
2. Between 2 MPa and 10 MPa, sandwiches with "optimal" binder thickness burn faster than AP alone.
3. Above 10 MPa, all sandwiches burn at the self-deflagration rate of AP.

These limits may differ with different binders. The trend in 3 probably does not apply to pressures above 14 MPa, where a transition in AP behavior occurs [14, 22].

### Deflagration Limit

Results of the spontaneous quench tests on tapered sandwiches are summarized in Fig. 6 for three binder materials [10, 11, 20, 21]. The error bars on the data points represent the range of variation of thickness of the binder lamina along the quenched edge, as measured in the SEM. Over the pressure range of 0.4–2.0 MPa, the sandwiches with any particular binder tended to quench at roughly the same binder thickness. Above 2.0 MPa, samples usually burned to completion, a result that is consistent with the fact that AP self-deflagrates above 2.0 MPa. At pressures below 0.4 MPa, the binder thickness for self-quenching became increasingly pressure dependent. Limited testing was made with samples with different degrees of taper of the binder lamina to test the possibility that the quench limit might be dependent on details of the approach to the limit. No statistically significant effect was evident. The different binders yielded significantly different

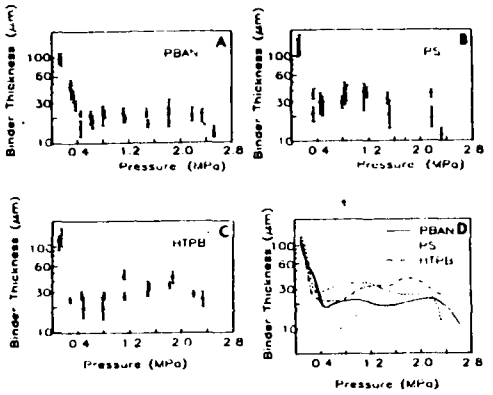


Fig. 6 Spontaneous quench limits for tapered sandwiches burning at constant pressure. (a) PBAN binder. (b) PS binder. (c) HTPB binder. (d) Summary.

quench limits in the 0.4–2.0 MPa range. Figure 7 shows a scanning electron microscope picture of a typical spontaneously quenched sample. The general features are similar to those of samples with binder lamina of uniform thickness quenched by rapid depressurization from comparable pressures. This indicates that approach of the tapered sandwich to self-quench does not involve development of any singular features of surface configuration. The thickness measurements in Fig. 6 were obtained from SEM pictures similar to Fig. 7, with suitable magnification.

### AP-Filled Binder Lamina Sandwiches

Test conditions are summarized in Table 1. Results of tests are summarized in Figs. 8–10. Figure 8 shows a comparison of quenched sandwiches with pure binder and with 1 : 1 AP-filled binder [20, 21]. From these tests (6.9 MPa, nominal lamina thickness 70 μm) there is an obvious difference between the behavior of sandwiches with and without AP in the binder. From extensive examination of samples with 1 : 1 laminae, it was evident that the region of protruding AP is widened and protrudes less with AP-filled laminae. The protruding region is flat on top, and the surface quality is smooth. The binder lamina is recessed and the surface of that lamina shows undulations of the same dimensional scale as the AP filler. However, no distinguishable AP particle surface is evident there. The details conform qualitatively to the general features 1–6 noted in the Introduction, but differ unambiguously from those of sandwiches with pure binder laminae in the details noted above. The differences become less evident at lower pressures.

Use of a higher mass ratio of AP to binder (7 : 3) in the "binder" lamina resulted in more conspicuous deviation from the results with pure binder laminae. The basic difference is illustrated for 6.9 MPa in Fig. 9 (upper right), which shows regions of both AP and binder adjacent to the AP–binder interface planes that are recessed relative to the protruding AP.

The comparison in Fig. 9 is for samples with filled binder laminae that are about 70 μm thick. With 1 : 1 AP–binder laminae, the profiles were not critically dependent on lamina thickness.


Fig. 7. Surface of a spontaneously quenched sample (test pressure 2.08 MPa).

However, for the 7 : 3 laminae it was found that the profile was highly dependent on lamina thickness (6.9 MPa) as shown in Fig. 10. With very thin laminae, the profile was similar to that with the 1 : 1 mixture. As lamina thickness increased, the lamina region became increasingly recessed, and the overall sample profile became V-shaped (a configuration indicating that the lamina-interface region is dominating the sandwich burning rate). As 7 : 3 lamina thickness was increased (Fig. 10), and increased burning rate resulted, the protrusion of the AP in the interface region became less and disappeared. The smooth bands also became localized very close to the interface planes. In that local region the AP surface was concave upward (evident in originals of Fig. 10), but the AP no longer protruded.

### Burning Rate of Bimodal Propellants

The burning rates are shown in Fig. 11. The singular feature of the rate versus pressure of these propellants is a step in the burning rate-pressure curves. The step occurs at higher pressure when the particle size of the fine fraction of AP is small. This trend is discussed further in the section "Interpretation of Results with Bimodal Propellants."

## DISCUSSION

The experimental results presented in this paper and its predecessor [10] represent parts of an evolving interplay between theory and experiment. Because of the complexity of the sandwich combustion process, it was judged at the outset that in the short term a realistic and comprehensive two-dimensional analytical model would be intractable. Accordingly the theory is based on qualitative arguments, and the experiments were designed to guide in formulation and evaluation of the theory. In this discussion, the qualitative theory will be presented in the form of a detailed description of a flame complex, accompanied by the basis for the details. To the extent that the basis for the

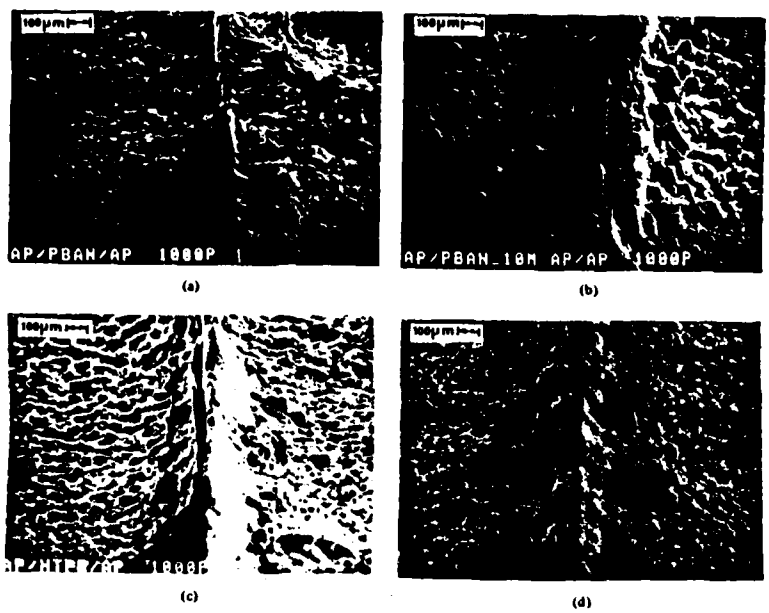


Fig. 8. Comparison of quenched surfaces of sandwiches (6.9 MPa). (a) Pure PBAN binder lamina. (b) 1 : 1 AP-filled PBAN binder lamina. (c) Pure HTPB binder lamina. (d) 1 : 1 AP-filled HTPB lamina.

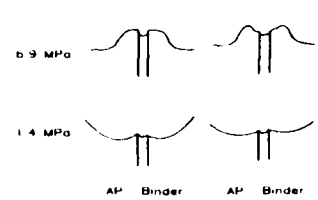


Fig. 9. Surface profiles of sandwiches with different AP-binder ratios in the binder laminae, and different pressures (PBAN binder, lamina thickness approximately 70 μm).

details involves the present experimental results, the results will be discussed more fully later (in interpretation sections) after outlining the theory of the flame complex.

Before presenting the flame theory, attention is directed to five previously reported features of combustion of AP and AP composites that will be treated as axiomatic in the theory and subsequent discussion.

1. Ammonium perchlorate self-deflagrates at pressures above about 2 MPa. This pressure limit is sensitive to temperature, AP purity, and heat losses, presumably because of the rather modest flame tempera-

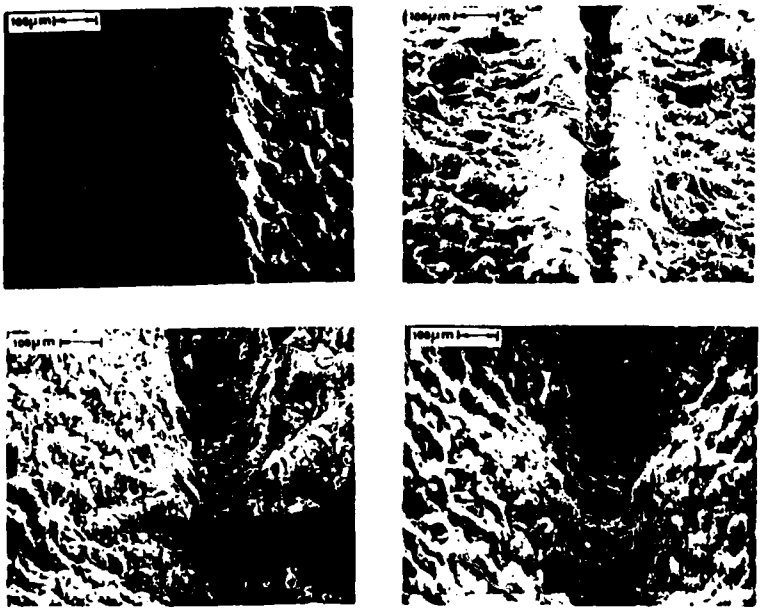

Fig 10 Effect of lamina thickness on quenched surface with AP-filled PBAN binder laminae (SEMs) AP binder ratio 7 : 3, 6 9 MPa

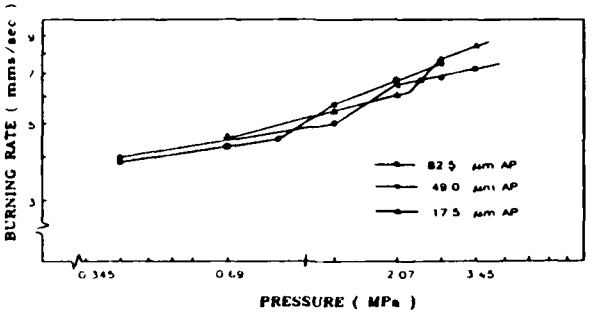


Fig 11 Burning rate of bimodal propellants 70% 400 μm AP, 17 5% fine AP, 12 5% PBAN binder Fine AP size as shown

ture available to "drive" the combustion [4, 13, 14, 19, 22, 23-27]

2. Self-deflagration of AP proceeds by a combination of a complex reaction in a surface liquid froth, along with a gas-phase flame. Heat release occurs in varying degrees at both sites [4, 13, 14, 16, 20, 22, 23, 25]. There are many references in the literature to condensed phase reactions, but such references do not acknowledge the unequivocal evidence for the existence of the reactive froth or distinguish what is meant by condensed phase in that context. When the issue is reduced to one of real dimensions, the reaction region in the wave in the solid is so thin that it would be difficult to separate condensed-*phase*, *surface*-, and *gas-phase reactions* in the froth. However, the gas-phase flame is generally treated as distinct from the froth under most conditions [25].
3. Heat release in reactions between AP and hydrocarbon binders occurs primarily in the gas phase [3-5, 10-12, 15-17, 23, 28]. (Contrary views can be found in early literature, and are often argued by investigators whose primary investigative tools are thermal analysis instruments.)
4. Burning rates of the composite systems are dependent on the structural details of the systems. This is generally attributed to the effect of propellant microstructure on location of gas-phase reaction sites (flames) (e.g., Refs. [1, 8, 15, 29-33]).
5. The gas-phase oxidizer-binder flames consist of a leading edge portion involving vapors that have already mixed, and a trailing portion governed by continued diffusion of oxidizer and binder vapors. The leading edge portion is described as having the properties of a kinetically limited premixed flame, and the trailing portion has the properties of a diffusion-limited flame [1, 9-12, 15, 21, 23, 31, 32]. Details and the relative importance of the two portions of the flame are matters of speculation, but are examined later in the context of the present results (the subject comes up in several of the later sections on interpretation of results of different experiments).

### Theory of the Flame Complex

Figure 12 is a sketch of the combustion zone of a burning sandwich, based on currently available evidence. The sketch represents only that portion of the combustion zone within about 150 $\mu$m of the plane of symmetry of the sandwich, and represents conditions for thin-binder sandwiches burning at intermediate pressures (3-6 MPa). The numbers in circles in the sketch designate regions in the combustion zone with unique features, regions that will be discussed in detail in the following. It should be understood that the objective of discussing these features of the combustion zone is to obtain a reasonably complete description that can be used to understand detailed experimental observations (or design experiments to test the model), and to begin to explain such global combustion behavior as burning rate and dynamic response of combustion to oscillations in the flow environment.

Region (1) *The Binder Lamina.* The exposed binder lamina is recessed in quenched thin-binder sandwiches [3, 5, 10-12, 15-17, 21, 23, 28]. The appearance of the bottom of the recess suggests that it was molten during burning (most binders tested). The recessed condition could be an artifact of the quench, since real-time observations during burning do not have sufficient resolution to validate the quench test results. However, it seems clear that the thin-binder laminae do not protrude during burning, as such a state would require that the protrusion be solid (in which case it would remain after the quench). Further, the speculation that the recess is caused by ejection of melt during quench [5] is put in doubt by the results with polysulfide binders, which burn without evidence of a melt but yield recessed binder laminae. Progressive increases in thickness of binder laminae lead to a change to protruding binder. For the most extensively tested binder (PBAN), the laminae became somewhat pro-

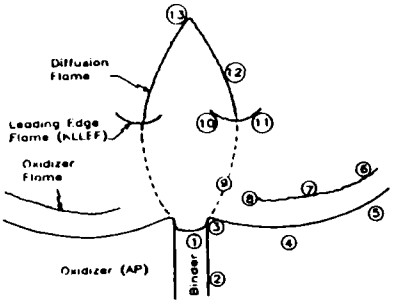


Fig. 12. Principal features of the combustion zone microstructure and processes as suggested by accumulated results: 1, binder lamina; 2, interface plane between binder and oxidizer; 3, oxidizer surface adjoining binder (smooth band); 4, leading edge of the oxidizer burning front; 5, oxidizer region that regresses at the normal AP self-deflagration rate; 6, AP flame; 7, leading edge region of AP flame; 8, oxidizer flame, modified by the anomalous decomposition in the smooth band (flame may be quenched); 9, oxidizer-fuel diffusion region, with stoichiometric surface indicated by broken line; 10-11, kinetically limited leading edge flame (KLLEF) (fuel-rich and oxidizer-rich sides); 12, diffusion flame; 13, tip of diffusion flame.

truding in the 50-90 $\mu$m thickness range (somewhat pressure-dependent), decidedly protruding for thicknesses over 110 $\mu$m. The trend was similar for HTPB and polysulfide binders.

Region (2) *The Interface Plane.* The oxidizer-binder interface is never the leading edge of the burning front [3, 5, 10, 15, 17, 21, 23, 28], *an observation that seems to rule out* binder-oxidizer interfacial reactions as significant contributors to burning rate at the pressures tested. The binder recess leaves a side wall that appears to be vertical in the interface plane, suggesting no AP decomposition in the recess. The bottom of the recess has the appearance of a meniscus, and there may be a film of binder on the sidewall of the recess (no evidence reported).

Region (3) *Protruding AP-Smooth Band.* Under all conditions tested (present work and Refs [3, 4, 10, 17, 21, 23, 28, 29]), the AP deflagration in the region near the *interface plane appears to be retarded relative to* region (4), and the AP surface there has a smooth quality suggestive of a different mode of decomposition than that occurring further out from the interface plane [3-5, 10-12, 15, 17, 21, 23, 28]. In earlier studies, these features were attributed to binder melt flow over the AP surface [3, 5, 16, 17, 21, 28], a conclusion that appears to be valid with thick laminae of *meltable binder. However, the smooth band and* protruding AP occur also with thin-binder laminae where flow is less probable, with nonmelting binders, and with a gold "heat sink" lamina in place of binder. As a result, it is theorized [21] that there is appreciable lateral heat flow into the endothermic binder, resulting in a lower AP surface temperature and a less exothermic or an endothermic surface decomposition (probably dissociative sublimation). This interpretation of region (3) behavior has been supported recently by detailed calculation of heat flow in a two-dimensional model of the combustion of contacting slabs of oxidizer and fuel [34], which *shows that lateral heat flow into the binder* lamina occurs.

Region (4) *The Leading Edge in the AP.* This region is generally located 25-50 $\mu$m from the interface planes (present work and Refs. [3, 5, 10-12, 15-17, 21, 28]); a transition from smooth to "flaky" surface occurs here on quenched samples, indicating a transition in the nature of the surface decomposition to an exothermally reacting froth more typical of AP self-deflagration. Region (4) represents that point on the surface profile where the energy flux from gas phase flames, surface reaction, and two-dimensional heat flow in the solid (including binder) yield the highest heat flux in the direction of burning. At low pressure (e.g., $<1.4$ MPa), the thickness of the thermal waves in the gas and solid are so large that surface heat fluxes are more uniform, and localized effects such as the region (4) leading edge are inconspicuous. The transition in AP surface decomposition disappears as the pressure is reduced below the AP self-deflagration limit—the evidence of reacting froth no longer is present anywhere [10, 21, 28, 36, 37].

Region (5) *AP-Self-Deflagration.* This region shows a surface essentially the same as for AP self-deflagration (including evidence of reactive froth), and surface regression rates are approximately the same as for self-deflagration [15, 21, 22]. At low pressure, the surface curves up toward vertical (Fig. 2a,d), reflecting the absence of sufficient heat flow from the AP-binder flame to sustain pyrolysis of the AP (the sandwiches were fuel-lean in overall stoichiometry). In contrast, at high pressure (e.g., 8-14 MPa), the AP self-deflagration rate exceeds the sandwich rate (Fig. 5b) (which is now overwhelmed by the heat drain to the endothermic binder), and region (5) becomes the leading edge of the AP burning front (Fig. 2c,f).

Region (6) *The AP Flame.* This flame is generally presumed to be present under conditions where AP self-deflagration is recognized to be possible, and such a flame is postulated in propellant combustion models [25]. The chemistry and location of the flame are matters of speculation, as the flame appears to be too close to the surface to be resolved experimentally. The heat release of the AP self-deflagration apparently is apportioned between the surface froth and this flame, probably in a way that is sensitive to pressure and other factors affecting energy balance and surface temperature [4, 5, 14, 23, 25]. At this point it is not certain that the flame is a "sheet." The irregular and frothy nature of the AP surface probably gives rise to nonuniform flow and a correspondingly nonuniform flame. Combustion photography has been reported [4, 37] to show turbulent flow from self-deflagrating AP, but it is doubtful that the AP flame region is resolved in such photography, and the "turbulence" may be surface-coupled nonuniform flow. It has been suggested [4, 14, 25] that the heat release shifts to the gas flame (6) from the froth site (5) as pressure is decreased toward the self-deflagration limit, and that the limit is related to loss of the reacting froth.

Region (7) *Leading Edge AP Flame.* This is a continuation of the AP flame into a region that must receive some heat from the AP-binder flame, leading to the higher regression rate of the surface at (4). This, in turn, implies a higher surface temperature in region (4).

Region (8) *Smooth Band Flame.* This region is unique in that the vapors from the underlying surface [region (3)] are postulated to be different from those for the rest of the AP flame. Lacking any direct experimental evidence, speculation about the nature of the flame is a precarious exercise. Indeed, this region may not have an AP flame at all—an interpretation that would be consistent with the idea that loss of the surface froth reaction is associated with deflagration limits [4, 14, 25]. Diffusion of heavy fuel molecules into this region may actually suppress the AP flame; thus it may instead be a thermal and chemical induction zone for a later AP-binder flame in region (11) [10, 11].

Region (9) *Oxidizer-Fuel Diffusion Region.* The dotted line in Fig. 12 represents the stoichiometric surface in a region of molecular

diffusion of vapors. This "surface" bends out over the region above the oxidizer surface because the oxidizer is relatively dilute compared with the fuel. While the vapors are fairly hot (roughly 600°C as they leave the burning surface), the initial vapor mixing occurs in a region of high heat loss, so oxidizer-binder reactions cannot raise the temperature precipitously, and rates remain low until further out in the mixing region. This region (9) merges with region (8), and the uncertainty about an AP flame in region (8) translates into an uncertainty about details of region (9). This same uncertainty has confronted propellant combustion modelers, who generally resolve it by somewhat arbitrary assumptions about "ignition delays" and/or flame structure. For the present, it will be assumed here that the AP flame reaches a quench limit somewhere in region (8), and that region (9) is a diffusion "fan" in which reaction rates are low because unfavorable balance of heat flow and insufficient mixing and chemical preparation of reactants prevent rapid temperature rise. However, one must keep in mind the qualitative features of regions (8), (9), and (10). Their interaction may be very pressure-dependent, and may oscillate during oscillations of the combustion environment.

Region (10–11) *Kinetically Limited Leading Edge Flame.* The diffusion region (9) prepares a flow in which an increasing oxidizer-fuel mixture develops by diffusion as convection carries the gases away from the surface. At some point in this mixing fan, the temperature becomes sufficient, relative to the two-dimensional heat flow, to support a flame. This flame is the leading edge of the diffusion flame, but unlike the diffusion flame [region (12)], its position in the mixing fan is strongly dependent on reaction kinetics, standing as it does in a partially premixed flow. Accordingly, the name "kinetically limited leading edge flame," KLLEF, is used here to designate the flame. The existence and nature of such a flame in sandwich burning is simply postulated on fundamental grounds, since no direct observation has been made, due to the problem of spatial resolution. However, it is important to note that every free (unattached) diffusion flame has a kinetically limited leading edge of some kind. The KLLEFs are of particular importance in the present problem because, *under some conditions, the majority of the oxidizer-fuel reaction occurs in the KLLEFs* (no fuel left for the diffusion flames). Such (KLLE) flames have been observed in studies of flame propagation in stratified air-fuel mixtures at 1 atm [38, 39]; such flames show a leading edge at the stoichiometric surface and trail off on the fuel-rich side [region (10)] and oxidizer-rich side [region (11)]. An analogous kinetically limited region of the flame is generally invoked also by modelers of propellant combustion [1, 29, 30–33], and has been postulated in reports on combustion down the interface between oxidizer and fuel slabs [9–11, 22, 23, 31]. Of particular note is the work of Fenn [31], who discussed the nature and role of a kinetically limited reaction region he called the "phalanx flame." Because of its importance in the present work, the nature of the KLLEFs will be discussed in some detail in several following sections.

Region (12) *Diffusion Flame.* In the region downstream from the KLLEF (Fig. 12), continued reaction occurs as further interdiffusion of fuel and oxidizer vapors occurs. The temperatures are high due to heat release further upstream and diffusion of hot reaction products, and the reaction rate is consequently controlled by the rate of mixing, rather than by reaction kinetics. The extent of this diffusion-limited portion of the flame is determined by the extent to which reactants have already been consumed by the KLLEF, and the extent of the fuel and oxidizer supply (i.e., thickness of the laminae that supply the reactants). According to classical theory, the diffusion flames locate themselves in such a way that oxidizer and fuel species will diffuse into the flames in stoichiometric proportions, with the reactants being fully converted to products at the flame surfaces. Thus the diffusion flame surfaces are continuations of the stoichiometric surfaces of regions (9); however, there are no oxidizer species in the space

between the flame surfaces in region (12), and no fuel species outside the flame surfaces. While this idealized "flame surface" approximation may not be quantitatively valid in the microflame situation of the present work, it is still a helpful concept for qualitative description of the situation.

Region (13) *The Stoichiometric Tip.* In Fig. 12 the flame complex is drawn for a thin-binder lamina, with oxidizer laminae thick enough to represent a sample with oxidizer-rich overall stoichiometry. As a result, the diffusion flame sheets close over the fuel, yielding a flame tip that is referred to here as a stoichiometric tip. The region above the tip presumably contains little or no fuel species when the diffusion flame is present in region (12). However, later discussion concerning the results of deflagration limit tests will involve the implications of a situation where the KLLEFs and diffusion flames fail to be established in the mixing region, and the entire region [levels (9)-(12)] is simply a two-interface diffusion region. In that situation, there are still stoichiometric surfaces and a stoichiometric tip, but the concentrations of fuel and oxidizer will not go to near zero at the stoichiometric surfaces as they do where the flames are present. In the configuration used here (thin-binder lamina), the mixture in the absence of a flame then will be increasingly oxidizer-rich as a function of distance above the stoichiometric tip, a condition that would be expected to affect the stability and location of any flame that might occur above the tip.

There are many features of sandwich burning that are not encompassed in the above description, features such as irregular burning at high pressure [10]; unsymmetrical burning with some binders [5]; melt flows with some binders and thick laminae [3, 5, 16, 17]; possibility of turbulent smearing of the flame complex [5]; intermittency of flames [5, 10, 15]; and general breakdown of the two-dimensional symmetry of the flame. These features are probably each significant under some conditions, but were apparently not qualitatively important with the thin-binder PBAN sandwiches and test conditions used most extensively here. In this context, it is appropriate to note that many observations of these nonideal features of sandwich burning that have been reported in the past have been based on observational methods that are misleading (e.g., limited spatial resolution) or test conditions and test samples not relevant to the studies reported here (e.g., thick binder). However, the issues raised merit continuing consideration in the future.

### Interpretation of Results of Binder Substitutions

The foregoing qualitative theory was evolved as a framework in which to understand the emerging results of the present studies. One of the more conspicuous experimental results was the smooth surface quality and protrusion of the AP in region (3). It was proposed that this region of the sample was deprived of heat by lateral transfer to the binder lamina, thus tending to hold down the surface temperature. Substitution of a nonconductive mica lamina led to elimination of the features of the profile attributed to the lateral heat drain, while substitution of a conductive gold lamina preserved these features. This result tends to support the lateral heat drain argument. At the same time, computer modeling of the heat flow problem was undertaken [34], and results of numerical studies indicate that heat flow would indeed occur from oxidizer to binder under the conditions of AP-HC binder sandwich burning. As will be seen later, the results of sandwich burning rate measurements also indicate that lateral heat flow to the binder occurs. Given the rather marginal heat balance situation characteristic of AP self deflagration, it is then not surprising that the AP surface regression is retarded in region (3). The persistent association of this with modified (smooth) surface quality suggests that the entire deflagration process is disturbed by the heat drain. This is interpreted here as a transition from normal self-deflagration with an exothermic froth layer to simple dissociative sublimation. The resulting loss of surface heat release of course enhances the retardation of surface regression. In effect,

the AP in region (3) is behaving as if it were below its self-deflagration limit, being pyrolized by heat flux from the gas-phase flames.

In this context, it may be important to note again that the features of region (3) have been attributed in the past to flow of molten binder over the AP surface. In experiments with binder laminae of thickness greater than 125 μm this interpretation is probably partly correct, at least with binders that yield high temperature surface melts. This is an unfortunate complication of the two-dimensionality of the experiment, which must also affect the gas-phase flame structure. This complication has been largely avoided in the presently reported work with thin-binder laminae, particularly PBAN binder.

### Interpretation of Deflagration Limit Results

The initial motivation for deflagration limit tests was to exploit an experiment that would be sensitive to the details of the flame complex and reaction kinetics. The systematic trends in the results (Fig. 6) at pressures below the AP self-deflagration limit posed a challenge that has yet to be exploited fully. However, some significant interpretation can be made now, interpretation that has been carried over to design of the bimodal propellant experiment and borne out by results of that experiment discussed in a later section about bimodal propellants.

In interpreting the deflagration limit, one turns to arguments regarding the two-dimensional energy field, and what happens as the binder lamina becomes increasingly thin while approaching the quench point. Figure 13 shows the trend one would expect of the combustion zone details with binder thickness. As the binder thickness decreases, the mixing regions above the AP-binder interfaces move closer together and the stoichiometric tip retracts toward the surface. The total fuel supply decreases, with a corresponding decrease in available combustion energy. Since this energy is dissipated two-dimensionally, one would expect burning rate and flame temperatures eventually to drop off with decreasing binder thickness. In such a situation, the energy balance ultimately becomes unstable and the "fire goes out." In the present situation, this may occur in either of two rather different ways that can be seen in Fig. 13. In part a, behavior at relatively low pressure is sketched. As binder thickness is reduced at constant pressure, the stoichiometric tip [region (13) in Fig. 12] retracts until it is coincident with the oxidizer-binder KLLEFs. Any further decrease in binder thickness would place the KLLEFs in a location beyond the stoichiometric tip. The flames would not be stable in that location, because it is a region where fuel concentration becomes more fuel-lean with distance from the surface, with a corresponding decrease in available flame temperature. Thus, if the flame does not quench spontaneously by the time the stoichiometric tip retracts to the flame position, it will do so then. Quench due to tip retraction is more likely at low pressure, where the flame stands relatively far from the surface, and it is postulated that the steep, low

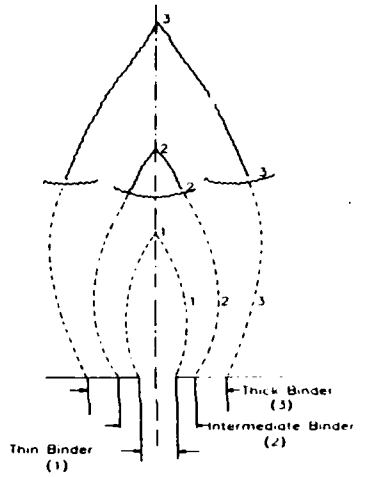


Fig. 13. Trend in oxidizer-binder combustion zone structure with thickness of the binder lamina (flames for different binder thicknesses superimposed). A. Very low pressure ($p < 0.4$ MPa) (stoichiometric tip is retracted for binder thickness #1).

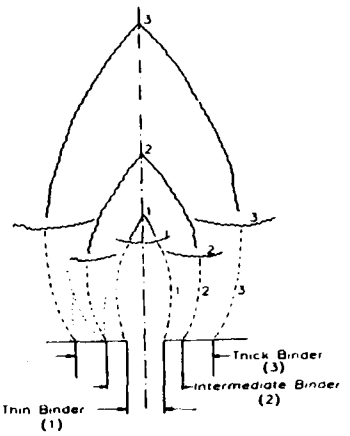


Fig. 13b. Low pressure ($0.4 < p < 2.0$ MPa).

pressure parts of the curves in Fig. 6 correspond to quenches involving approach to the tip retraction. The dotted extension of the steep part of the curve at higher pressure is intended to suggest the locus of stoichiometric tip retraction that would result if the flame position were to continue to change with pressure in the manner of the low pressure curve.

Following the above interpretation, the experimental results (Fig. 6) suggest that around 0.4 MPa the flame stability becomes marginal before stoichiometric tip retraction. At higher pressures, the KLLEFs are located near the sample surface under stable burning conditions. By the time the binder thickness has decreased to 40 μm or so (Fig. 13b), the mixing regions and KLLEFs have substantially merged and the entire flame complex has become very small, but the KLLEFs still stand well down in the mixing regions. The limit of flammability becomes dependent on the energy balance of this small flame burning down a narrow slot in the sample. With decreasing binder thickness, the burning rate drops off, and quench occurs when available heat from the flame can no longer support the losses. In the pressure range $0.4 < p < 2.0$, the approach to quench evidently does not depend on stoichiometric tip retraction, and the trend with pressure accordingly is different from that at lower pressure. The relative insensitivity to pressure suggests that approach to quench is governed by pressure insensitive diffusion processes, but this needs clarification by appropriate quantitative analysis. As in all quench events, the chemical kinetics become critical at the approach to the limit because of decreasing flame temperatures. In this limit domain, the final retreat of the flame may still be precipitated by withdrawal to the unstable region beyond the stoichiometric tip due to falling flame temperature, even in this higher pressure range. Presumably this is a "terminal aspect" of quench, which no longer dominates the pressure dependence of the quench limit. The effect of binder type on quench limit (Fig. 6) in this "diffusion dominated" domain appears to be related to the mode of decomposition of the polymer, and corresponding nature of the fuel molecules in the mixing region (9). PBAN binder (which quenches at the lowest binder thickness) is expected to yield relatively small vapor molecules, while HTPB will yield large molecules that must be further broken down to support a flame. It is postulated that this chemical induction process requires a longer time with HTPB than PBAN, with a correspondingly larger KLLEF standoff distance and lower flame stability. The calculated stoichiometric flame temperature of the HTPB/AP flame is higher than that for PBAN/AP, a condition that adds plausibility to a fuel kinetics explanation of the difference in quench limit.

The arguments regarding pressure dependence of quench limit due to stoichiometric tip retraction (Fig. 13a) can be stated in simple analytical terms by application of diffusion theory to determine the height of the stoichiometric tip. At pressures approaching the quench limit, the KLLEF is near the tip, and the stoichiometric surface is almost entirely below the flame. If one assumes the entire stoichiometric surface is within a simple laminar mixing flow, the stoichiometric tip height can be esti-

mated by the same analysis used in the Burke-Schumann diffusion flame theory [40] (in that analysis, it is assumed that the coupling function $\alpha_f - \alpha_{ox}$ is equal to zero at the flame, which is assumed to be at the stoichiometric surface with $\alpha_f = \alpha_{ox} = 0$; however, the analysis does not depend on $\alpha_f = \alpha_{ox} = 0$, and the "flame surface" calculation is really a stoichiometric surface calculation whether or not a flame is present). While the Burke-Schumann theory is only approximate, and cast in cylindrical coordinates, we shall adopt the qualitative result that the stoichiometric tip height can be obtained as a nondimensional function of fuel-oxidizer stoichiometry and relative thickness of fuel and oxidizer laminae. This height, $\eta_t$, is related to the dimensional height by

$$\eta_t = k y_t D/v = k y_t(\rho D)/(\rho v). \quad (1)$$

where $k$ depends on the relative dimensions of the oxidizer and fuel flows, $y_t$ is the actual tip height, $D$ is a diffusion coefficient, and $v$ is the convective flow velocity. In such analyses it is usually satisfactory to assume that the product $\rho D$ is independent of pressure [40]. The product $\rho v$ can be represented for pyrolizing solids as

$$\rho v = \rho_s r, \quad (2)$$

where $\rho_s$ is the density of the solid and $r$ is the regression rate of the surface (which is viewed in this analysis as remaining flat). If $r$ is represented by a typical burning rate function such as

$$r = C p^n, \quad (3)$$

then

$$y_t = (\rho v)\eta_t/k(\rho D),$$

$$y_t = \rho_s C p^n \eta_t/k\rho D,$$

$$y_t = (\rho_s C \eta_t/k\rho D) p^n, \quad (4)$$

where the expression in parentheses is insensitive to pressure. Thus the tip height increases with pressure according to the factor $p^n$, where $n$ is typically between 0.2 and 0.6.

The foregoing argument, albeit simplistic in nature, suggests that above the quench limit, a gradual reduction in pressure would lead to a decrease in tip height and an increase in KLLEF standoff distance, a situation that is conducive to a decisive role for the "loss of KLLEF" due to retreat into the unstable situation at and above the stoichiometric tip. As noted above, loss of the KLLEFs depends also on a detailed two-dimensional energy balance, which apparently plays a more important role at higher pressure (0.4-2.0 MPa), where the very thin binder simply cannot maintain a sufficient fuel supply (and heat release) to overcome the heat losses. Under these conditions the KLLEFs apparently remain below the stoichiometric tip until the heat balance is so unfavorable that low flame temperature on the stoichiometric surface leads to either spontaneous quench of the flame or retreat of the KLLEFs into the unstable region beyond the tip. The difference in the nature of the quench limit trend for the different binders in the 0.4-2.0 MPa range suggests that flame kinetics still play a significant role in that pressure range. Above 2 MPa, sandwiches with thick oxidizer laminae burn regardless of binder thickness, because the AP burns as a monopropellant. Thus, the binder thickness limit for quench goes to zero at higher pressure in Fig. 6.

### Sandwich Burning Rate

The experimental results indicate that the overall burning rate of the sandwich is dominated by the AP rate at pressures between 10 and 14 MPa, but that the AP-binder flame can have a significant effect at lower pressure (and, of course, dominate the rate below the AP self-deflagration limit). This is evident in Fig. 5, and is consistent with the larger features of quenched burning surfaces (Fig. 2). In terms of the flame complex in Fig. 12, one would expect that burning rate would be governed by heat release in a region of the flame complex relatively close to and on the burning surface. This region has been referred to [18, 20, 32, 33] as the "propagation velocity controlling" (PVC) region. Under conditions where the sandwich rate is higher than the AP rate (Fig. 5b), the PVC region encompasses part of the binder-oxidizer flame, including the KLLEF. The PVC region is the region in which energy flow affects the temperature at the leading edge of the

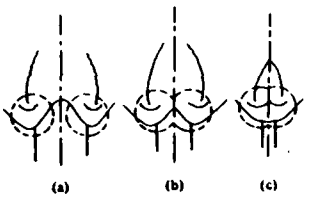


Fig. 14. Propagation velocity controlling regions (a) Thick binder lamina. (b) Binder lamina 70-100 μm (c) Binder lamina ~ 50 μm.

burning front. When the binder lamina is thick, the flame complexes above the two interface planes burn independently. There is a PVC region for each interface plane (dotted circles, Fig. 14a). In this situation, diffusion of heat (and chemical species in the gas) proceeds much as if the binder lamina were of infinite thickness, and the burning rate is independent of binder thickness. There is a threshold thickness of the binder lamina around 150 μm for PBAN binder below which burning rate becomes sensitive to binder thickness (Fig. 5). This corresponds to the onset of interaction of the two PVC regions (Fig. 14b). Under these conditions, heat transfer from the AP laminae to the fuel lamina is decreased (because there is a smaller heat sink). The heat that is transferred is retained within the PVC region and is reflected as higher temperatures in the flame in the PVC region. In addition, fuel dilution of the mixing regions on the fuel-rich sides of the stoichiometric surfaces will be reduced in the gas-phase diffusion field. One would anticipate that the fuel-rich portion of the KLLEF [region (10) in Fig. 12] would therefore be hotter and extend further into the fuel-rich region, with correspondingly larger heat release. In effect, the AP at the leading edge of the burning front experiences less lateral heat drain in the solid and more heat supply from the gas flame, with a corresponding enhancement of burning rate.

As binder thickness is reduced further, the total fuel supply is reduced until it is all consumed in the PVC region (i.e., none is left for the outer region of the trailing diffusion flame). Continued decrease in binder thickness thus eventually leads to decrease in heat release in the PVC regions, which are also substantially overlapping (Fig. 14c). Following the increase in burning rate caused by concentration of the two PVC regions, this trend to limitation in fuel supply must lead with thinner binders eventually to a decreasing burning rate (Fig. 5a). When pressures are above the AP self-deflagration limit, the sandwich rate will drop off with decreasing binder thickness until the AP deflagration rate is reached. At lower pressure, the rate will drop off until a combustion limit is reached (Fig. 6).

It is interesting to note that the foregoing arguments did not draw on the details of behavior in regions (8) and (9) of Fig. 12, which have been described earlier as unknown. The results of quench tests indicate that the protrusion of AP near the interface planes and the characteristic smooth surface of the AP there persist over the whole range of test conditions and are evident even on spontaneous burnout of tapered binder samples. This suggests that behavior in regions (8) and (9) is not changing qualitatively. This, in turn, seems to be most compatible with the view that the AP vapors from this region are diluted by fuel vapors and fail to establish a near-surface AP flame, delaying heat release until the KLLEF location. At low pressure, the leading edge of the burning front [region (4)] receives heat primarily from the KLLEF and secondarily from the trailing diffusion flame. Above the AP self-deflagration limit, the leading edge receives heat also from the AP reactions in regions (4)-(7). Above about 7 MPa (10 MPa for "optimal" binder thickness), the leading edge receives heat primarily from the AP reactions in regions (4)-(7). Thus the character of the propagation velocity controlling region changes with binder thickness and pressure, and the burning rate trends suggest the nature of the changes (see later discussion of pressure dependence and Fig. 18 presented there).

### Sandwiches with AP-Filled Binder Laminae

The range of test conditions in the investigation of AP-filled binder laminae was rather limited, and the results consequently are probably more provocative than enlightening. The investigation was done before the burning rate study, and, in retrospect, the choice of 6.9 MPa for most of the tests probably limited the amount and interpretability of the results. However, they do merit some discussion.

The presence of a protruding region of the AP laminae on the tests with thin-binder lamina (Figs. 9, 10) indicates that lateral heat flow from the AP laminae to the filled binder lamina is still a factor in these tests. The smooth surface quality of the protruding region is still present. The peak of the protruding region is flattened off, compared with the pure-binder sandwiches. This suggests that the AP-binder flame is in closer proximity to that region, a conclusion that would be consistent with the fact that much of the oxidizer for that flame is premixed in the binder lamina. The recess of the binder lamina and lesser recess of a thin region of the adjacent AP, in the tests with 7 : 3 AP/binder mix in the binder lamina, seem to be indicative that the 7 : 3 mix burns on its own, a result consistent with past propellant experience (e.g., Ref. [41]).

Increasing the thickness of the 7 : 3 AP-filled binder lamina resulted in an increase in sandwich burning rate, as revealed by the development of V-shaped surface profiles (Fig. 10). The burning rate of the 7 : 3 AP/binder mix alone was not determined, so it is not possible to determine from the present data whether the KLLEFs on the stoichiometric surfaces contributed significantly to the rate or not. The details of the flame structure over a 7 : 3 AP/binder propellant with 10 $\mu$m AP are also not known. However, the observations and interpretations of "smooth bands" near AP-binder interfaces suggest that the 10 $\mu$m AP particles sublime (i.e., the solid and surface processes in the "fuel" lamina are still endothermic). The results of the sandwich deflagration limit tests suggest that KLLEFs may not hold in the individual mixing fans of small AP particles, in which case the flame would be more nearly a flat premixed flame over the 7 : 3 lamina. While these are rather speculative extensions of the results of tests on sandwiches with pure binder laminae, they are fundamental to the nature of the flame over the surface of the AP-filled binder laminae. This concept of stability of a KLLEF in the mixing fan from AP particles is pursued further in the bimodal propellant tests.

### Interpretation of Results with Bimodal Propellants

The idea of stoichiometric tip retraction that was proposed to explain the pressure-sensitive parts of the deflagration limit curves (Fig. 6) has much broader relevance than the tapered sandwich experiment. In propellant combustion, there are stoichiometric surfaces and KLLEFs also, and the presence or absence of the KLLEFs on the stoichiometric surfaces would be expected to be important to the burning characteristics of the propellant. Of course, the issue is not a simple one of a deflagration limit, because the propellant surface is a chaotic array of oxidizer and binder surfaces of different dimensions. Yet one may reasonably ask of each point on the surface, is there a KLLEF on the neighboring mixing region, or not? Presumably the answer will depend on pressure, and the dimensions of the local fuel and oxidizer surfaces. In that case, at low pressure, KLLEFs may be attached to individual mixing regions only at localities on the surface where relatively wide fuel and oxidizer surface elements are involved. As pressure is increased, conditions become more favorable for holding of KLLEFs, so these near-surface, high-temperature flamelets will be present on a larger range of oxidizer particle sizes. This has obvious implications for pressure dependence of burning rate, but involves a very different argument than those used in present burning rate models. In particular, it suggests a role of propellant microstructure that acts through pressure dependence of stability of near-surface microflames, rather than the usual mixing rate arguments.

In view of the difficulty of either observing the postulated microflame behavior or con-

structing analytical models to test the foregoing concepts, an experiment was sought in which the relevance of the concepts would be revealed by singular burning rate behavior. The burning rate tests on bimodal propellants were run for this purpose (Fig. 11). The virtue of bimodal propellants is that the burning surface can be viewed as consisting of "large" areas of oxidizer (each large particle) interspersed with areas of a binder-fine oxidizer mixture (this description applies if the particle size of the coarse oxidizer is much larger than the particle size of the fine oxidizer). In such a propellant, the question of KLLEF holding on the local mixing fans becomes less statistical, since mixing fans are divided into two categories (fine particle fans and coarse particle fans). The thesis of the experiment was that KLLEFs would hold on the coarse particle mixing fans over the whole range of pressures of interest, but hold on the mixing fans of individual fine oxidizer particles only at high pressure. If this reasoning were correct, one would expect that a curve of burning rate versus pressure would show a break to higher burning rate at the pressure for establishment of KLLEF holding on fine particles. Further, one would expect the break in the curve to occur at higher pressure when the fine particles are smaller. The break in the curve would be sharp if the size distributions in the two oxidizer modes were very narrow, and less abrupt with broader size distributions.

The burning rate results in Fig. 11 constitute a test of the foregoing arguments, and show the breaks in the burning rate curves, with the predicted dependence on size of fine AP particles. These results not only support the mechanistic argument, but also provide an interesting means of tailoring burning rate. It should be recalled that the size distribution of the fine AP in these propellants was not particularly narrow; since the effect on burning rate is nonetheless clear-cut, there appears to be considerable latitude for control of the burning rate curve by careful combinations of narrow-cut particle fractions.

The reader may have noted in the foregoing steady burning arguments that a deflagration limit concept previously called "stoichiometric tip retraction" was being used as a concept of KLLEF holding or nonholding. In the sandwich deflagration limit situation, the stoichiometric surfaces were closed over the binder in an oxidizer-rich system. In the propellant, the overall stoichiometry is fuel-rich, so one may imagine that the stoichiometric surfaces close over the oxidizer particles. The stoichiometric tips are close to the surface for small particles, far from the surface for large particles, a condition on which the rest of the argument is founded. However, the KLLEF holding-nonholding argument depends on the local oxidizer-fuel mixture being far enough from the stoichiometric condition to provide a strongly fuel-rich condition above the stoichiometric tips of the fine particles. If this condition were not met, the KLLEFs might hold at any height; i.e., the instability above the tips would be removed. This effect was demonstrated in the sandwich burning tests with AP-filled binder laminae, where a 1 : 1 AP : fuel ratio in the lamina appeared to yield no near-surface flames in the 10 $\mu$m AP, while a 7 : 3 AP : fuel ratio caused the thicker laminae to burn down ahead of the normal sandwich burning front in spite of the small AP particle size. It is not likely in this latter case that the KLLEFs were held on the individual mixing fans, but they nonetheless established locations close enough to the surface to dominate burning rate when the mixture was not too fuel-rich. In the case of the bimodal propellant tests, the mixture ratio of the binder-fine AP matrix was chosen to be very fuel-rich to assure that KLLEFs would not hold close above the stoichiometric tip.

## Dependence of the Combustion Zone

### Details on Pressure

The model of combustion zone structure in Fig. 12 corresponds to the region of the sandwich and flame complex within 150 $\mu$m or less from the oxidizer-binder interface planes, and for a midrange pressure (3-5 MPa). The differences in surface profiles with pressure have been

described in the foregoing. These differences are indicative of substantial pressure dependence of the flame complex, and a proper use of the model of combustion zone structure would require consideration of these differences. Because pressure dependence is so important to combustion of propellants, the relevant material on pressure dependence of the sandwich flame complex is discussed more systematically here. The discussion is confined to thin-binder sandwiches and pure binders that do not produce melt flows onto the AP surface in such sandwiches. The discussion will address the regions (1)–(13) of Fig. 12 progressively. The pressure range covered is roughly 0.4–10 MPa.

*Region (1).* The binder lamina here is recessed relative to the immediately adjoining AP for lamina thickness less than 40 $\mu$m, and protrudes for binder thickness greater than about 80 $\mu$m. The trend has not been catalogued in detail, but is not notably pressure-dependent.

*Region (2).* The interface planes of this region do not show evidence of interfacial burning or other singular behavior over the range of conditions noted here.

*Regions (3) and (4).* The AP immediately adjoining the interface planes [region (3)] protrudes under all conditions (relative to the AP further from the interface). This is also the "smooth band" region. At low pressure, the protrusion is only marginally evident (0.1 MPa). At high pressure (see Fig. 3), the protrusion is dramatic (10 MPa) [10, 11, 15]. The width and nature of the smooth band [and location of associated outer edge at region (4)] are relatively insensitive to pressure except to the extent that height of the region of AP protrusion changes. The lateral distance to the outer edge of the smooth band has not been determined systematically, but is typically in the 20–50 $\mu$m range. Thus the leading edge of the AP surface [region (4)] is always some distance from the interface plane, being located just beyond the smooth band. This is the point of maximum heat flux to the surface. At pressures above 7 MPa, the leading edge may extend as a flat profile (Fig. 2) all the way to the outer edge of the sample (depending on binder thickness), indicating that the AP burning rate exceeds the rate attributable to the sandwich (consistent with Fig. 5b).

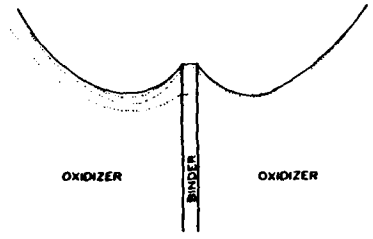


Fig. 15. Temperature field in the solid phase. (Dotted lines are calculated isotherms, Ref. [34]).

*Region (5).* The pressure dependence of this region was described earlier. It behaves like self-deflagrating AP (above 2 MPa), and controls the burning rate above 7–10 MPa (Fig. 5b). Below 2 MPa the AP is pyrolized by the AP–binder flame.

From the results just summarized [(1)–(5)], it can be inferred that the maximum heat flux to the solid phase (and maximum AP surface temperature) occurs at region (4). The temperature field in the solid must then be qualitatively similar to the sketch in Fig. 15. Such profiles are consistent with earlier observations of the boundary of the crystal phase change layer (240°C isotherm) in quenched samples [3], and with profiles calculated in a two-dimensional model of the two-slab burning problem [34]. These results seem to establish unambiguously that heat flows from the AP to the binder over the whole pressure range.

The extent of the region in the AP in which lateral heat transfer is important must be of the same order as the thermal wave thickness in the solid. The thickness of this heated layer can be calculated from estimated thermal properties of the ingredients, surface temperatures, and burning rates (which are pressure-dependent). The thickness can also be estimated from experimental observations of the thickness of the crystal

phase change layer on quenched AP samples [3, 39]. The latter results show that the temperature falls from 550–600°C down to 240°C in a distance of 8 μm at 10 MPa, and a distance of 58 μm at 1 MPa. These results are consistent with estimates based on thermal properties and burning rates. The resulting dimensions are of the same order as the width of the region of retarded AP regression and smooth band [region (3)], indicating not only that lateral heat transfer to the binder is present (based on isotherm profiles), but is effective in the dimensional domain postulated in the model. The total effect of the lateral heat drain from the AP on the surface regions depends upon its effect on the flame complex (heat source distribution). Thus, the total effect of pressure on the condensed-phase temperature field or surface profile cannot be estimated without consideration of the pressure dependence of the flame complex. Judging from the wide change in surface profile in region (3) (Fig. 3 and Ref. [15]) over the pressure range (especially above 7 MPa), the pressure dependence of the heat source distribution is a major factor in determining this part of the surface profile and temperature field in the solid.

*Region (6).* The pressure dependence in this region is simply that of the AP self-deflagration flame [25]. It seems likely that more of the total exothermic reaction of the AP occurs in this flame at low pressure than at high pressure, since evidence of the froth reaction on quenched samples becomes minimal as the low pressure self-deflagration limit of the AP is approached. Below that pressure, the gas-phase AP flame may still be present in locations where heat losses are low and heat flow from the oxidizer-binder flame can support the AP flame. Since no direct observations of the AP flame have been reported, the above arguments are inferences from indirect evidence, and are, at best, of only qualitative validity.

*Region (7).* The qualitative argument concerning the AP flame in region (6) is also relevant to region (7), but in this region there is no doubt that the flame receives heat from the AP–binder flame, because the burning rate of the underlying AP is higher than the AP self-deflagration rate (Fig. 5b) at pressures below 7–10 MPa (depending on binder thickness). Above this pressure the AP combustion is not enhanced locally by the oxidizer-binder flame, and regions (4) and (7) cease to have unique existence (the curves in Fig. 5b converge into a single curve, which is the AP self-deflagration rate). The minimum pressure for the AP flame to be present at region (7) is not known; below the AP self-deflagration limit, its presence would depend on the presence and condition of the AP–binder flame.

*Region (8).* As noted earlier, the status of the AP flame in this region is uncertain at all pressures. From the extreme protrusion of the AP in this region at high pressure, it seems likely that there is no local AP flame; i.e., the AP flame in region (7) encounters a quench limit on the region (8) side due to lateral heat drain into the solid and reduced heat supply from the AP–binder flame. It is this reasoning that led to the speculation earlier that there was no AP flame in region (9). The evidence for this is convincing at high pressure because of the extreme AP protrusion, but presence of a quench limit for the AP flame between regions (7) and (9) seems plausible also at lower pressures. This hypothesis is supported by the relatively low pressure sensitivity of the related features in the underlying surface (smooth band and AP protrusion) in the lower pressure range.

*Region (9).* This region is a mixing "fan" between oxidizer and fuel flow. Such regions occur in pairs, and the members of each pair interact increasingly with each other at greater distance out from the surface. While these interactions have been stressed in explaining burning rate trends and deflagration limits, a quantitative analysis of such pairs of mixing fans is not available. Some insight into pressure dependence of the flame complex can be gained by examining a simpler, more tractable representation of the single mixing fan problem. For that purpose, it will be assumed that oxidizer

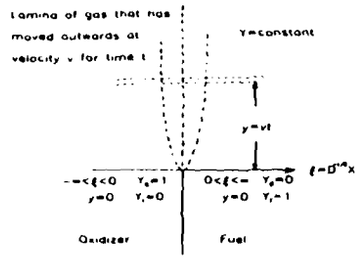


Fig. 16 Description of a single mixing fan. The broken upward lines are constant composition lines. The horizontal broken lines represent a volume element convected upward at velocity $v$

and binder vapors leave the surface as parallel flows of equal velocity, $v$, and temperature, and that this condition is preserved out to the KLLEF [regions (10), (11)]. In that case, a layer of gas emerging from the solid at a specific time can be located later at a definite "$y$" position (Fig. 16) that is proportional to time. It will be assumed that mixing of the two gases in a convected layer proceeds by molecular diffusion, and only in the lateral direction (i.e., vertical diffusion velocities are small compared to convective velocity). Using the equations for a binary system with diffusion coefficients $D_{12} = D_{21}$, diffusion in the $x$ direction in a convective layer proceeds according to Fick's Law

$$YV = -D\frac{dY}{dx} \tag{5}$$

where $Y$ is a mass fraction of one of the gases and $V$ is diffusion velocity. For a given volume (length) element in the moving layer of gas, conservation of a species $Y$ requires that

$$\frac{dY}{dt} = -D\frac{d^2Y}{dx^2} = -\frac{d^2Y}{d\xi^2}, \tag{6}$$

where

$$\xi = xD^{-1/2}. \tag{7}$$

For this purpose, note that the initial condition on $Y$ is the same for all pressures; i.e., $Y_o = 1$ at the oxidizer surface and $Y_f = 1$ at the fuel surface. The initial mixing is primarily close to the interface plane where concentration gradients are high, and the boundary conditions at "large" $x$ have little effect. Assuming this to be valid in all of region (9), the solutions to Eq. (6) in the region of interest are closely approximated by a single pair of time-dependent mass fraction profiles (one for $Y_o$ and one for $Y_f$),

$$Y_i = Y_i(\xi, t) = Y_i\left(\xi, \frac{y}{v}\right), \qquad i = o, f, \tag{8}$$

where $y/v$ reflects the convection time of the layer outward from the surface at velocity $v$ out to the height $y$.

To the extent that pressure does not affect the validity of assumptions about boundary conditions at "large" $x$, a set of solutions, $Y = Y(\xi)$, corresponding to various values of $t$, applies for all pressures; the pressure dependence is contained in the relation of $\xi$ to $x$, and of $t$ to $y$, which are necessary to convert Eq. (8) into concentration fields in $x$ and $y$ coordinates. The relation of $\xi$ to $x$ in Eq. (7) depends on pressure through $D$, which is inversely proportional to $p$ [40]. Thus

$$x = (K_1 p^{-1/2})\xi. \tag{9}$$

The $y$ position for a given $t$ is given by

$$y = vt, \tag{10}$$

where $v$ is the velocity from the surface, assumed to be pressure dependent, but independent of $y$. Applying mass continuity at the surface, and assuming the burning rate depends on pressure according to Eq. (3) (where $n$ is typically between 0.2 and 0.5), and the continuity expression (2) is used;

$$v = (\rho_s C_p^n/\rho_s) = K_2 p^{n-1}, \tag{11}$$

where $K_2$ is independent of $p$, then

$$y = K_2 p^{n-1} t. \tag{12}$$

$y$ is the distance a layer travels from the surface in the time, $t$. Suppose one considers mixing fans at different pressures, and seeks the transverse concentration profile in each fan that corresponds to a specific convection time $t_1$. Equation (12) indicates the $y$ coordinate of that concentration profile, Eq. (8) gives the concen-

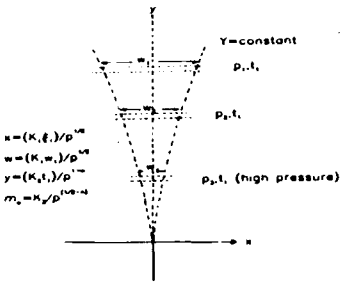


*Fig. 17. Dependence of the location and span of a convected layer of gas in the mixing fan on pressure. The spans $w$ are the distances between specific composition lines corresponding to the convection and diffusion time $t_1$, shown for three different pressures. (Figure is sketched to show trend, not calculated.)*

tration profile for that time $t_1$ (in the $\xi$ coordinate), and Eq. (9) provides the conversion of the profile to the $x$ coordinate. Examining these equations, the $t_1$ profile moves in closer to the surface as pressure increases, and the profile contracts in the $x$ direction. This pressure dependence of the mixing region is illustrated qualitatively by the sketch in Fig. 17. The span of the layers sketched in Fig. 17 corresponds to a specific span of $\xi$ for the time $t = t_1$, and corresponding mass fraction profile $Y_{t_1}(\xi)$. However, the mass flow through the segments at different pressures are not the same. Thus, if the width of the segment is designated by "$w$,"

$$\dot{m} = \rho v w,$$

which depends on pressure according to

$$\dot{m} \propto p \cdot p^{n-1} \cdot p^{-1/2} = p^{n-1/2}. \tag{13}$$

The reason for addressing the trend of conditions in a specific span of $Y_{t_1}(\xi)$ as a function of pressure is explained in the following.

*Region (10)–(11)* refers to a transverse flame in the mixing region. While there is no direct observational data about such micro flames, their behavior will be argued here on the basis of more traditional theory and observation of macro flames. The "KLLEF" is probably crescent-shaped [38, 39] with leading edge on the stoichiometric surface. It extends outward laterally into the mixing region to an extent limited by flammability limits in the off-stoichiometric mixture. Presumably, the location ($y$ coordinate) and span (width in the mixing field) are dependent on pressure. The flame is kinetically limited in the sense that it stands in a premixed flow, but that flow is a diffusion fan, and the response of the flame to pressure (e.g., standoff distance from the surface) depends also on the state of mixing as a function of $y$. This will be examined by a very simplified model in the following.

Suppose that, under a given set of conditions, a KLLEF exists and is approximated by a planar flame analogous to the mixing layers described for region (9) (Fig. 17). Then this KLLEF would be associated with a specific concentration profile [Eq. (8)], flow time from the surface, and a span of $\xi$ corresponding to fuel-rich and oxidizer-rich flammability limits. At a higher pressure, assume that these same concentration conditions determine the flame location and span (i.e., that the position of the flame is dominated by adiabatic flame temperature). Thus the preceding description of pressure dependence of segments of the mixing layer applies also to the KLLEF, and the flame position and span at each pressure are given by applying Eqs. (9) and (12) to the $t$ and $\xi$ span of *the flame at the higher reference pressure*. Thus the flame would move closer to the surface and contract laterally as pressure increased in the manner described for the mixing fan analysis and Fig. 17 (including decrease in mass flux through the KLLEF with increasing pressure).

Described in the foregoing terms, one might ask, in what way does the description reflect the "kinetically limited" aspect of the flame? This is embedded in the postulate that the flame positions itself at each pressure so as to maintain the same flame temperature profile and chemical induction time. This seems to be a reasonable approximation in view of the exponential temperature dependence of reaction rate on temperature. However, the molecular collision rate

does increase with pressure, and the flame probably advances more than the amount predicted by Eq. (12). In doing so, the span of the flame would be further reduced, and the mass flux through the flame would be reduced more than indicated by Eq. (13). Thus the advance of the flame with increasing pressure also contracts the flame and decreases the total heat release.

Given the two-dimensional nature of the heat transfer from the flame, a more complete two-dimensional analysis would be required to quantify the argument further. In such an analysis it would be necessary to consider more carefully the boundary conditions. We have argued earlier that interaction of adjoining mixing fans is an important factor in the effect of binder thickness on burning rate and deflagration limits, indicating the necessity to quantify the above simplistic argument for realistic description of pressure dependence of KLLEFs with thin-binder sandwiches and/or low pressures.

### The Overall Flame Complex

The details of the flame complex and its dependence on binder thickness and pressure are summarized in Fig. 18. The stoichiometric tip is shown with a height that decreases moderately with decreasing pressure (row 1 → 4), due to lower mass flow rate [Eq. (4)] and decreases with binder thickness (columns a → c). The KLLEF standoff distance increases (row 1 → 4) as pressure decreases [Eq. (12)], and a correspondingly large portion of the fuel is consumed in the KLLEF at lower pressure [Eq. (13)]. When the binder thicknesses decreases (columns a → c) the amount of fuel to be consumed decreases, and the KLLEF consumes a correspondingly larger portion. In the process, the KLLEFs stand closer together (Figs. 13, 14). This merging of diffusion fields is more conservative of energy in the PVCs, giving rise to the increase in burning rate with decreasing binder thickness (Fig. 5a) [the earlier arguments regarding individual mixing fields, and Eqs. (12) and (13), are less applicable to this situation]. In the limit of very thin binder, the AP-binder flame makes a decreasing contribution (row 2, column c), and burning rate returns toward the AP rate (Fig. 5a), or quenches (row 4, column c) if pressure is below the AP self-deflagration limit (Fig. 6).

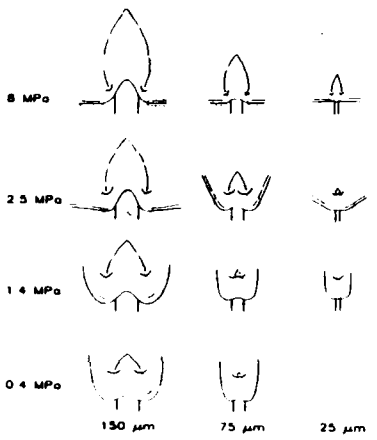


Fig. 18 Dependence of flame complex on pressure for various binder thicknesses (dotted curves are constant-concentration profiles, wavy lines are flames, solid lines are surfaces). (Sketches based on combined results of present study.)

The AP flame is present at all pressures down to 2.5 MPa or lower, and dominates the burning rate in the pressure range 10-14 MPa at all binder thicknesses, and at extremes of binder thickness down to about 5 MPa (Fig. 5a,b). The AP flame may be established locally at lower pressures in locations of maximum support from the AP-binder flame (rows 3, 4, column a). Over the range of conditions of interest, the heat release from the AP decomposition is apportioned between a surface froth reaction and a flame reaction, the exact proportionment and dependence on pressure being matters of speculation.

The components of the flame are interdependent in ways that are established in only qualitative terms. Some portion of the inner ends of the AP flames seems to be quenched by heat loss to the binder lamina (in the smooth band region),

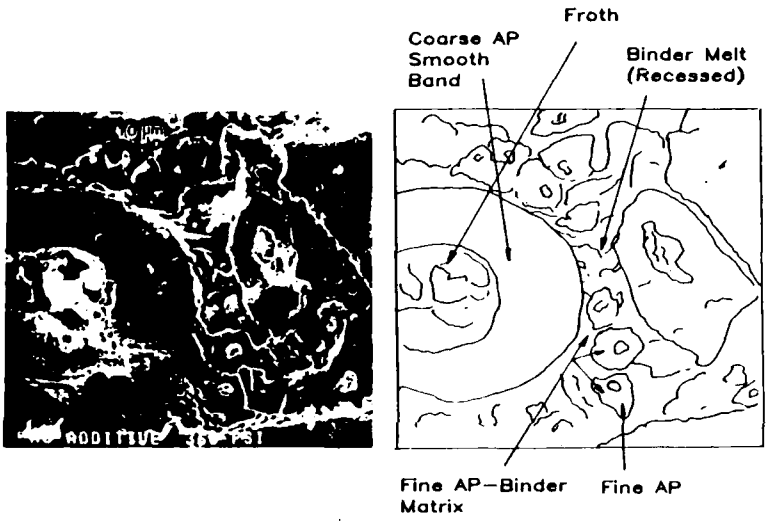


Fig. 19 Quenched burning surface of an AP PBAN propellant burned at 1.24 MPa (bimodal AP size distribution) showing features analogous to quenched sandwiches.

with the result that the mixing fans apparently always involve intermediate decomposition products of AP. This must be a significant factor in the location and nature of the KLLEF, which, in turn, affects the amount of reactants remaining for the diffusion flame. In any consideration of burning rate of a propellant or of steady or nonsteady interaction of the flow environment with rate, these details of the interaction of different parts of the flame complex, and associated spatial distribution of heat release, are crucial questions about which more quantitative information is needed.

## COMMENT

The practical purpose of studies of sandwich burning is to clarify the controlling mechanisms of composite propellant burning. There should be no illusions about the strategy. It cannot clarify all relevant aspects of propellant combustion, and the difficulties of studying propellants do not all go away when one turns to sandwich studies. The present results do indicate that a good deal can be learned about combustion zone structure in the context of the "simple" sandwich system. It should be no surprise that the resulting view of the combustion zone is two-dimensional, not one-dimensional, since the sandwich system is two-dimensional. However, it should be recognized that those (two-dimensional) features of the sandwich combustion zone that are within 50 $\mu$m of the interface planes between laminae have their counterpart on propellant surfaces, where oxidizer crystals are typically 100–150 $\mu$m in diameter. If we are to understand composite propellant combustion, we must deal with the same multidimensional features of the combustion zone that are present in sandwich burning.

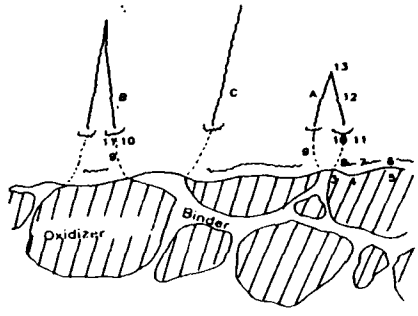


Fig. 20. Flame complex for an AP propellant as inferred from present studies. Note that "closure" of the diffusion flame is only local, i.e., may seem to close over the fuel in locations where the binder is thin, but appears to close over the AP at a location further around the AP particle where the fuel is thicker. These features change with time during burning of particles, as does the surface profile of the particle itself. Note: numbers designate regions of the flame complex described in Fig. 12 and in the text. The letters represent (A) flame closure over a region of thin binder; (B) flame closure over oxidizer in a fuel-rich region; (C) a region where closure is in transition between closure over fuel and closure over oxidizer (i.e., no closure when viewed three-dimensionally).

The sandwich results show the gas-phase, surface, and subsurface processes to be all multidimensional, and all closely coupled. Pyrolysis of the binder is aided by lateral heat flow from the oxidizer. The heat drain from that region of the oxidizer causes a local change in the mode of vaporization of the oxidizer, and a change in site of its heat release. This anomalous vaporization must have some effect on the near-surface oxidizer-binder flame. While there are conditions (e.g., high pressure) where this locally coupled aspect of the behavior in the PVC region may not be important to the mean burning rate, it appears that under most rocket motor conditions, realistic modeling of either steady or unsteady combustion of AP-HC binder propellants must address the three-dimensionally coupled nature of the processes in the entire combustion wave. It does not require much imagination to see the same surface features on quenched propellant samples (Fig. 19) that have been discussed here for sandwich burning. By the same token, the structure of the flame complex can also be postulated with reasonable confidence (Fig. 20). In the case of the propellant, some further consideration must be given to propagation of the flame between successive particles [42], and to the question of the least-time path of the burning front through the more complicated propellant matrix [15].

One final note is owed to all discerning readers. In research on propellant combustion, the difficulties of either analytical modeling or direct measurement of the flame complex lead to indirect strategies of postulate and proof. An inevitable consequence is that "proofs" are generally inferences based on qualitative arguments related to indirect evidence such as burning rate and combustion limits. We have striven to amass as much unambiguous evidence as possible in support of our interpretations, but do not want to leave any illusions about outstanding problems. For example, the *concept of a kinetically limited leading edge flame* has been used in one form or another by various modelers without rigorous modeling. It is pictured in the

present report as a transverse flame sheet in the O–F mixing flow. But we are uncertain what reactants are present in the mixing flow, what "induction" reactions occur in that flow, or whether the concept of a flame "sheet" is relevant in such a microscopic domain. The evidence suggests that the "KLLEF" concept is qualitatively relevant and useful, but the details are not amenable to direct observation by available methods, and have not yet been realistically modeled analytically. Further, the presence of the KLLEF poses a problem in correct calculation of the diffusion flame and height of the stoichiometric tip that has not been addressed. The sketches in this paper suggesting KLLEF locations and stoichiometric tip heights are based on consistency with the arguments in the interpretation of results (including those in Ref. [34]). The real behavior may involve unsteady behavior or vortical breakdown of the diffusion fans or diffusion flames, and the concept of stoichiometric tip retraction (loss of the KLLEF) suggested in the discussion of experimental results may be a simplistic interpretation of a more complicated phenomenon. These issues are stressed here as a matter of scientific integrity, and in the interest of a more dynamic attack on remaining problems.

*The research reported here was conducted under sponsorship of the U.S. Office of Naval Research, with technical monitorship by Dr. R. S. Miller.*

## REFERENCES


1. Beckstead, M. W., Derr, R. L., and Price, C. F., *AIAA J.* 8:2200-2206 (1970).
2. Powling, J., *Eleventh Symposium (International) on Combustion*, The Combustion Institute, 1967, pp. 447-456.
3. Hightower, J. D., and Price, E. W., *Astronautica Acta* 14:11-21 (1968).
4. Hightower, J. D., Price, E. W., and Zurn, D. E., CPIA Publication No. 162, Vol. I, December 1967, pp. 527-534.
5. Boggs, T. L., and Zurn, D. E., *Combustion Science and Technology* 4:279-292 (1972).
6. Brown, W. E., Kennedy, J. R., and Netzer, D. W., *Combustion Science and Technology* 6:211-222 (1972).
7. Abraham, M., III, and Netzer, D. W., *Combustion Science and Technology* 11:75-83 (1975).
8. Nadaud, L., *Combust. Flame* 12:177-195 (1968).
9. Ermolaev, B. S., Korotkov, A. I., and Frolov, Yu. V., *Fizika Goreniya i Vzryva* 6:277-285 (1970).
10. Price, E. W., Handley, J. C., Panyam, R. R., Sigman, R. K., and Ghosh, A., *AIAA J.* 19:380-386 (1981).
11. Price, E. W., Sigman, R. K., and Panyam, R. R., Georgia Institute of Technology, Atlanta, GA, September 1981.
12. Price, E. W., Panyam, R. R., and Sigman, R. K., CPIA Publication No. 329, Vol. I, November 1980, pp. 37-51.
13. Hightower, J. D., and Price, E. W., *Eleventh Symposium (International) on Combustion*, The Combustion Institute, 1967, pp. 463-472.
14. Boggs, T. L., Price, E. W., and Zurn, D. E., *Thirteenth Symposium (International) on Combustion*, The Combustion Institute, 1971, pp. 995-1008.
15. Price, E. W., Handley, J. C., Strahle, W. C., Sheshadri, T. S., Sigman, R. K., and Ghosh, A., Georgia Institute of Technology, Atlanta, GA, September 1980.
16. Boggs, T. L., Zurn, D. E., Strahle, W. C., Handley, J. C., and Milkie, T. T., Naval Weapons Center, NWC TP 5514, 1973.
17. Varney, A. M., and Strahle, W. C., *Combustion Science and Technology* 4:197-208 (1972).
18. Price, E. W., and Sambamurthi, J. K., CPIA Pub. No. 333, Vol. I, October 1981, p. 223.
19. Boggs, T. L., Zurn, D. E., and Netzer, D. W., *Combustion Science and Technology* 7:177-183 (1973).
20. Price, E. W., Panyam, R. R., Sambamurthi, J. K., and Sigman, R. K., Annual Report on Office of Naval Research Contract N00014-79-C-0764, Georgia Institute of Technology, Atlanta, GA, February 1983.
21. Price, E. W., Panyam, R. R., Sambamurthi, J. K., and Sigman, R. K., CPIA Publication No. 366, Vol. I, October 1982, p. 81.
22. Boggs, T. L., *AIAA J.* 8:867-873 (1970).
23. Price, E. W., and Flandro, G. A., CPIA Publication No. 366, Vol. I, October 1982, p. 73.
24. Cohen Nir, E., *Combust. Flame*, 20:419-435 (1973).
25. Guirao, C., and Williams, F. A., *AIAA J.* 9:1345-1356 (1971).
26. Boggs, T. L., and Zurn, D. E., *Combustion Science and Technology* 4:227-232 (1972).
27. Levy, J. B., and Friedman, R., *Eighth Symposium (International) on Combustion*, The Combustion Institute, Williams and Wilkins Co., Baltimore, 1962, p. 66.
28. Hightower, J. D., and Price, E. W., CPIA Publication No. 105, Vol. I, May 1966, pp. 421-435.

29. Cohen, N. S., *17th Aerospace Sciences Meeting*, January, 15-17, 1979, New Orleans, LA, AIAA Paper 79-0160.
30. Summerfield, M., Sutherland, G. S., Webb, M. J., Taback, H. V., and Hall, K. P., in *Solid Propellant Rocket Research*, Progress in Astronautics and Rocketry Series, Vol. 1, Academic Press, New York, 1960, pp. 141-182.
31. Fenn, J. B., *Combust. Flame* 12:201-216 (1968).
32. Belyaev, A. F., and Bakhman, N. N., *Combustion, Explosion and Shock Waves* 2:1-17 (1966).
33. Bakhman, N. N., and Librovich, V. B., *Combust. Flame* 15:143-155 (1970).
34. Panyam, R. R., Thesis, Georgia Institute of Technology, Atlanta, GA, June 1983.
35. Handley, J. C., Price, E. W., and Ghosh, A., CPIA Publication No. 308, Vol. 2, October 1979, p. 127.
36. Boggs, T. L., Kraeutle, K. J., *Combustion Science and Technology* 1:75-93 (1969).
37. Murphy, J. L., and Netzer, D. W., *AIAA J* 12:13-14 (1974).
38. Phillips, H., *Tenth Symposium (International) on Combustion*, The Combustion Institute, 1965, pp. 1277-1283.
39. Ishakawa, N., *Combustion Science and Technology* 31:109-117 (1983).
40. Williams, F. A., *Combustion Theory: the Fundamental Theory of Chemically Reacting Flow Systems*, Addison-Wesley, Reading, MA, 1965.
41. Schmidt, W. G., Loving, R. L., and Poynter, A. L., AFRPL TR-81-19, April 1981.
42. Strahle, W. C., *AIAA J.* 16:843-847 (1978).

*Received 17 December 1984; revised 6 September 1985*

United Technologies Corp. 4
Chemical Systems Division
P. O. Box 358
Sunnyvale, CA 94088
Attn: Dr. Robert S. Brown
Dr. C. M. Frey
Dr. R. W. Hermsen
Dr. R. R. Miller

University of Akron 1
Institute of Polymer Science
Akron, OH 44325
Attn: Prof. Alan N. Gent

University of California 1
Berkeley, CA 94720
Attn: Prof. A. G. Evans

University of Delaware 1
Department of Chemistry
Newark, DE 19711
Attn: Dr. T. C. Brill

University of Waterloo 1
Dept. of Mechanical Engineering
Waterloo, Ontario
CANADA
Attn: Dr. Clarke E. Hermance

Naval Air Systems Command 1
NAVAIR-320G
Jefferson Plaza 1, RM 472
Washington, DC 20361
Attn: Mr. Bertram P. Sobers

Morton Thiokol, Inc. 1
Director, Advanced Technology
Aerospace Group
3340 Airport Rd.
Ogden, UT 84405
Attn: Dr. O. A. Flanigan

Air Force Office of Scientific 1
Research
Directorate of Chemical &
Atmospheric Sciences
Bolling Air Force Base
Washington, DC 20332
Attn: Dr. Donald L. Ball

Naval Surface Weapons Center 1
Code R11
White Oak
Silver Spring, MD 20910
Attn: Dr. H. G. Adolph

Naval Weapons Center 3
Code 3205
China Lake, CA 93555
Attn: Mr. Lee N. Gilbert
Dr. L. Smith
Dr. C. Thelen

Naval Weapons Center 1
Code 3858
China Lake, CA 93555
Attn: Dr. E. Martin

Pennsylvania State University 1
Dept. of Mechanical Engineering
University Park, PA 16802
Attn: Prof. Kenneth Kuo

Princeton Combustion Research 2
Laboratories, Inc.
1041 U. S. Highway One North
Princeton, NJ 08540
Attn: Dr. Martin Summerfield
Dr. J. Ben Raven

Princeton University 1
School of Engineering and Applied
Sciences
Dept. of Mech. Eng. & Aero. Eng.
The Engineering Quadrangle
Princeton, NJ 08544
Attn: Dr. Forman A. Williams

Purdue University 1
School of Mechanical Engineering
TSPC Chaffee Hall
West Lafayette, IN 47906
Attn: Mr. John R. Osborn

Rockwell International Corp. 1
Rocketdyne Division
8A08
6633 Canoga Ave.
Canoga Park, CA 91304
Attn: Mr. Joseph E. Flanagan

Space Sciences, Inc. 1
135 Maple Avenue
Monrovia, CA 91016
Attn: Dr. M. Farber

Naval Weapons Center 1
Code 385
China Lake, CA 93555
Attn: Mr. Herb Richter

SRI International 1
333 Ravenswood Ave.
Menlo Park, CA 94025
Attn: Mr. J. T. Rosenberg

Naval Surface Weapons Center 1
Code R13
White Oak
Silver Spring, MD 20910
Attn: Dr. C. S. Coffey

Aerojet Strategic Propulsion Co. 1
Bldg. 0525, Dept. 2131
P. O. Box 15699C
Sacramento, CA 95813
Attn: Dr. G. E. Manser

Dr. Norman Cohen 1
141 Channing St.
Redlands, CA 92373

The BDM Corporation 1
2227 Drake Ave.
Huntsville, AL 35805
Attn: Dr. J. K. Sambamurthi

Morton Thiokol, Inc. 1
Huntsville Division
Huntsville, AL 35807-7501
Attn: Dr. Robert B. Kruse

Jet Propulsion Laboratory 1
California Institute of Technology
Mail Stop 507-241
4800 Oak Grove Dr.
Pasadena, CA 91109
Attn: Dr. Leon Strand

Hercules, Inc. 1
Bacchus Works
P. O. Box 98
Magna, Utah 84044
Attn: Dr. Ken McCarty

Sandia Laboratories 1
Livermore, CA 94550
Attn: Dr. R. Armstrong

Mr. G. Daniel Oldre 1
ONR Resident Representative
O'Keefe Building, Room 206
Georgia Institute of Technology
Atlanta, GA 30332

Defense Technical Information Center 12
Bldg. 5, Cameron Station
Alexandria, VA 22314

Director 6
Naval Research Laboratory
Code 2627
Washington, DC 20375